Finite Element Analysis of Incompressible Flows Past Two Circular Cylinders
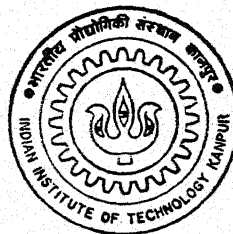
by

Akhilesh Raghuvanshi

DEPARTMENT OF AEROSPACE ENGINEERING

INDIAN INSTITUTE OF TECHNOLOGY KANPUR

FEBRUARY, 1996

Finite Element Analysis of Incompressible Flows Past Two Circular Cylinders

A Thesis Submitted

in Partial Fulfillment of the Requirements

for the Degree of

Master of Technology

by

Akhilesh Raghuvanshi

to the

DEPARTMENT OF AEROSPACE ENGINEERING
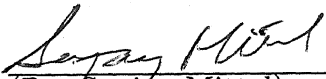
INDIAN INSTITUTE OF TECHNOLOGY, KANPUR

February,1996

AE- 1996 — M — RAG — FIN

CERTIFICATE

Certified that the work contained in the thesis entitled *"Finite Element Analysis of Incompressible Flows Past Two Circular Cylinders"*, by *"Akhilesh Raghuvanshi"*, has been carried out under my supervision and that this work has not been submitted elsewhere for a degree.

(Dr. Sanjay Mittal)

Department of Aerospace Engineering,

Indian Institute of Technology,

Kanpur.

February,1996

iii
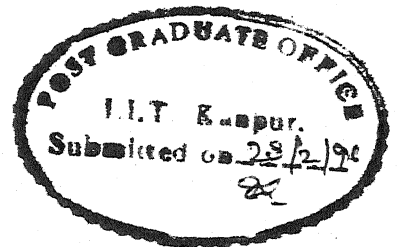
Acknowledgements

I would like to express my deepest gratitude to all those who have helped me in my thesis work.

Contents

List of Figures

ix

Abstract

In the present study, stabilized space-time finite element formulations have been used to simulate unsteady incompressible flows involving two cylinders at various relative locations at low Reynolds numbers. The equation system resulting from the finite element discretization of these problems have been solved iteratively. In all the cases we observe significant interaction between the flows around the two cylinders.

In the first problem, we study the effect of placing a small control cylinder in the wake of another larger cylinder. As observed by other researchers, in the past, our results show that under certain conditions , the control cylinder can suppress the vortex shedding mechanism. The second problem involves two cylinders of equal size that are allowed to move due to the fluid dynamic forces acting on them. Such problems fall in the general class of fluid-body interaction.

The results we present include the pressure, vorticity and stream function fields at various time instants during the temporal evolution of the flow field, time histories of the drag and lift coefficients, amplitude of the drag and lift coefficient oscillations, the phase relationships between the drag and lift oscillations associated with each cylinder and Strouhal number for each flow field.

Chapter 1

Introduction

1.1   Motivation

Fluid-body interaction causes vibration/flutter of the structure immersed in fluid. Flow-induced vibration is a term to denote those phenomena associated with the response of structures immersed in or conveying fluid flow. The term covers those cases in which an interaction develops between fluid-dynamic forces and the inertia, damping or elastic forces in the structures. The study of these phenomena draws on three disciplines: (1) structural, (2) mechanical vibration, and (3) fluid dynamics.

Flow induced vibration comprises complex and diverse phenomena; subcritical vibration of nuclear fuel assemblies, galloping of transmission lines, flutter of pipes conveying fluid, and whirling of heat exchanger tube banks are typical examples. Recently, flow-induced vibration has been studied extensively for several reasons. First with the use of high strength materials, structures become more slender and more susceptible to vibration. Second, the development of advanced nuclear power reactors requires high-velocity fluid flowing through components, which can cause detrimental vibrations. Third, the dynamic interaction of structure and fluid is one of the most fascinating problems in engineering mechanics. The

increasing study is evidenced by many conferences directed to this subject and numerous publications, including reviews and books. In a broad sense, flow-induced vibration encompasses all topics on the dynamic responses of structures submerged in a flow.

1.2   Overview

We begin by stating Navier Stokes equations for incompressible flows in chapter 2. Thereafter, equation of motion for a rigid body in two dimensions that moves under the action of body forces and surface traction have been given. The motion of the body is constrained by a system of linear springs and dampers. We have adopted Galerkin least square formulation for the finite element computation of incompressible flows. For the formulation used, the stabilization of the numerical method is achieved by adding to the Galerkin formulation, a series of stabilizing terms. These terms can be obtained by minimizing the sum of the the squared residual of the momentum equation integrated over each element domain. This kind of stabilization is known as the GLS (Galerkin/ Least square) stabilization.

Most of the results presented in this thesis involve large scale computation of unsteady flows. The computational cost associated with the space-time finite element formulations using piece wise linear function in time is quite heavy. Generalized minimal residual (GMRES) iteration algorithm has been used to reduce the cost involved. The GMRES method is based on the minimization of the residual norm over a krylov space. For details of GMRES method refer [6][1].

In chapter 3 we talk about the vortex shedding and its suppression at low Reynolds number behind a circular cylinder. We state and show that vortex shedding behind circular cylinder can be altered and suppressed altogether (or 'controlled') over a limited range of Reynolds number by a proper placement of second,

---

[1]Numbers in brackets designate References at the end of this report

much smaller, cylinder in the near wake of the main cylinder. This interesting phenomenon of suppression of vortex shedding is the subject of chapter 3.

In chapter 4 a study has been conducted and presented for the flow field around two cylinders of same diameters at various locations with respect to one another and to find the cylinders' response to the flow.

For the present study, stabilized space-time finite element formulations in the form of Fortran codes were already available for single cylinder case[2]. These were modified and new grid was generated to accommodate the second circular cylinder of any diameter at any location downstream of first cylinder. The grid generated was block structured which enabled us to put any reasonable number of data points in any block/region of the flow field and thus capture the boundary layer flow field sufficiently. The results presented in the present study are a part of an ongoing investigation of flow past circular cylinders. All computations were performed at DEC-ALPHA-3000 systems and HP-9000/715 series machines at computer center at I.I.T. Kanpur. Post processing of data was done on HP-9000/834 Workstations (tsrxs') and HP-9000/715 Workstations.

---

[2]see acknowledgements

Chapter 2

Governing Equations And Finite Element Formulations

2.1 The Governing Equations

Let $\Omega_t \subset \mathbb{R}^{n_{sd}}$ and $(0,T)$ be the spatial and temporal domains respectively, where n_{sd} is the number of space dimensions, and let Γ_t denote the boundary of Ω_t. The subscript "t" implies the time-dependence of the spatial domain. The spatial and temporal coordinates are denoted by $\mathbf{x}$ and t. The Navier-Stokes equations governing incompressible fluid flow are

$$\rho(\frac{\partial \mathbf{u}}{\partial t} + \mathbf{u} \cdot \nabla \mathbf{u} - \mathbf{f}) - \nabla \cdot \boldsymbol{\sigma} = 0 \quad \text{on } \Omega_t \; for \; (0,T), \tag{2.1}$$

$$\nabla \cdot \mathbf{u} = 0 \quad \text{on } \Omega_t \; for \; (0,T). \tag{2.2}$$

Here ρ, $\mathbf{u}$, $\mathbf{f}$ and $\boldsymbol{\sigma}$ are the density, velocity, body force and the stress tensor, respectively. The stress tensor is written as the sum of its isotropic and deviatoric parts:

$$\boldsymbol{\sigma} = -p\mathbf{I} + \mathbf{T}, \quad \mathbf{T} = 2\mu\boldsymbol{\varepsilon}(\mathbf{u}), \quad \boldsymbol{\varepsilon}(\mathbf{u}) = \frac{1}{2}((\nabla \mathbf{u}) + (\nabla \mathbf{u})^T), \tag{2.3}$$

4

where p and μ are the pressure and viscosity. Both the Dirichlet and Neumann-type boundary conditions are accounted for, represented as

$$\mathbf{u} = \boldsymbol{g} \ on \ (\Gamma_t)_g, \quad \mathfrak{n} \cdot \boldsymbol{\sigma} = \mathbf{h} \ on \ (\Gamma_t)_h, \tag{2.4}$$

where $(\Gamma_t)_g$ and $(\Gamma_t)_h$ are complementary subsets of the boundary Γ_t. The initial condition on the velocity is specified on Ω_0:

$$\mathbf{u}(\mathbf{x}, 0) = \mathbf{u}_0 \quad on \ \Omega_0, \tag{2.5}$$

where $\mathbf{u}_0$ is divergence free.

2.2 Finite Element Formulations

2.2.1 Fixed Domains – Semi-Discrete Formulation

Consider a finite element discretization of Ω (the subscript t has been dropped for the fixed domain) into subdomains Ω^e, $e = 1, 2, ..., n_{el}$, where n_{el} is the number of elements. Based on this discretization, for velocity and pressure we define the finite element trial function spaces $\mathcal{S}_{\mathbf{u}}^h$ and $\mathcal{S}_p^h$, and weighting function spaces $\mathcal{V}_{\mathbf{u}}^h$ and $\mathcal{V}_p^h$. These function spaces are selected, by taking the Dirichlet boundary conditions into account, as subsets of $[\mathbf{H}^{1h}(\Omega)]^{n_{sd}}$ and $\mathbf{H}^{1h}(\Omega)$, where $\mathbf{H}^{1h}(\Omega)$ is the finite-dimensional function space over Ω. The stabilized finite element formulation of Eq. (2.1)-(2.2) is written as follows: find $\mathbf{u}^h \in \mathcal{S}_{\mathbf{u}}^h$ and $p^h \in \mathcal{S}_p^h$ such that $\forall \mathbf{w}^h \in \mathcal{V}_{\mathbf{u}}^h$, $q^h \in \mathcal{V}_p^h$

$$\int_\Omega \mathbf{w}^h \cdot \rho \left(\frac{\partial \mathbf{u}^h}{\partial t} + \mathbf{u}^h \cdot \nabla \mathbf{u}^h - \mathbf{f} \right) d\Omega + \int_\Omega \boldsymbol{\varepsilon}(\mathbf{w}^h) : \sigma(p^h, \mathbf{u}^h) d\Omega + \int_\Omega q^h \nabla \cdot \mathbf{u}^h d\Omega$$
$$+ \sum_{e=1}^{n_{el}} \int_{\Omega^e} \frac{1}{\rho} \left(\tau_{\text{SUPG}} \rho \mathbf{u}^h \cdot \nabla \mathbf{w}^h + \tau_{\text{PSPG}} \nabla q^h \right) \cdot$$

$$\left[\rho\left(\frac{\partial \mathbf{u}^h}{\partial t} + \mathbf{u}^h \cdot \nabla \mathbf{u}^h - \mathbf{f}\right) - \nabla \cdot \boldsymbol{\sigma}(p^h, \mathbf{u}^h)\right] d\Omega^e$$

$$+ \sum_{e=1}^{n_{el}} \int_{\Omega^e} \delta \nabla \cdot \mathbf{w}^h \rho \nabla \cdot \mathbf{u}^h d\Omega^e = \int_{\Gamma_h} \mathbf{w}^h \cdot \mathbf{h}^h d\Gamma \quad (2.6)$$

Remarks

1. In the variational formulation given by Eq. (2.6), the first three terms and the right-hand-side constitute the Galerkin formulation of the problem.

2. The first series of element-level integrals are the SUPG and PSPG stabilization terms added to the variational formulations. In the current formulation τ_{PSPG} is the same as τ_{SUPG} and is given as

$$\tau = \left(\left(\frac{2 \parallel \mathbf{u}^h \parallel}{h}\right)^2 + \left(\frac{4\nu}{h^2}\right)^2\right)^{-\frac{1}{2}}. \quad (2.7)$$

3. The second series of element-level integrals are added to the formulation for numerical stability at high Reynolds numbers. This is a least-squares term based on the continuity equation. The coefficient δ is defined as

$$\delta = \frac{h}{2} \parallel \mathbf{u}^h \parallel z, \quad (2.8)$$

where

$$z = \begin{cases} \left(\frac{Re_u}{3}\right) & Re_u \leq 3 \\ 1 & Re_u > 3 \end{cases},$$

and Re_u is the cell Reynolds number.

4. Both stabilization terms are weighted residuals, and therefore maintain the consistency of the formulation.

2.2.2 Deforming Domains – Space-Time Formulation

In order to construct the finite element function spaces for the space-time method, we partition the time interval $(0, T)$ into subintervals $I_n = (t_n, t_{n+1})$, where t_n and t_{n+1} belong to an ordered series of time levels $0 = t_0 < t_1 < \cdots < t_N = T$. Let $\Omega_n = \Omega_{t_n}$ and $\Gamma_n = \Gamma_{t_n}$. We define the space-time slab Q_n as the domain enclosed by the surfaces Ω_n, Ω_{n+1}, and P_n, where P_n is the surface described by the boundary Γ_t as t traverses I_n. As it is the case with Γ_t, surface P_n is decomposed into $(P_n)_g$ and $(P_n)_h$ with respect to the type of boundary condition (Dirichlet or Neumann) being imposed. For each space-time slab we define the corresponding finite element function spaces $(\mathcal{S}_{\mathbf{u}}^h)_n$, $(\mathcal{V}_{\mathbf{u}}^h)_n$, $(\mathcal{S}_p^h)_n$, and $(\mathcal{V}_p^h)_n$. Over the element domain, this space is formed by using first-order polynomials in space and time. Globally, the interpolation functions are continuous in space but discontinuous in time.

The stabilized space-time formulation for deforming domains is then written as follows: given $(\mathbf{u}^h)_{n-}$, find $\mathbf{u}^h \in (\mathcal{S}_{\mathbf{u}}^h)_n$ and $p^h \in (\mathcal{S}_p^h)_n$ such that $\forall \mathbf{w}^h \in (\mathcal{V}_{\mathbf{u}}^h)_n$, $q^h \in (\mathcal{V}_p^h)_n$

$$
\int_{Q_n} \mathbf{w}^h \cdot \rho \left(\frac{\partial \mathbf{u}^h}{\partial t} + \mathbf{u}^h \cdot \nabla \mathbf{u}^h - \mathbf{f} \right) d\Omega + \int_{Q_n} \varepsilon(\mathbf{w}^h) : \sigma(p^h, \mathbf{u}^h) dQ + \int_{Q_n} q^h \nabla \cdot \mathbf{u}^h dQ
$$

$$
+ \sum_{e=1}^{n_{el}} \int_{Q_n^e} \frac{1}{\rho} \tau \left[\rho \left(\frac{\partial \mathbf{w}^h}{\partial t} + \mathbf{u}^h \cdot \nabla \mathbf{w}^h \right) - \nabla \cdot \sigma(q^h, \mathbf{w}^h) \right] \cdot
$$

$$
\left[\rho \left(\frac{\partial \mathbf{u}^h}{\partial t} + \mathbf{u}^h \cdot \nabla \mathbf{u}^h - \mathbf{f} \right) - \nabla \cdot \sigma(p^h, \mathbf{u}^h) \right] dQ
$$

$$
+ \sum_{e=1}^{n_{el}} \int_{Q_n^e} \delta \nabla \cdot \mathbf{w}^h \rho \nabla \cdot \mathbf{u}^h dQ + \int_{\Omega_n} (\mathbf{w}^h)_n^+ \cdot \rho \left((\mathbf{u}^h)_n^+ - (\mathbf{u}^h)_n^- \right) d\Omega = \int_{(P_n)_h} \mathbf{w}^h \cdot \mathbf{h}^h dP \quad (2.9)
$$

This process is applied sequentially to all the space-time slabs $Q_1, Q_2, \ldots, Q_{N-1}$. In the variational formulation given by Eq. (2.9), the following notation is being used:

$$
(\mathbf{u}^h)_n^\pm = \lim_{\varepsilon \to 0} \mathbf{u}(t_n \pm \varepsilon), \quad (2.10)
$$

$$
\int_{Q_n} (\ldots) dQ = \int_{I_n} \int_{\Omega_n} (\ldots) d\Omega \, dt, \quad (2.11)
$$

$$\int_{P_n} (\ldots) dP = \int_{I_n} \int_{\Gamma_n} (\ldots) d\Gamma dt. \tag{2.12}$$

The computations start with

$$(\mathbf{u}^h)_0^- = \mathbf{u}_0, \tag{2.13}$$

where $\mathbf{u}_0$ is divergence free.

Remarks

5. The fourth term in Eq. (2.9) is a least-squares term based on the momentum equation, and plays the roles of both the PSPG and the SUPG operators.

6. The sixth term enforces weak continuity of the velocity field across the space-time slabs.

Chapter 3

Formation and Suppression of vortex shedding

3.1 Preview and relevant studies

In this chapter results are presented for computations of flows past a circular cylinder with another smaller cylinder placed in its wake. These computations are based on the stabilized space-time finite element formulation. In addition to the results from other relevant studies conducted by other researchers, we report the results for the same problem obtained with the stabilized space-time formulation. Computations are carried out for the various relative locations of the two cylinders to study the effect of control cylinder on the flow structure and on the nature of vortex shedding in the wake of first cylinder.

Vortex shedding[1] behind circular cylinders can be altered and suppressed altogether (or 'controlled') over a limited range of Reynolds numbers, by a proper placement of a second, much smaller, cylinder[2] in the near wake of the main cylinder.

---

[1]No specific physical process is implied by the use of the word 'shedding' which, for convenience, will be used subsequently without the quotes.

[2]we'll call it control cylinder for convenience now onwards

This has been shown by P.J. Strykowski and K.R. Sreenivasan [7] and E. Berger [1]. The authors have taken temporal growth rate measurements of the velocity fluctuations and it reveals that the presence of the smaller cylinder reduces the growth rate of the disturbances leading to vortex shedding and that its suppression, accompanied by the disappearance of sharp spectral peaks, coincide with negative temporal growth rates. It is argued that the presence of the secondary cylinder has the effect of altering the local stability of the flow by smearing and diffusing concentrated vorticity in the shear layers behind the body. A related effect is that the secondary cylinder diverts a small amount of fluid into the wake of the main cylinder. A unified explanation of the formation and suppression of the vortex street is attempted and it is suggested that the vortex shedding is associated with temporally unstable eigenmodes which are heavily weighted by the near field. It is also shown that the absolute instability is relevant upto a point, in explaining vortex shedding, whose suppression can similarly be associated with altering the instability in the near wake region from absolute to convective.

Strykowski and Sreenivasan have reported results from experiments primarily on flow behind circular cylinders, and have emphasized a method of suppression of low Reynolds number vortex shedding in their paper [7]. They have substantiated their experimental finding by numerical simulation. We decided to carry out present study because of several reasons. There were many drawbacks associated with the numerical scheme and the kind of grid chosen by the authors. The authors in their numerical scheme have simulated the 'control cylinder' by forcing the stream-wise and normal velocity components to vanish at six grid points at $X/D = 1.2$ and $Y/D = 1.2$ occupying an area of side equal to $1/7D$, where D is diameter of larger cylinder and coordinates x & y have been taken with respect to origin at the center of larger cylinder. We found that the second cylinder can be represented in a much better way by using a block structured grid. Besides this

the authors have computed the natural wake development to the vortex shedding state after which the 'control cylinder' was suddenly introduced. But this is not natural because in practical situations, a cylinder can not be introduced all of a sudden. Furthermore, as soon as the cylinder is introduced suddenly, the divergence free condition for incompressible flows is violated and it is known that the violation of this condition can result in spurious, numerical modes.

These reasons cast doubt over the appropriateness of the numerical scheme and the kind of grid used by the authors. These reasons along with need of independent investigation of the phenomena (vortex suppression) at different location of the control cylinder motivated us to carry out the present study. We have tried to avoid all the shortcomings of the method used by the authors by using better numerical scheme, finer grids which enable us to study the flow part control cylinder closely. This could not be done using numerical scheme used by the Strykowski and Sreenivasan. To eliminate the effect of outer boundaries we carry out the computations in much bigger physical domain $(-8.0 < X/D > 22.5)$ and $(-8.0 < Y/D > 8.0)$ compared to the domain $(-3.4 < X/D < 9.7)$ and $(-6.0 < Y/D < 6.0)$ used by the earlier authors.

Strykowski and Sreenivasan have reported in their study that there is a finite spatial domain[3] within which the placement of the control cylinder can suppress the vortex street. This spatial domain shrinks with increasing diameter ratio (D/d) (where D = diameter of larger cylinder, d = diameter of smaller cylinder). When the control cylinder is placed anywhere within this region the vortex street is suppressed completely. Furthermore the contours are symmetric about the line $y = 0$, indicating that a single control cylinder placed on either side of the wake can be effective.

The authors in their paper [7] have shown that the proper placement of

---

[3]We'll call it vortex suppression region now onwards for convenience

a control cylinder suppresses vortex street formation at low Reynolds number up to about 80. Now keeping the control cylinder in position, if the Reynolds number is further increased, the vortex street reappears at a higher Reynolds number. The effect of the control cylinder is not merely to elevate the critical Reynolds number to a higher value, because the control cylinder produces a non trivial influence even at Reynolds number above which complete suppression is impossible. One consequence of the suppression of the vortex street is the concentration of the bulk of the momentum defect to a narrower region than in the natural case, and the corresponding enhancement of the maximum momentum defect.

3.2   Computational Study

3.2.1   Computational domain and grid

In the present study computational value of the cylinder diameter and the free stream velocity are 2.0 and 1.0 respectively and the time step size is 0.1. The dimensions of the computational domain, normalized by the cylinder diameter are 30.5 and 16.0 in the flow and cross flow directions, respectively. The normalized zero displacement location for the first cylinder is (8,8) relative to the lower left corner of the flow domain. We take the origin to be at the center of first cylinder. We have computed the flow for two grids and four locations of the control cylinder.

In the coarse grid a total of 5048 elements and 5219 nodal points are used, and for a finer grid these numbers are 9696 and 9441. Both of these grids are used to solve for the flow field and thus to get the values of flow variables u, v & p at each nodal point. In figure 4.2 grid used for the present control cylinder case is shown. In these figures close view of the grid around the main cylinder and control cylinder is also shown.

Based on location of the control cylinder we can divide the control cylinder problem into following categories.

1. In the first problem, control cylinder is located at far downstream location at $X/D = 5.0$ and $Y/D = 5.0$. Coarse grid is used to get the flow field at Reynolds number of 100. This computation is carried out to establish confidence in our implementation of the two cylinder case. Since the two cylinders are fairly far apart, we expect very little interference of the second cylinder on the first (upstream) one.

2. Second location of the control cylinder for which we compute the flow is $X/D = 1.0$ and $Y/D = 1.0$. We carry out this computation for $Re = 80$ using coarse grid.

3. Third location of the control cylinder is $X/D = 2.0$ and $Y/D = 1.0$. We carried out these computations on two grids. First, computations are carried out at Reynolds numbers, 100 and 80 on coarse grid and later the same computations are carried out using finer grid.

4. Fourth and final location of the control cylinder is $X/D = 2.0, Y/D = 0.8$. In this case solution is obtained at Reynolds numbers, 100 and 80 and computations are carried out using only the fine grid.

Reynolds number is based on the free stream velocity (U_∞) and diameter (D) of larger upstream (main) cylinder. Symmetric conditions are imposed at the upper and lower computational boundaries and the traction-free condition is imposed at the outflow boundary.

3.2.2   Findings of the computations

- In the first case the control cylinder is located at a far downstream location

with respect to the first cylinder; $X/D = 5.0, Y/D = 5.0$ the Reynolds number is 100. As expected, no effect of the presence of control cylinder is observed in the immediate wake of the first cylinder. Pressure, vorticity and streamlines contours are shown in figure 3.9 for this case. Vortex shedding is observed from both upper and lower surfaces of the main upstream cylinder. Strouhal number for this case for the main cylinder is 0.167 which is same as observed by Mittal [6] for the single cylinder case at the same Reynolds number. Strouhal number for control cylinder is 0.0236.

- The control cylinder is located at $X/D = 1.0$ and $Y/D = 1.0$ in our second computation for the control cylinder case. This location of the control cylinder is inside the boundary of the vortex suppression region. We first compute the flow to get steady state solution at $Re = 100$. Then we do the computations at $Re = 80$ to get unsteady solution. We find that vortex shedding is not observed and amplitudes of lift and drag coefficients do not change significantly till $t = 100$, but change in the flow pattern due to the presence of control cylinder is perceptible. Figure 3.10 & 3.11 show pressure, vorticity and streamline contours at starting $(t = 0.0)$ and end $(t = 100.0)$ of the computations. We observe that vortex shedding never starts for this case even towards the end of the computations. Pressure, vorticity and streamlines contours given in these figures show that strength of the vorticity formed in this case is lower compared to that in the case in which we put the cylinder at far downstream location.

- **Computations using coarse grid**

As mentioned earlier upper limit of Reynolds number upto which 'control phenomena' can be observed is 80. So as a part of the computations for third case of the control cylinder problem, the unsteady flow field at $Re = 100$ past

two cylinders is computed using coarse grid keeping the control cylinder at $X/D = 2.0$ and $Y/D = 1.0$. This location of the control cylinder is near the boundary of the vortex suppression region. Since only sketchy boundary of the region of vortex suppression has been given by Strykowski and Sreenivasan, present location of the control cylinder could not be ascertained to be either inside or outside of the region. We choose this location to study effect of presence of control cylinder located near the boundary on the flow field behind main cylinder. The periodic solution for flow past a fixed cylinder is obtained by introducing a short term perturbation to the symmetric solution. Thus computations were carried out till $t = 500$ at which, main cylinder started shedding the vortices. Notice that the Reynolds number, here, is higher than the critical Reynolds number for which the control cylinder suppresses the shedding. In figure 3.12 pressure, vorticity and stream lines contours are plotted at $t = 500$ i.e. at the end of computation for $Re = 100$. We observe that due to presence of the control cylinder, flow tends to get pushed into the wake of the main cylinder, which sheds vortices. No vortex shedding is observed behind control cylinder because Reynolds number for control cylinder is (based on the free-stream velocity) 14.3, which is much below the critical value (40) of Reynolds number at which a cylinder starts shedding vortices as observed in earlier related studies. Strouhal number is found to be 0.153 for the main cylinder and 0.0216 for the control cylinder. Notice that this value of the Strouhal number for the main cylinder is smaller than one observed for a single cylinder.

Reynolds number of the flow is now reduced to 80 (by changing the kinematic viscosity (ν)) to find, if from this unsteady solution we can get the quasi-steady solution. Computation are then carried out till $t = 500$ and variations of C_L, C_D, (Coefficients of lift and drag) change in pressure field, vorticity field

and stream lines contours with respect to time are observed. As shown in the plot 3.4 values of these coefficients fluctuate with respect to time for both the cylinder, while amplitude of these fluctuations decay with time. In the end both the cylinders acquire constant values of these coefficients and the flow reaches steady state. Final, steady state values of lift and drag coefficients for upstream cylinder are close to 0.01 and 1.30 and that for control cylinder are -0.32 and 2.5.

- **Computations using fine grid**

The computations, described above, are repeated on a finer mesh. As is mentioned above, in this case, the control cylinder is placed at a location that is very close to the boundary of the region, discovered by Strykowski & Sreenivasan, that results in the vortex suppression from the main cylinder. Our computations on a coarse mesh indicate that the present location leads to vortex shedding suppression. To study the effect of numerical diffusion, we decided to compute this case on a finer mesh. It is well known that a finer mesh results in lesser numerical diffusion & therefore one can expect results that are closer to experimental observations.

Coefficients of lift and drag are plotted in figure 3.5 & figure 3.6 for the present case for Reynolds number of 100 and 80 respectively. Pressure, vorticity and streamline contours in the flow at Reynolds number of 100 & 80 and at the end of the computations for each case are shown in figure 3.19 & figure 3.20. We observe that the solution that we get in this case is quite different from the one that we get using coarser grid, especially for Reynolds number of 80. We find that, in the present case, presence of the control cylinder does not completely suppress the vortex shedding due to main cylinder. Though presence of the control cylinder has some effect on the flow as strength of the vorticities is lesser at the end of the computations for Reynolds number 80

as compared to that for Reynolds number 100. This is evident also from the time histories of the coefficients of lift and drag at Reynolds number of 80. These plots show that though fluctuations in the values of these coefficients is observed in this case too, and amplitude of this fluctuations decay with time till $t = 100$, but after this time amplitude of the fluctuations attains constant value. If we compare the mean values of these coefficients, we find that the mean values for Reynolds number of 100 are approximately same as that we get using coarse grid, but for Reynolds number of 80 these values are higher. Strouhal number for the first cylinder is 0.1695 at Reynolds number of 100 and 0.1575 at Reynolds number of 80.

- In the fourth problem, we use fine grid to solve the flow at Reynolds number of 100 & 80. In this problem the location of the control cylinder with respect to the main cylinder is $X/D = 2.0, Y/D = 0.8$. This location of the cylinder is inside the vortex suppression region. Computations are first carried out at Reynolds number of 100 till vortex shedding is established and flow reaches a periodic state. In figure 3.21 pressure, vorticity and streamlines contours are plotted at $t = 700$, at the end of computation for $Re = 100$. Figure 3.7 shows coefficients of lift and drag of both the cylinders for this location of the control cylinder. We observe that lift and drag coefficients for both the cylinders fluctuate with non-dimensional time (t) and mean values of these coefficients for the main cylinder are close to -0.01 and 1.385 while that for control cylinder these values are -0.5 and 0.27 respectively. Strouhal number for the flow is 0.1613.

Taking this unsteady solution at Reynolds number of 100 as initial condition (t=0.0), flow is computed for Reynolds number of 80, till t=1200 keeping the position of both the cylinders same. Pressure, vorticity and streamlines contours at various time instants are plotted in figure 3.8. Time histories of

coefficients of lift and drag are plotted in figure 3.8. Time histories of lift and drag coefficients of both the cylinders show that values of these coefficients fluctuate with non-dimensional time (t) for Reynolds number 80 too, but amplitude of these fluctuations decays with respect to non-dimensional time (t). Computations were carried out till amplitude of this fluctuation reduced to negligible value compared to the amplitude at the start of the computations. We observe that flow reaches steady state as is evident from pressure, vorticity and streamlines contours plots also. Steady state values of lift and drag coefficients for the main cylinder are -0.02 and 1.39 while for control cylinder these values are -0.3 and 1.68. Figure 3.22, 3.23, 3.24, 3.25, 3.26 & 3.27 give constant pressures, vorticity and streamlines contours in the flow at various time instants. These plots shows that strength of the vorticities behind main cylinder reduces with non-dimensional time (t) and finally the vortex shedding is completely suppressed. Two eddies remain attached to the main cylinder, while flow far behind the main cylinder reaches steady state.

3.2.3 Discussion and conclusions

As we have mentioned earlier, the 'control' phenomena is most likely to be related to changes occurring in the neighbourhood of the vortex shedding cylinder. It is our premise that the understanding of this 'control' will lead to an improved understanding of the vortex shedding itself. Here we try to connect the special features of this phenomena, because it is in these features that the key to the explanation must lie. Observations and premises related to this study given by other authors are also given in the following discussion on the control phenomena and the underlying physical mechanism.

∎ *Notable features of the present suppression method*

From our studies, it is clear that the control is possible only when the near field is manipulated in some way; In our first study control cylinder is not effective when placed downstream at X/D of 5.0, while for all other positions of the control cylinder in the near field of the main cylinder some effect of the presence of control cylinder is observed. We infer that the vortex shedding phenomena must be associated with the near field dynamics. Also Strykowski & Sreenivasan have shown in their experimental studies that the effect is not one of setting up an asymmetry, because two control cylinders are more effective than a single one.

Our second and fifth studies suggest that vortex shedding can be inhibited either by letting the flow to develop at Reynolds number below the critical value of 100, while control cylinder is placed inside the vortex suppression region or by reducing the Reynolds number to the subcritical value after the flow has acquired the unsteady state at higher Reynolds number. In our second study, control cylinder is kept in the vortex suppression region and Reynolds number which is 80, is below critical value of 100. We find that in this study vortex suppression is not observed even towards the end of the computations and flow remain steady. While in the fifth study, we first place the control cylinder in the vortex suppression region and let the flow acquire steady state. We then reduce the Reynolds number to 80. We observe that strength of the vorticities starts reducing and at the end of the computations, flow attains steady steady state. We thus observe that final effects of both the cases are same.

A similar important observation, made by Strykowski & Sreenivasan, is that the suppression is not a dynamic effect resulting from some type of interaction between the unsteady flow field of the vortex shedding and the control cylinder. A point in favour of this view given by them is that suppression at a given low Reynolds number below the critical value is achieved equally well either by bringing the control

cylinder into an appropriate position after the vortex shedding has started in the normal way, or by positioning the cylinder in that same position prior to setting up the flow. In the former case the existing vortex patterns disappear, while in the latter case vortex shedding is banished from appearing. It is of fundamental interest to note that the final effects of both scenarios are the same.

▮ *Physical explanation of the mechanism of vortex street suppression*

At the end of the discussions on the 'control phenomena', we now try to give the essential physics of vortex shedding itself based on the observations made by various researchers who have done the similar studies.

At low Reynolds numbers, the vorticity pumped into the wake from the boundary layers on the cylinder can be diffused away from the shear layer surfaces merely by viscous action. The classical view held by the researchers is that, as the flow Reynolds number increases, viscous diffusion alone cannot keep up with the increased vorticity production in the upstream boundary layers, and vortices break away at regular intervals, constituting 'vortex shedding'.

Vorticity distribution and circulation in the wake shear layer is important to the formation of the natural 'vortex street'. Abernathy & Kronauer have postulated in their paper [3] that it is not necessary to have a wake producing body to form a 'vortex-street'. The body is necessary to generate the shear layers, of course, but the main point is that it is the interaction of the shear layers, independent of the body, which forms the 'vortex-street'. A direct consequence is that it is not the reduction in base pressure which forms the 'vortex-street' but the formation of the 'vortex-street' through shear layer interaction which results in a decrease in the base pressure. Gerrard [4] has described the 'vortex street' formation to be a function of the 'diffusion length' and 'formation length'. Gerrard's model predicts that the circulation in the shear layer must be of a sufficient magnitude before one

shear layer draws the other across the wake center plane. Further this interaction must take place before a critical distance (formation length) is reached. In Gerrard's terminology the 'vortex street' could be inhibited if either the shear layer vorticity distribution was diffused (over a critical diffusion length) or the shear layers were prevented from interaction (over a critical formation length), the essential point being that the spreading of the shear layer means that only a part of it is drawn across to the other side.

Pressure, vortex and streamlines contours in figure 3.12, 3.17 & 3.18 suggests that a small amount of fluid is diverted into the near-wake region from the free stream, although to widely varying extents depending on the precise position of the control cylinder.

One must expect fluid diversion and the vorticity redistribution to be related. The numerically generated vorticity fields with the presence of control cylinder in the near wake and in the far downstream location show that the properly placed control body redistributes vorticity in the shear layer in which it resides, but has remarkably little direct influence in the opposite shear layer. Strykowski and Sreenivasan have stated in their paper [7] that a partial cancellation of the vorticity results in the portion of the shear layer closest to the wake center line. Correspondingly an enhancement of the vorticity must occur farther off-axis. We can in general reduce a shear by either decreasing the velocity in the high speed stream or increasing the velocity in the low speed stream. It appears that a properly placed control cylinder may satisfy both these criteria by a combination of its velocity defect and its ability to redirect the oncoming flow. We may thus conclude that the properly placed control cylinder weakens the shear layer by spreading the vorticity gradient over a larger distance; i.e. diffusing vorticity. Using the formation-length terminology of Gerrard, a properly placed control cylinder increases the diffusion length, or equivalently, thickens the shear layer. According to Strykowski and

Sreenivasan, if the circulation is reduced below some threshold level in the formation region, the mutual attraction between the opposing shear layers will be too weak to form the vortex roll up. An interesting prediction made by Gerrard was that as the shear layers were weakened, but before the 'vortex street' was eliminated the shedding frequency would be reduced because the weaker shear layers could not as rapidly 'pull' each other across the wake. Consistent with this model, we observe that the weakened shear layers result in a reduced shedding frequency even when the 'vortex street' is not eliminated.

3.3   Suggestions on further study

In our study of the control phenomena, out of various parameters associated with the problem we have studied the variation of only two of them: the location of the control cylinder and Reynolds number of the flow. Further study of the phenomena can be done by altering other parameters such as Reynolds number, diameter of the control cylinder. The control cylinder can be allowed to oscillate and rotate which could give very interesting results such as vortex induced oscillations of the control cylinder and the alteration in the vortex shedding process due to fluid body interaction.
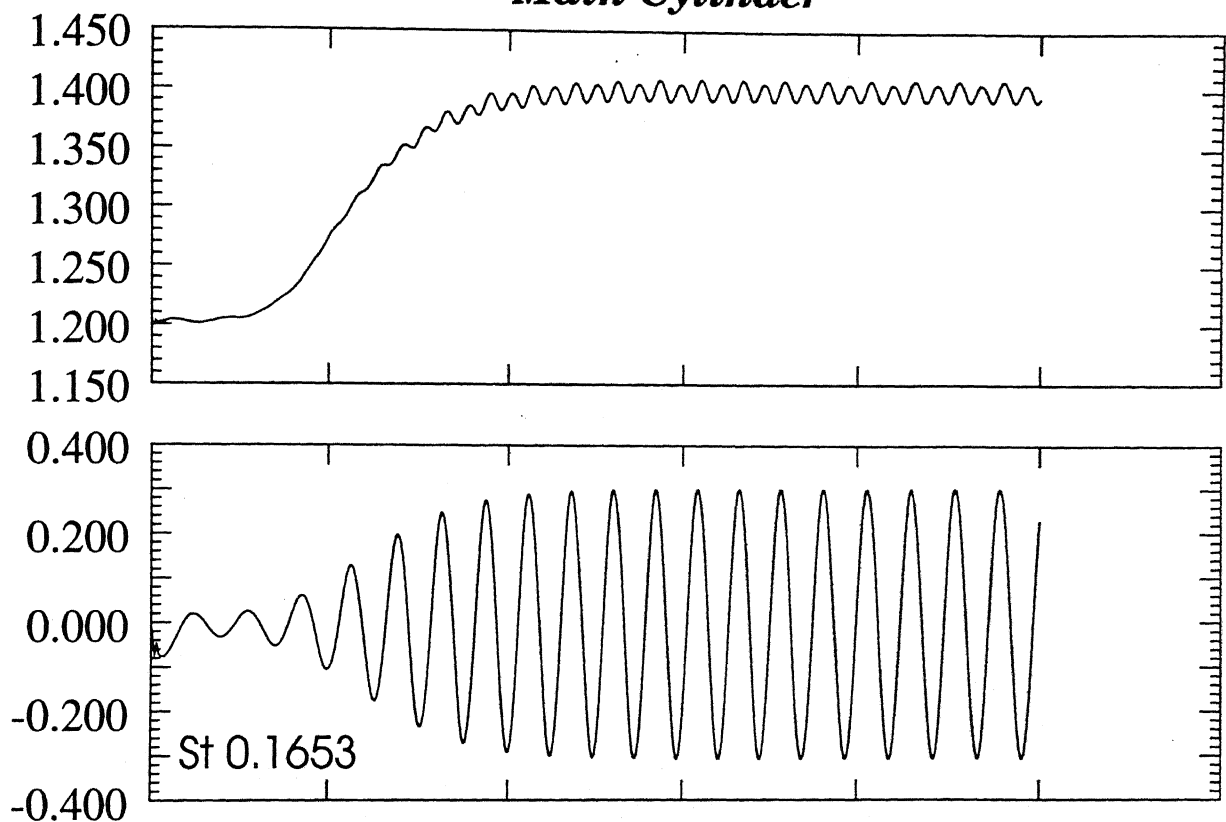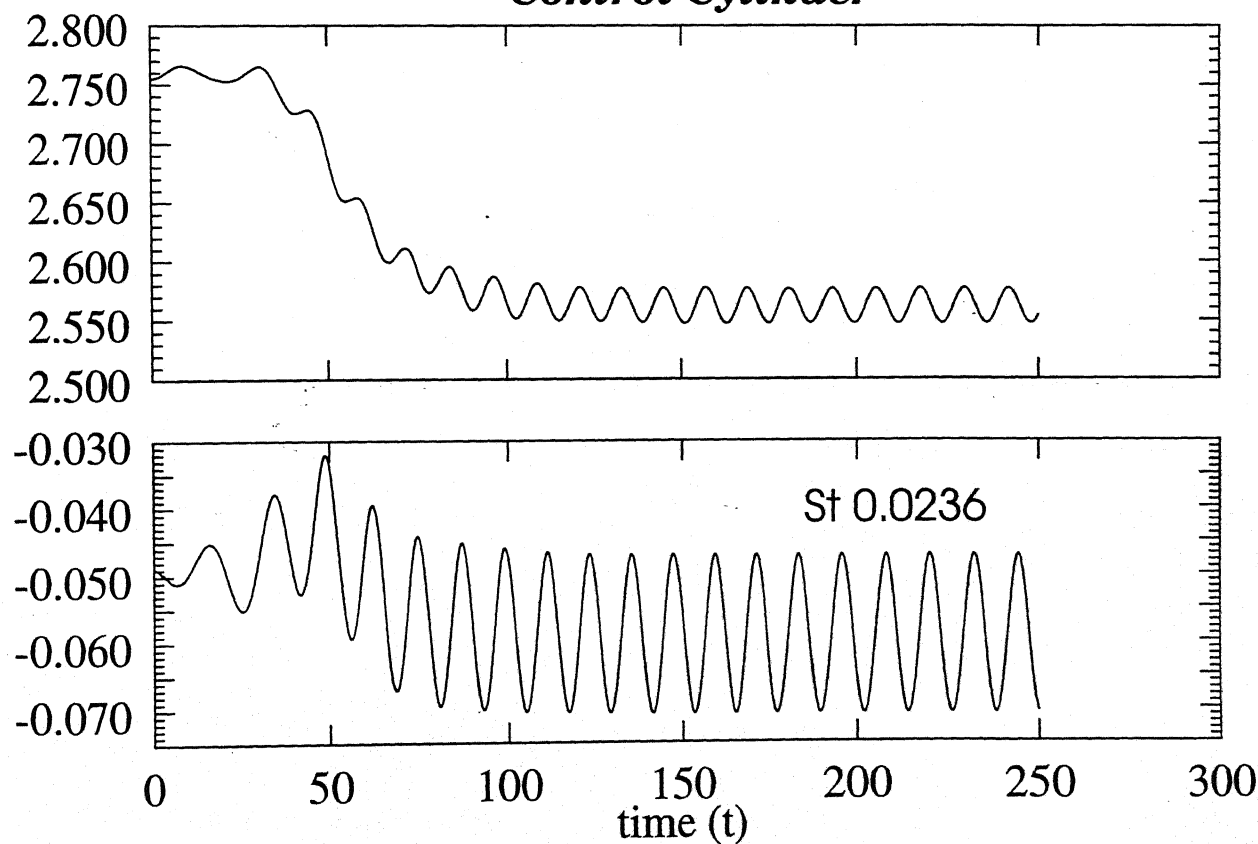
Figure 3.1: Coefficients of lift and drag at Re = 100 for control cylinder problem using Coarse Grid: Control cylinder at X/D = 5.0, Y/D = 5.0
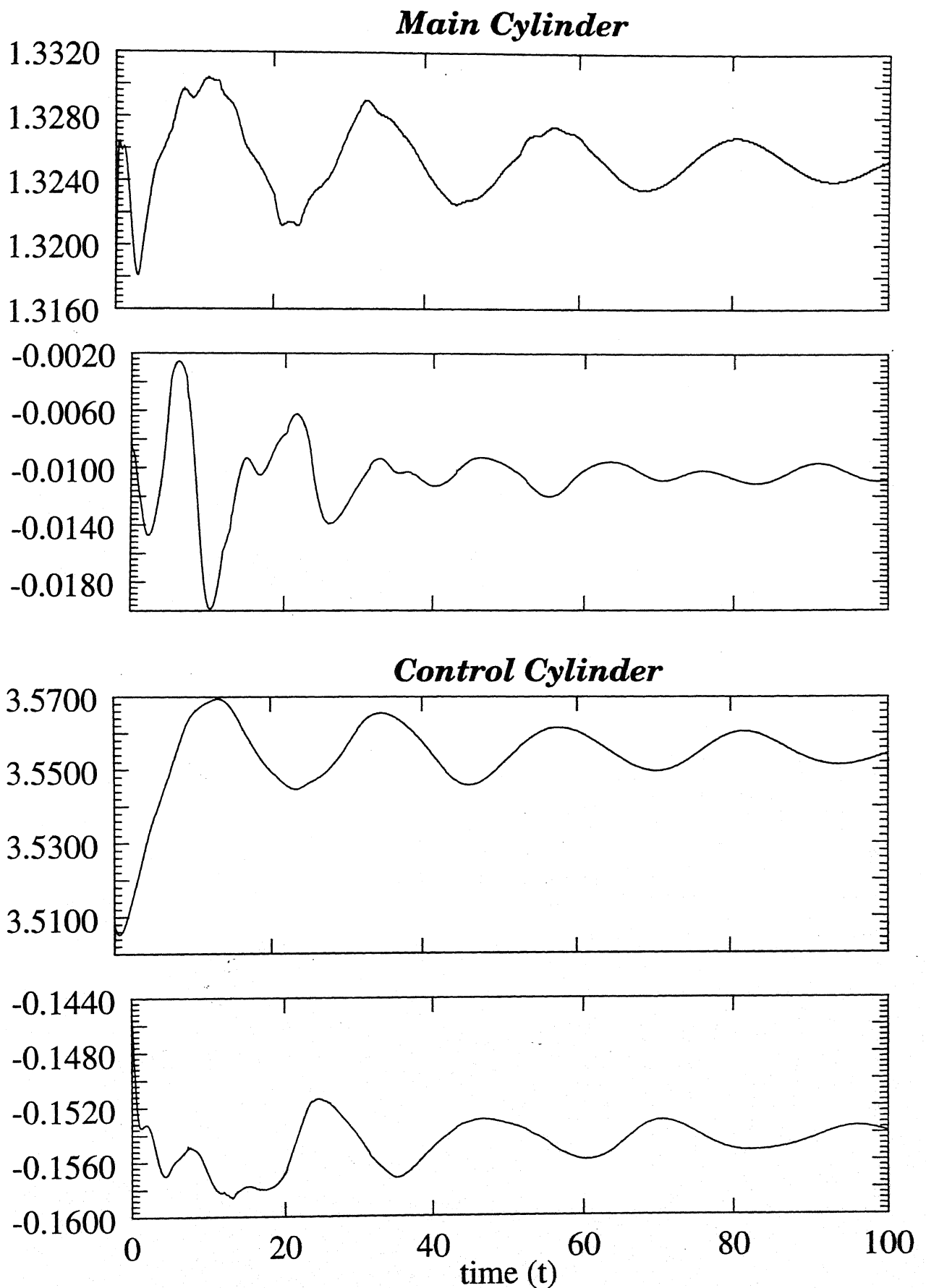
Figure 3.2: Coefficients of lift and drag at Re = 80 for control cylinder problem using Coarse Grid: Control cylinder at X/D = 1.0, Y/D = 1.0
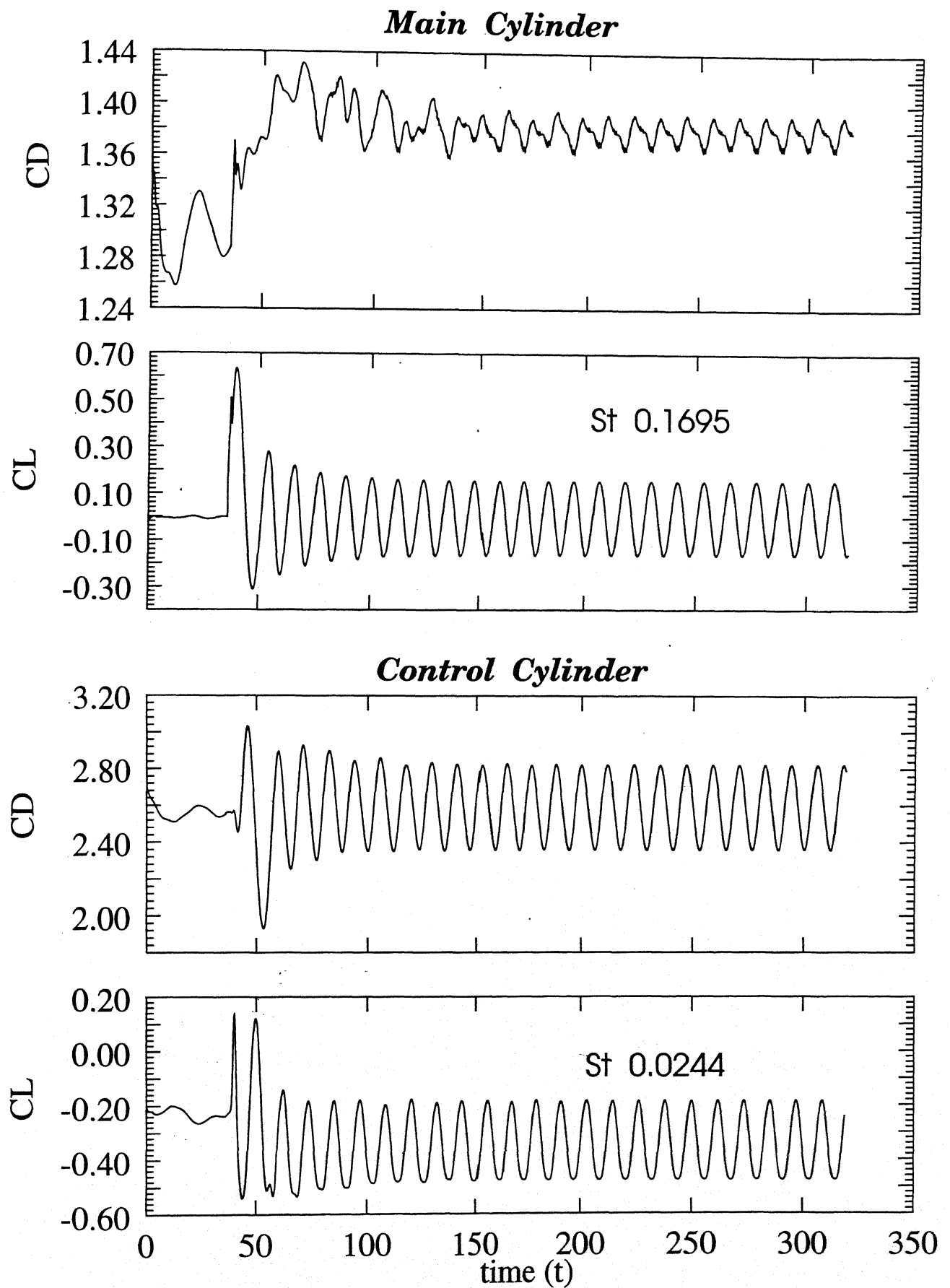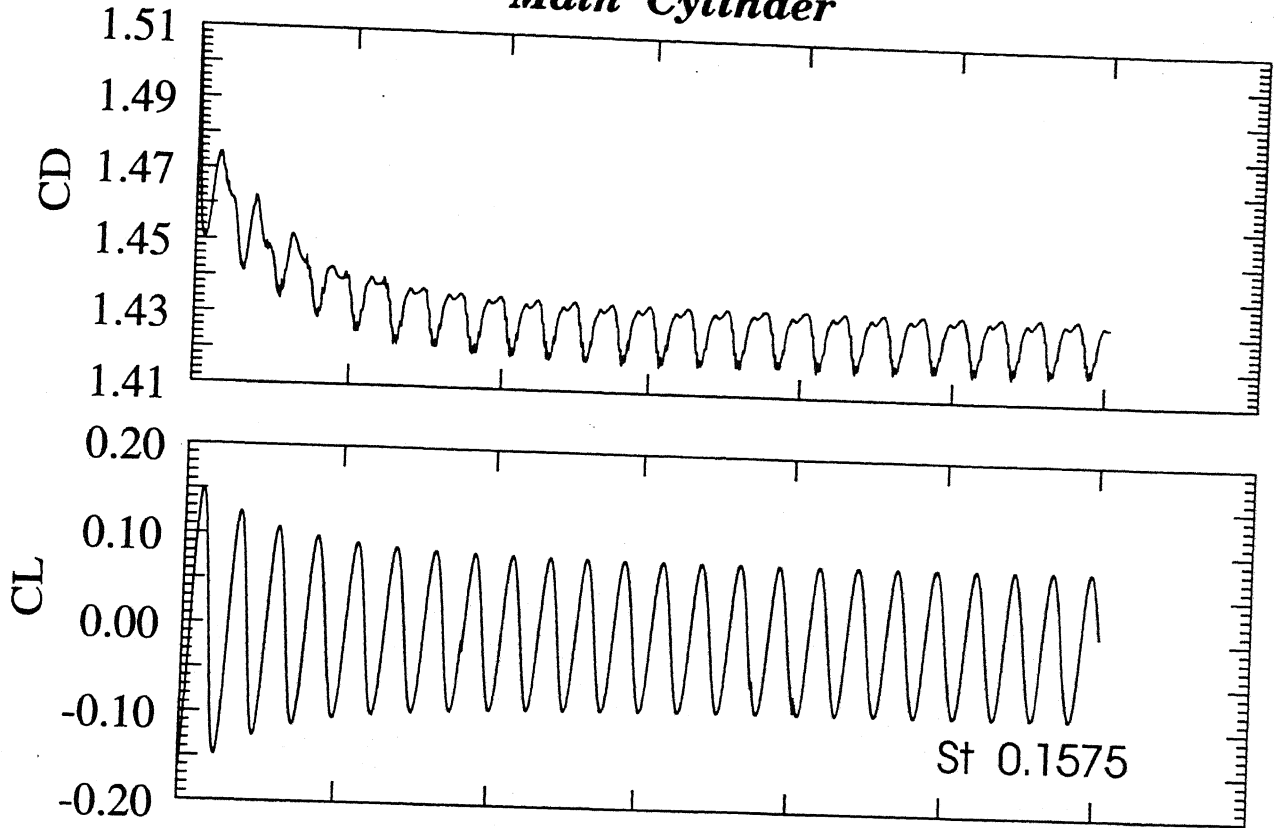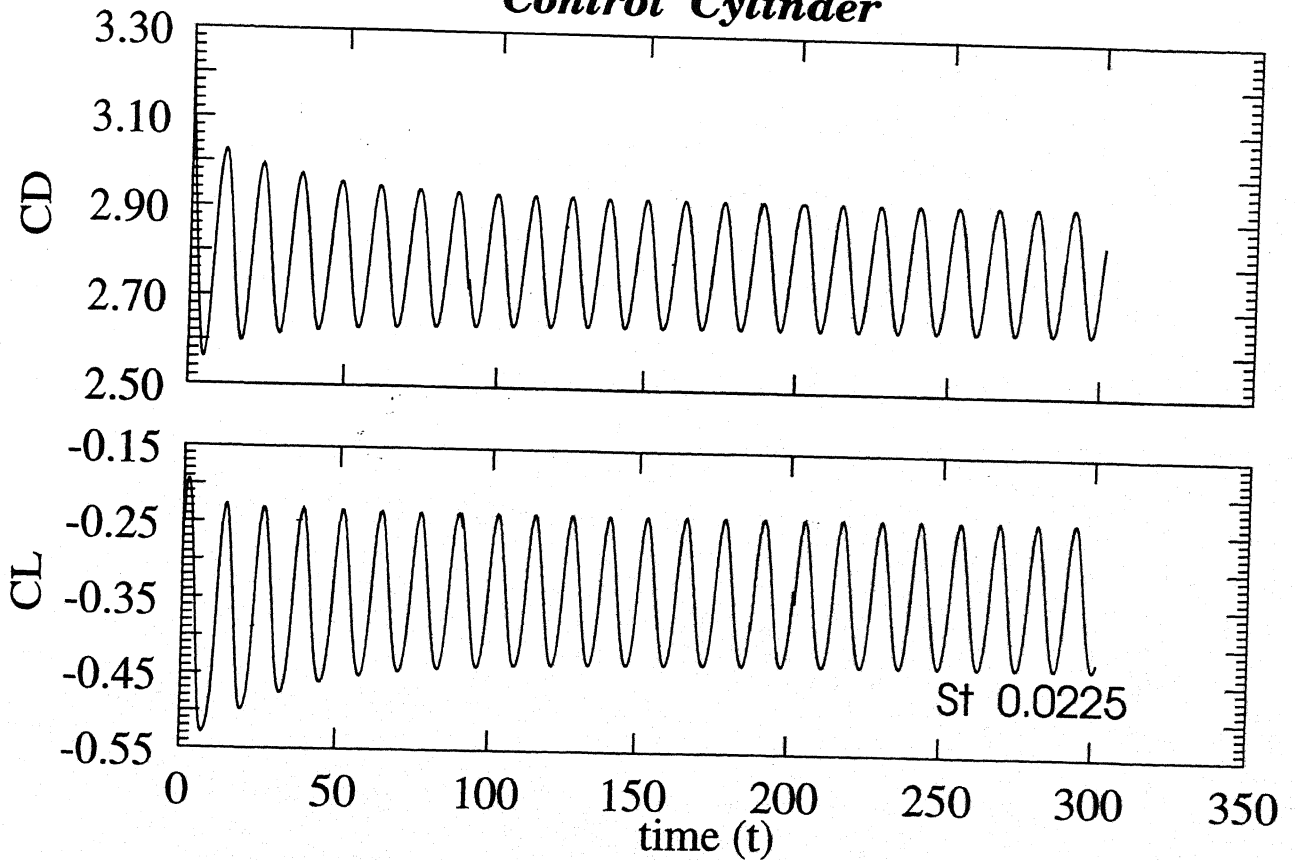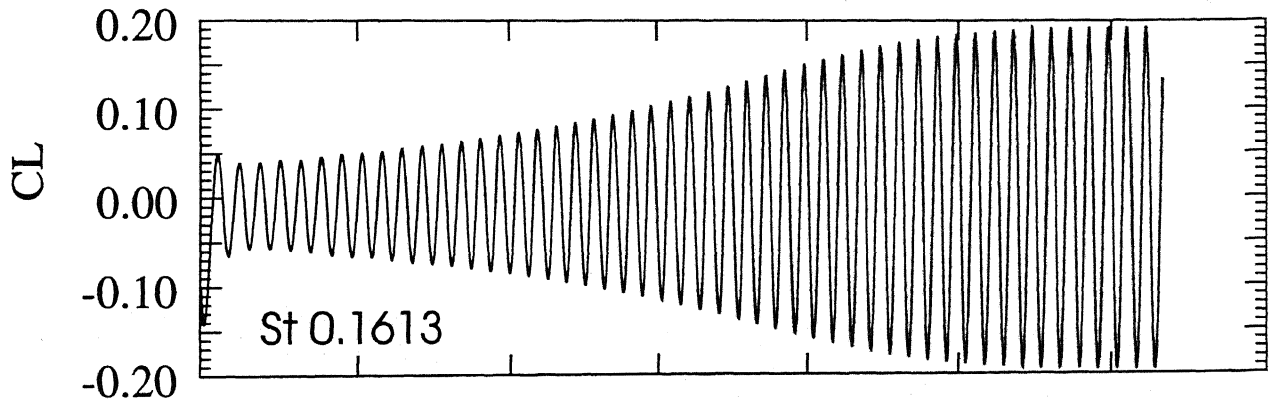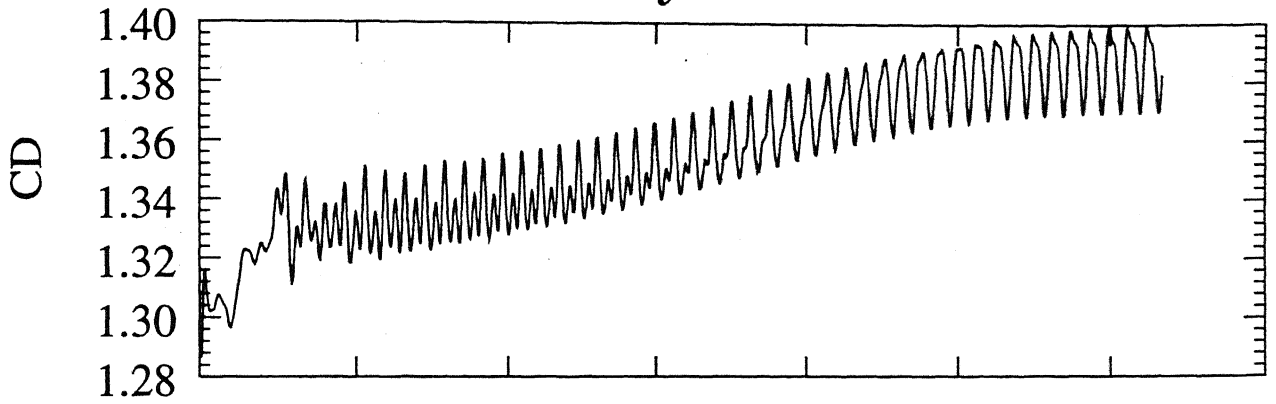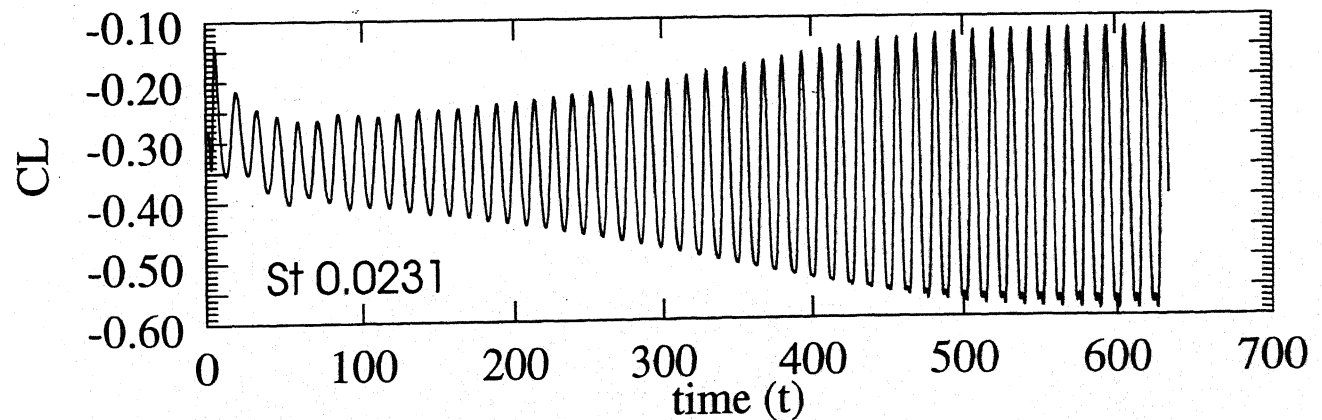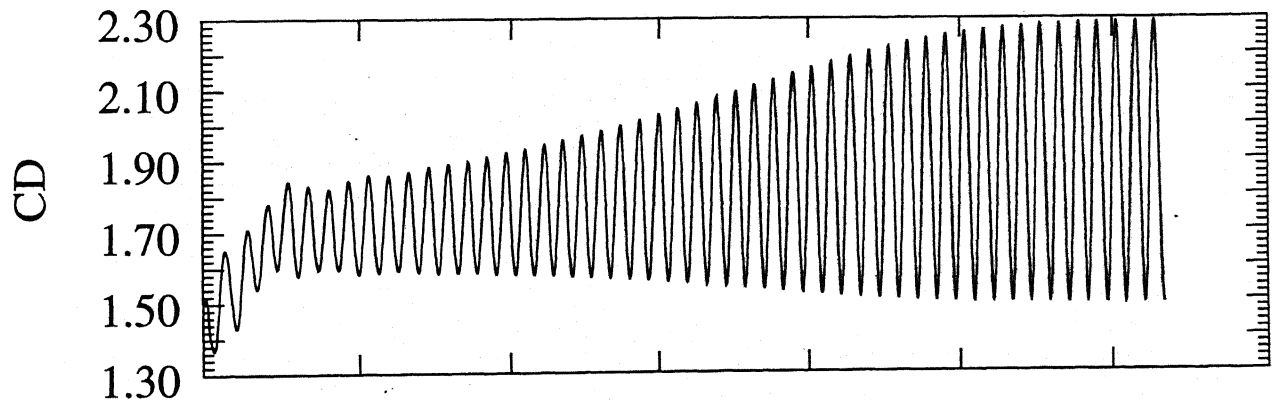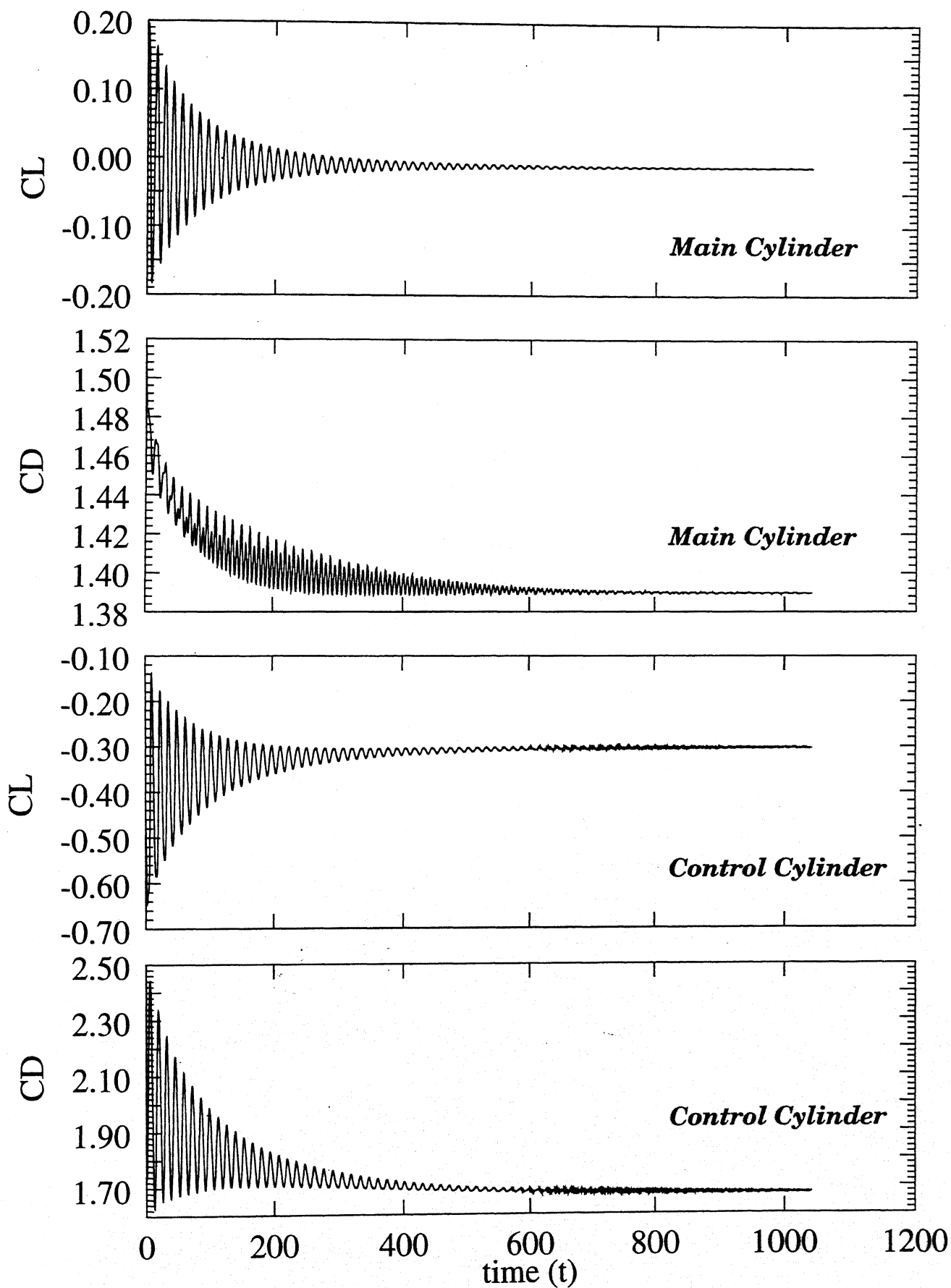
Main Cylinder

St 0.1527

Control Cylinder

St 0.0216

time (t)
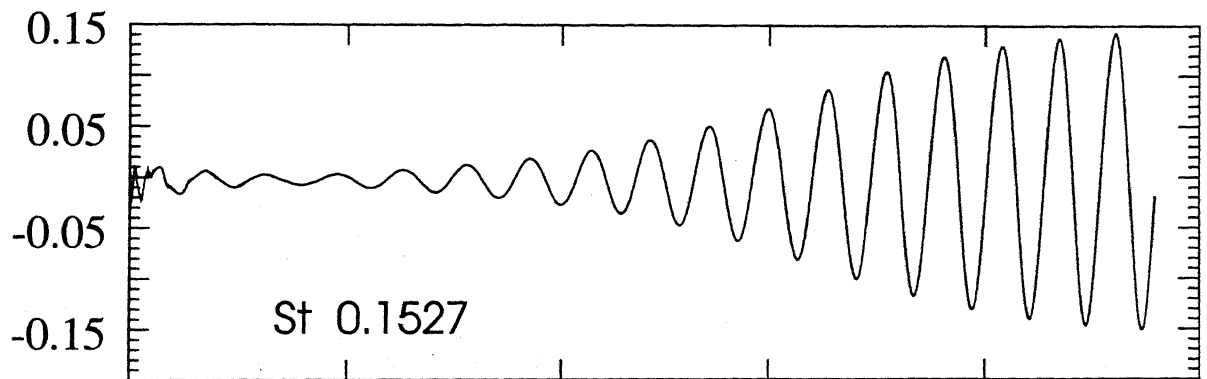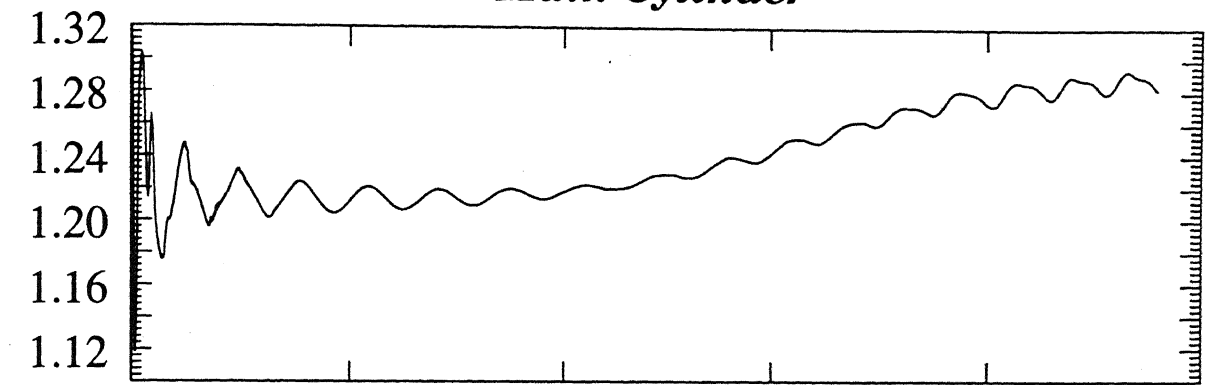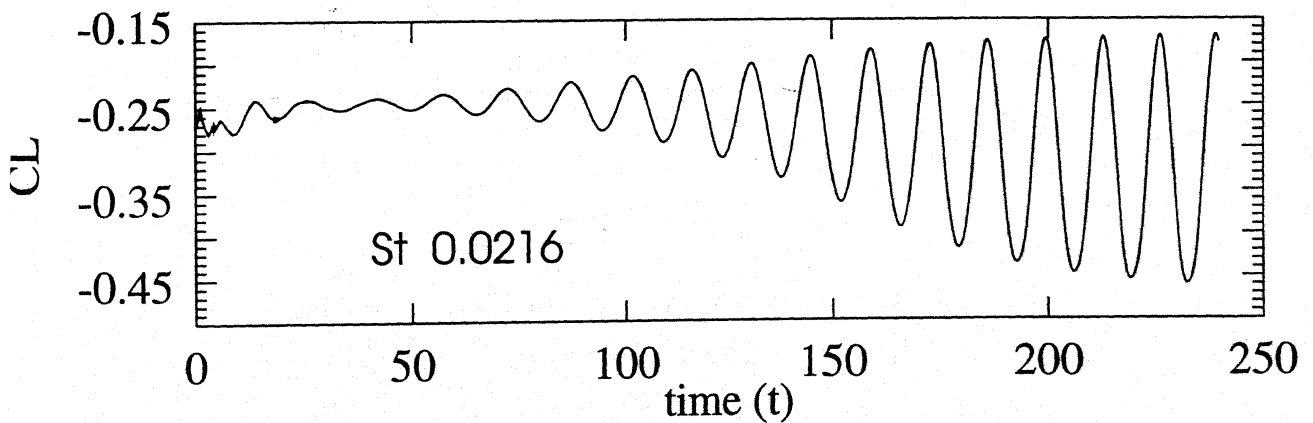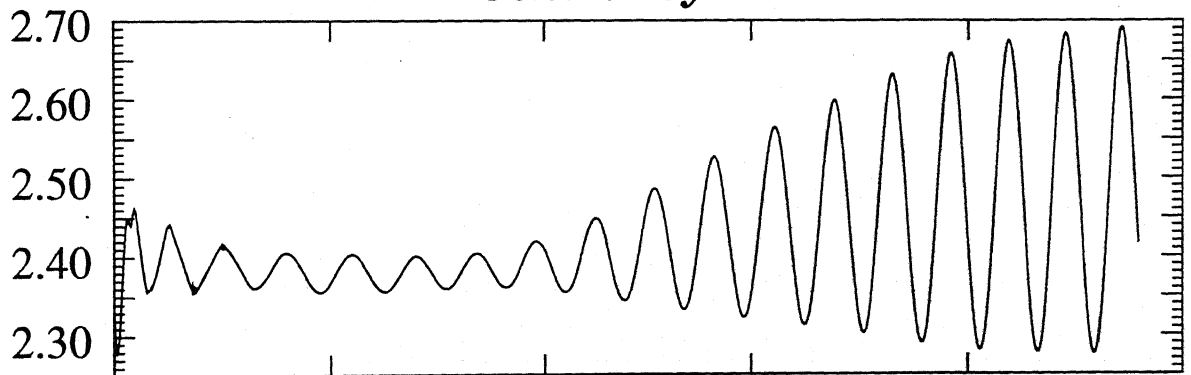
Figure 3.3: Coefficients of lift and drag at Re = 100 for control cylinder problem using Coarse Grid: Control cylinder at X/D = 2.0, Y/D = 1.0

Figure 3.4: Coefficients of lift and drag at Re = 80 for control cylinder problem using Coarse Grid: Control cylinder at X/D = 2.0, Y/D = 1.0

Figure 3.5: Coefficients of lift and drag at Re = 100 for control cylinder problem using Fine Grid: Control cylinder at X/D = 2.0, Y/D = 1.0

Figure 3.6: Coefficients of lift and drag at Re = 80 for control cylinder problem using Fine Grid: Control cylinder at X/D = 2.0, Y/D = 1.0.

Main Cylinder

St 0.1613

Control Cylinder

St 0.0231

time (t)

Figure 3.7: Coefficients of lift and drag at Re = 100 for control cylinder problem using Fine Grid: Control cylinder at X/D = 2.0, Y/D = 0.8

Figure 3.8: Coefficients of lift and drag at Re = 80 for control cylinder problem using Fine Grid: Control cylinder at X/D = 2.0, Y/D = 0.8
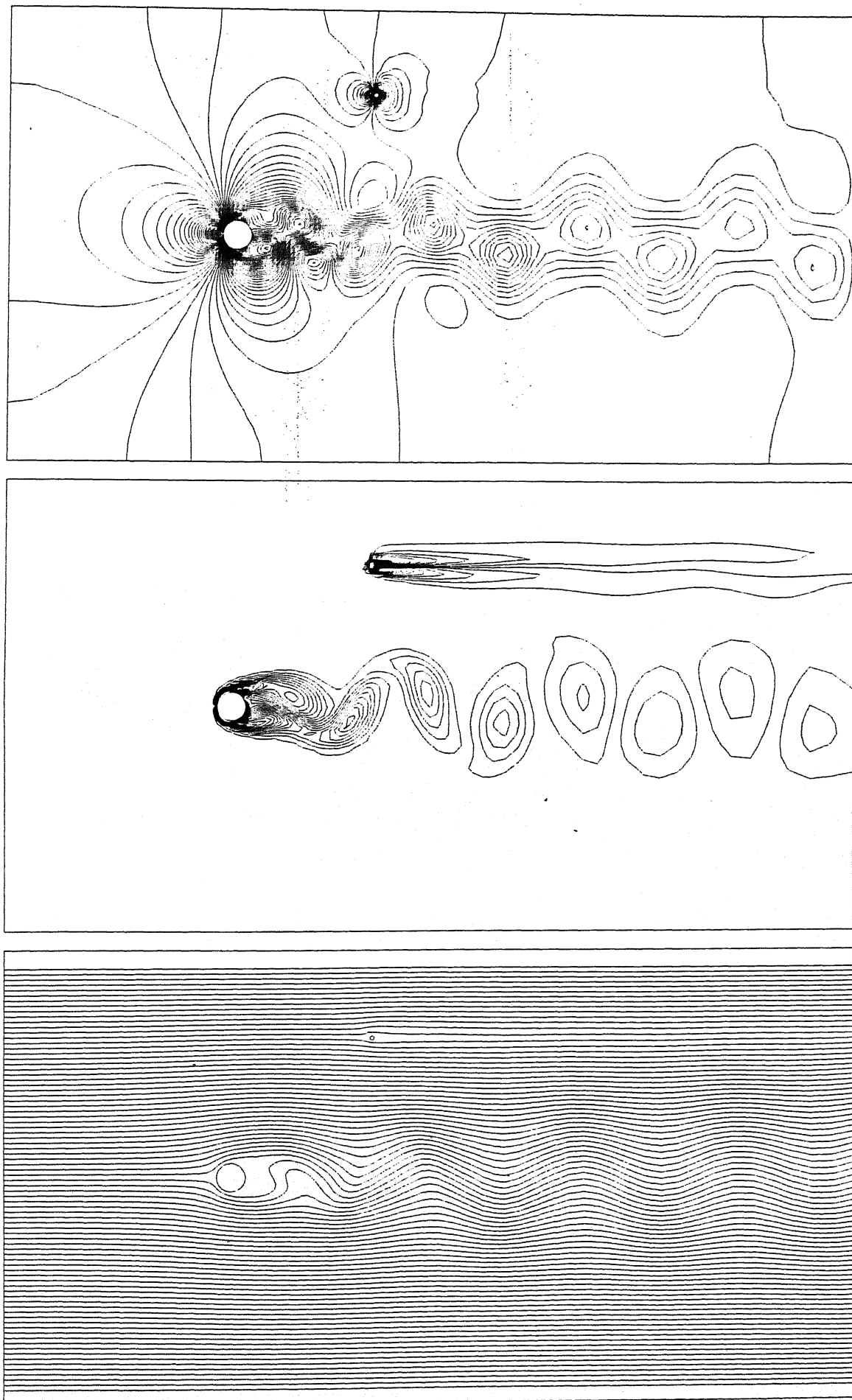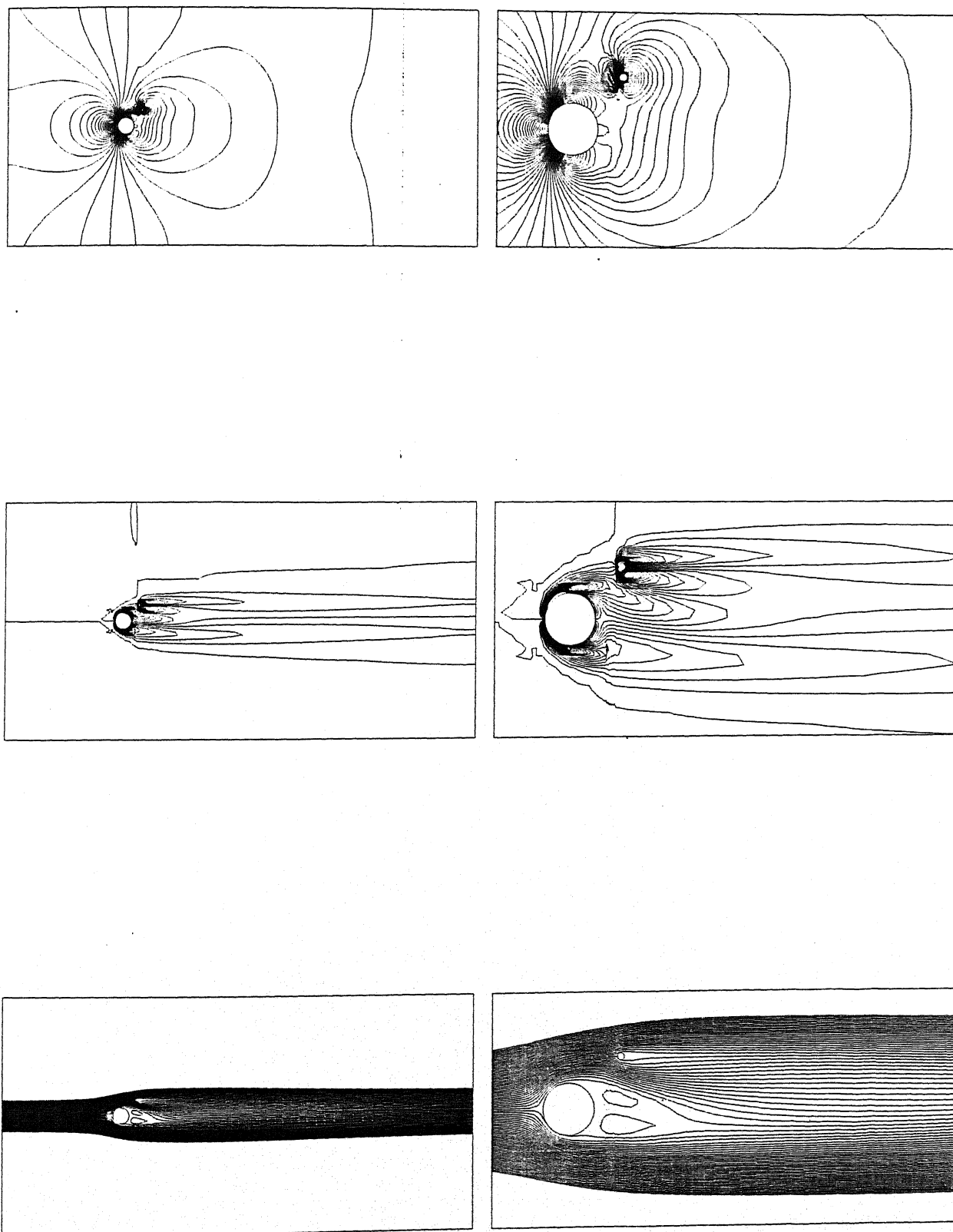
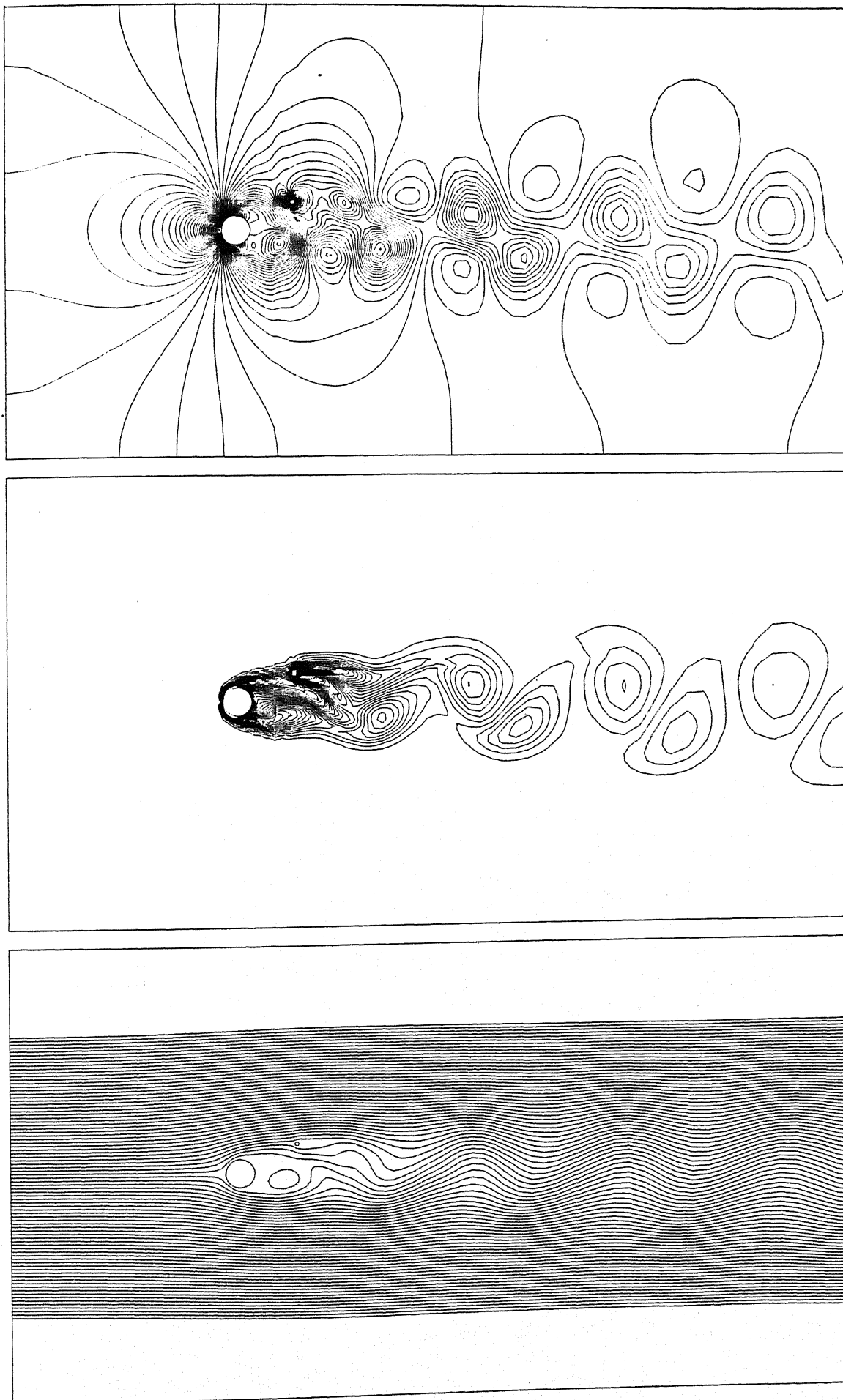Figure 3.9: Pressure, Vorticity and Streamlines plots at Re = 100 for control cylinder problem using Coarse Grid: Control cylinder at X/D = 5.0, Y/D = 5.0
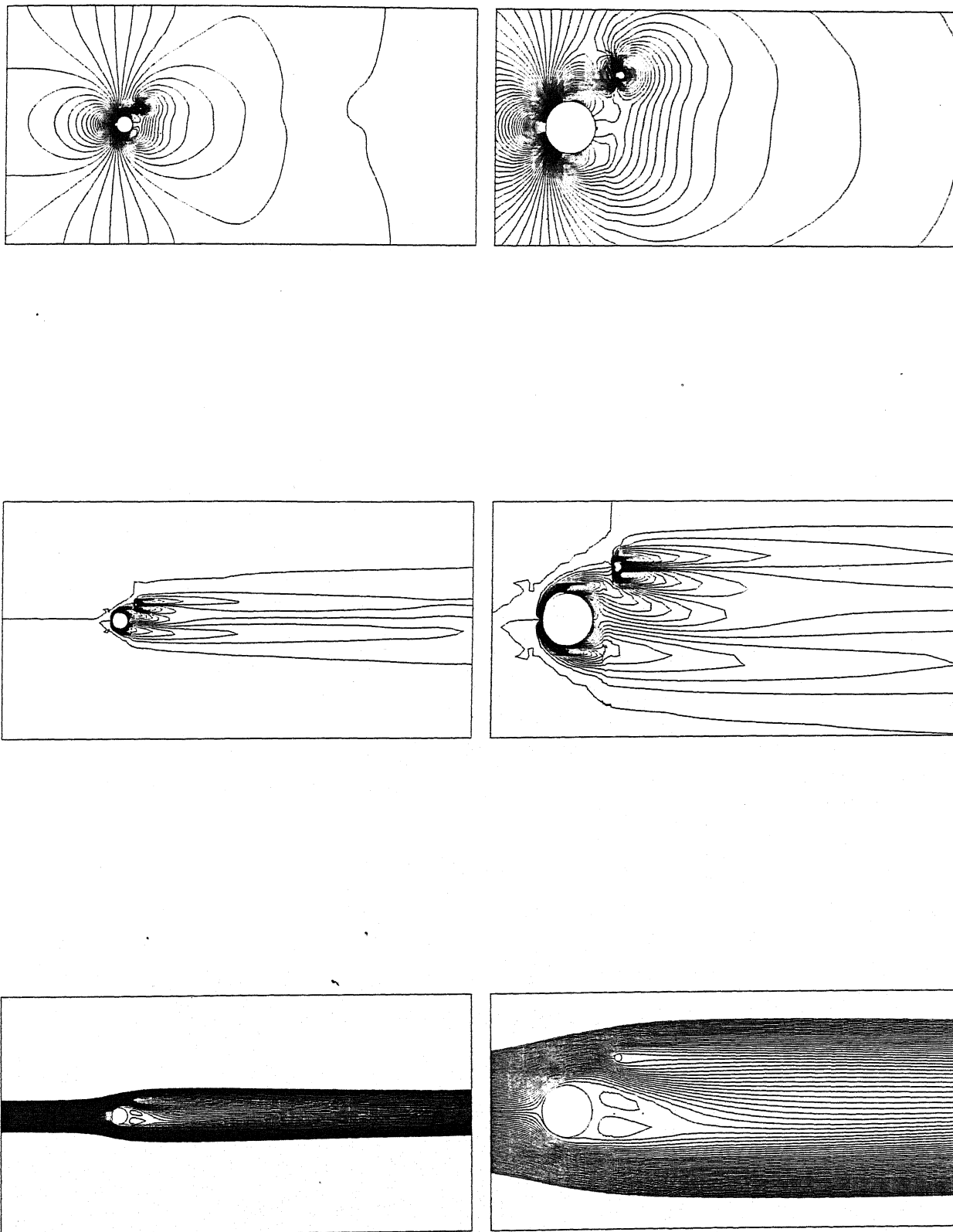
Figure 3.10: Pressure, Vorticity and Streamlines plots at Re = 80 for control cylinder problem using Coarse Grid: Control cylinder at X/D = 1.0, Y/D = 1.0, t = 0.0

Figure 3.11: Pressure, Vorticity and Streamlines plots at Re = 80 for control cylinder problem using Coarse Grid: Control cylinder at X/D = 1.0, Y/D = 1.0, t = 100.0

Figure 3.12: Pressure, Vorticity and Streamlines plots at Re = 100 for control cylinder problem using Coarse Grid: Control cylinder at X/D = 2.0, Y/D = 1.0
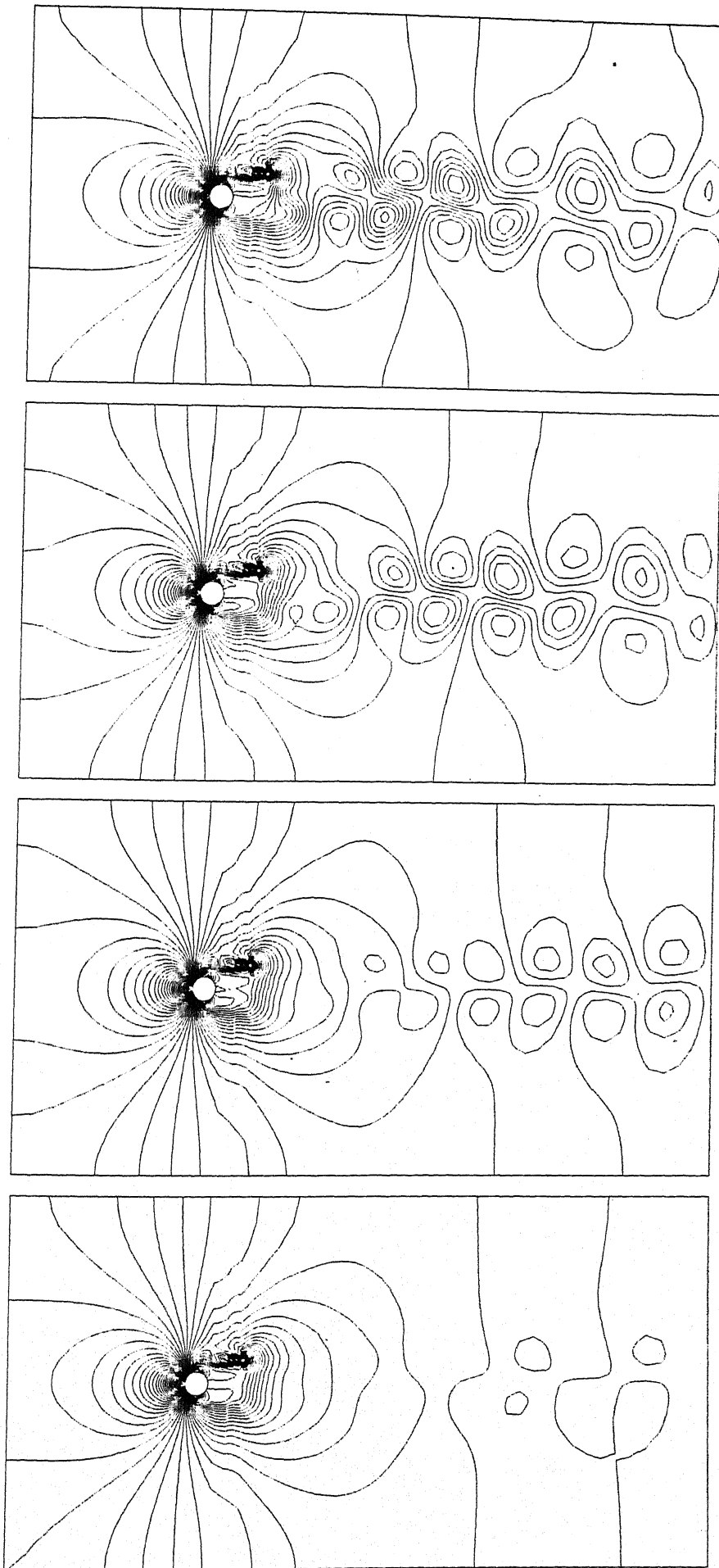
Figure 3.13: Pressure contours at various time instants for Re = 80 for control cylinder problem using Coarse Grid: Control cylinder at X/D = 2.0, Y/D = 1.0
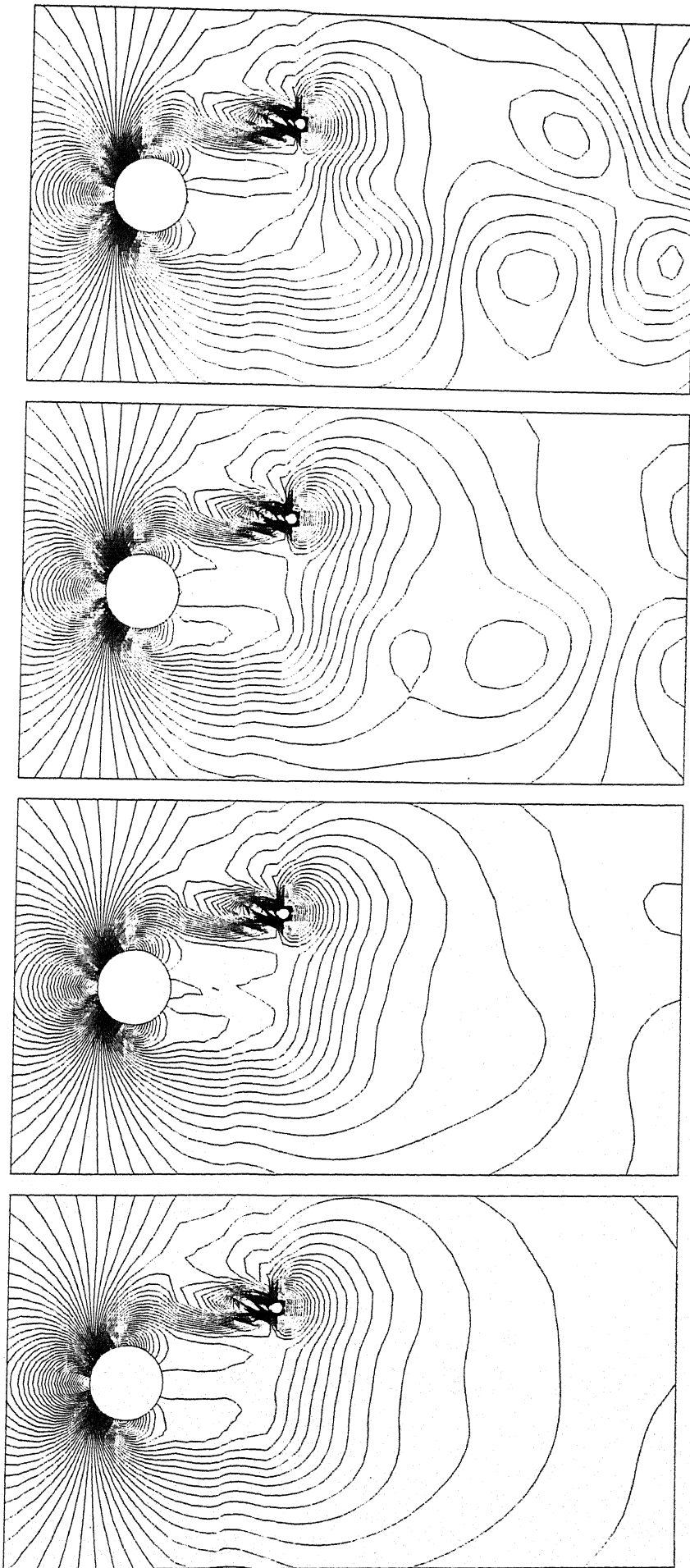
Figure 3.14: Close view of Pressure contours at various time instants for Re = 80 for control cylinder problem using Coarse Grid: Control cylinder at X/D = 2.0, Y/D = 1.0
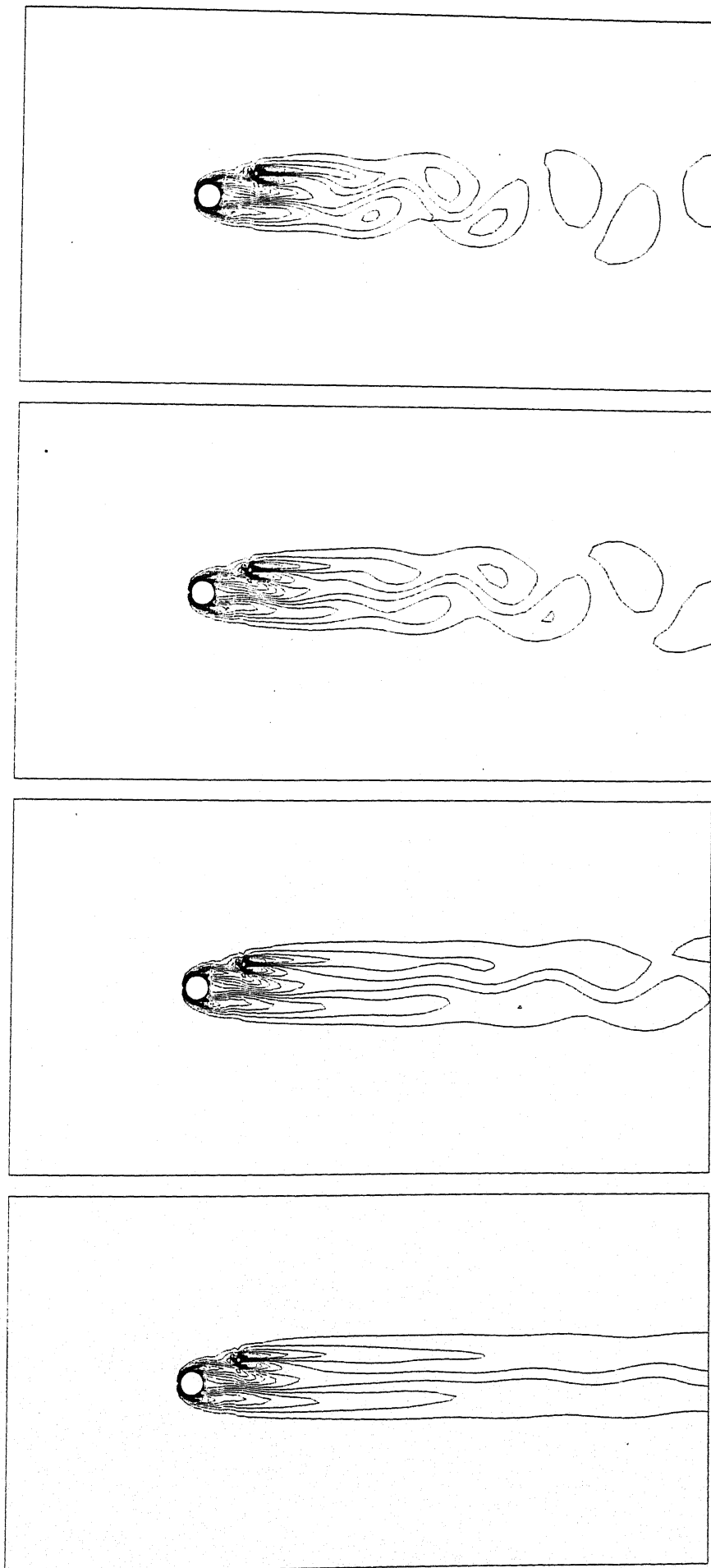
Figure 3.15: Vorticity contours at various time instants for Re = 80 for control cylinder problem using Coarse Grid: Control cylinder at X/D = 2.0, Y/D = 1.0
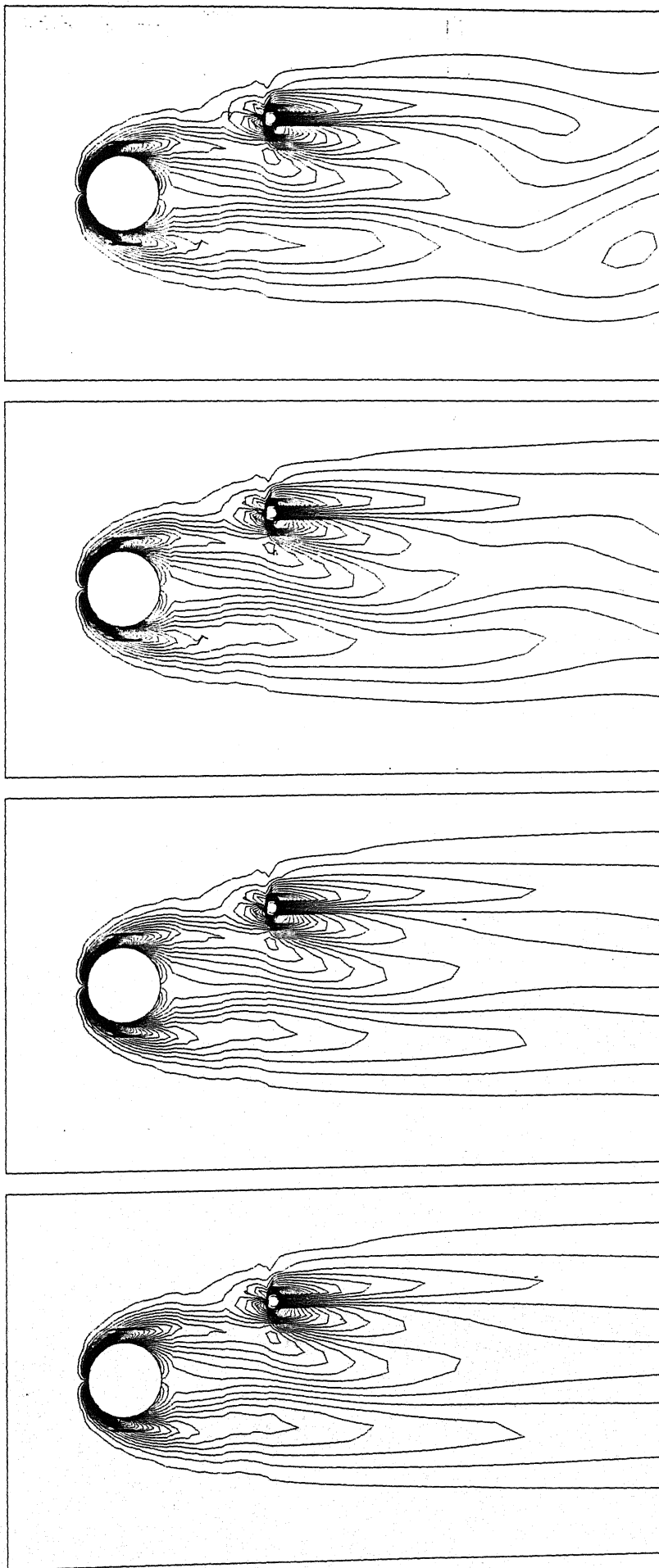
Figure 3.16: Close view of Vorticity contours at various time instants for Re = 80 for control cylinder problem using Coarse Grid: Control cylinder at X/D = 2.0, Y/D = 1.0
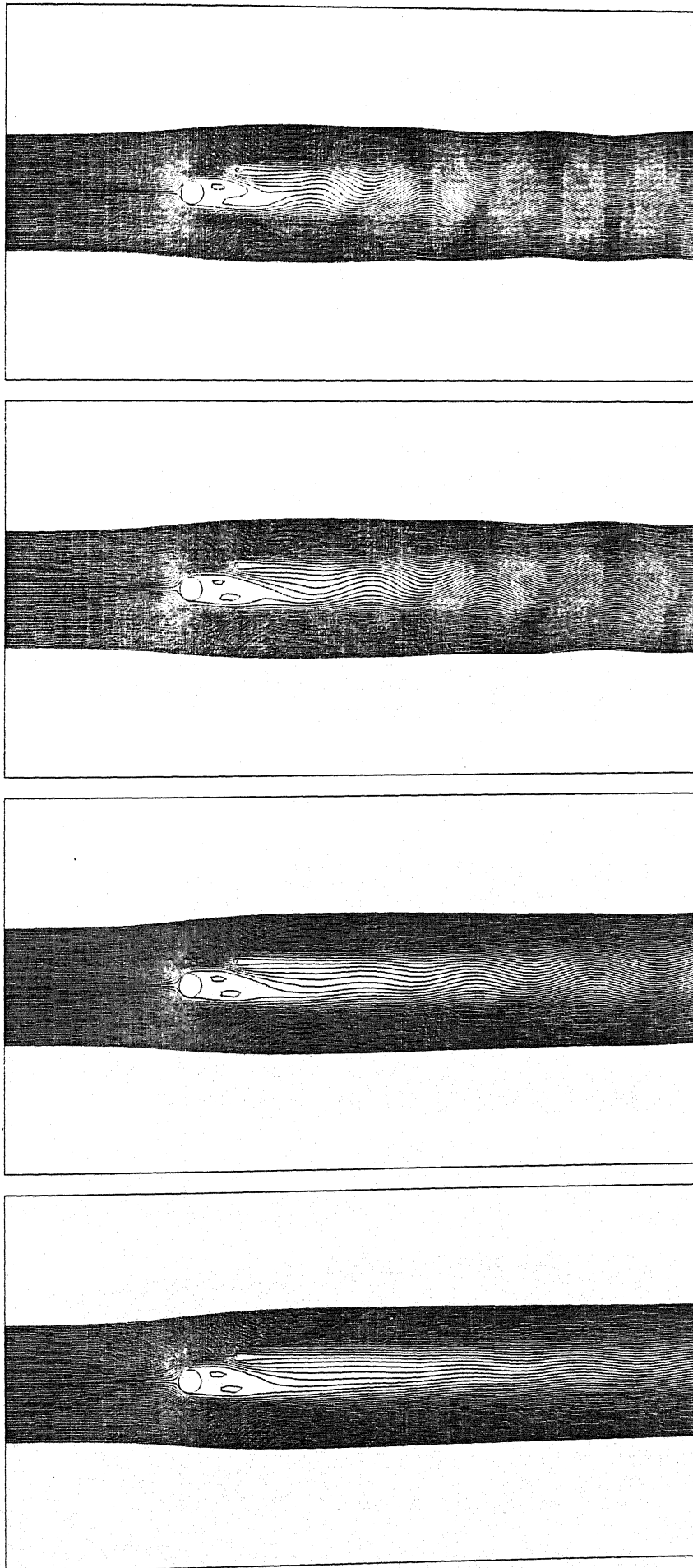
Figure 3.17: Streamlines at various time instants for Re = 80 for control cylinder problem using Coarse Grid: Control cylinder at X/D = 2.0, Y/D = 1.0
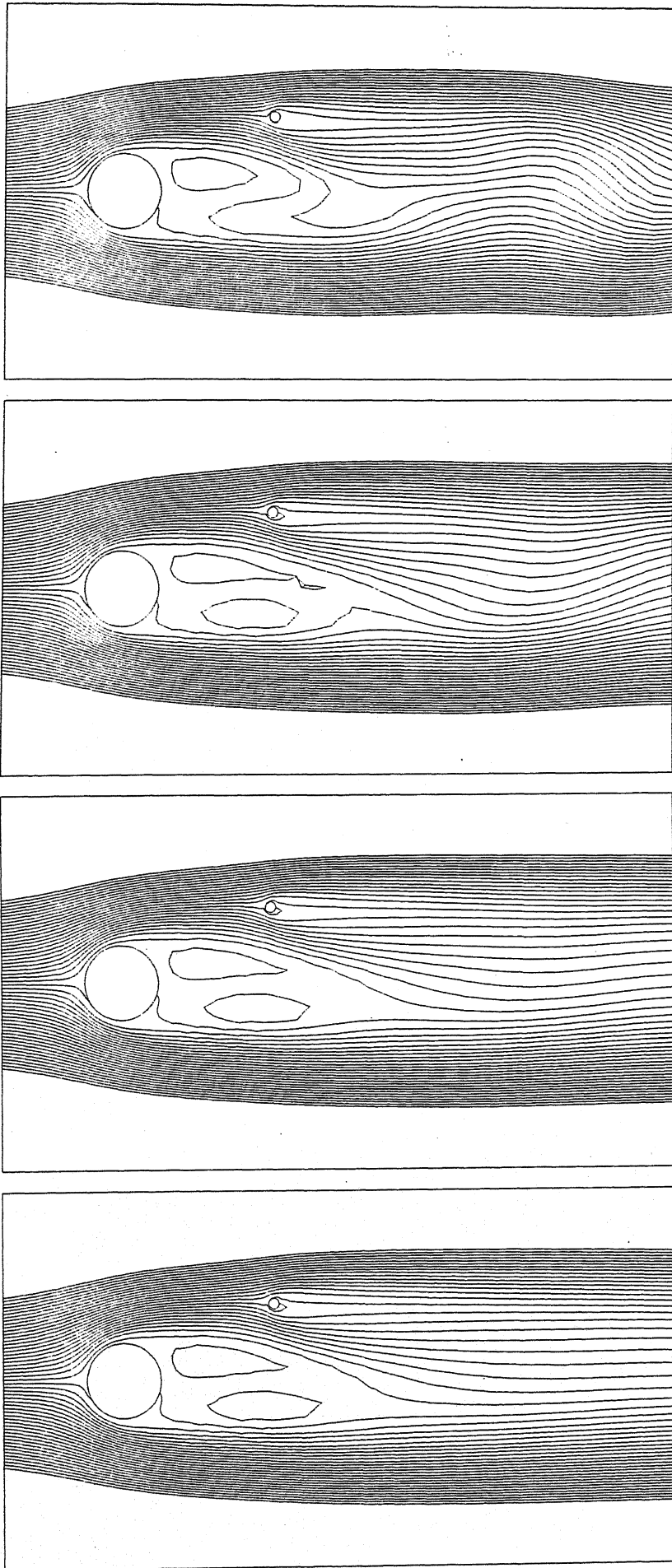
Figure 3.18: Close view of Streamlines contours at various time instants for Re = 80 for control cylinder problem using Coarse Grid: Control cylinder at X/D = 2.0, Y/D = 1.0
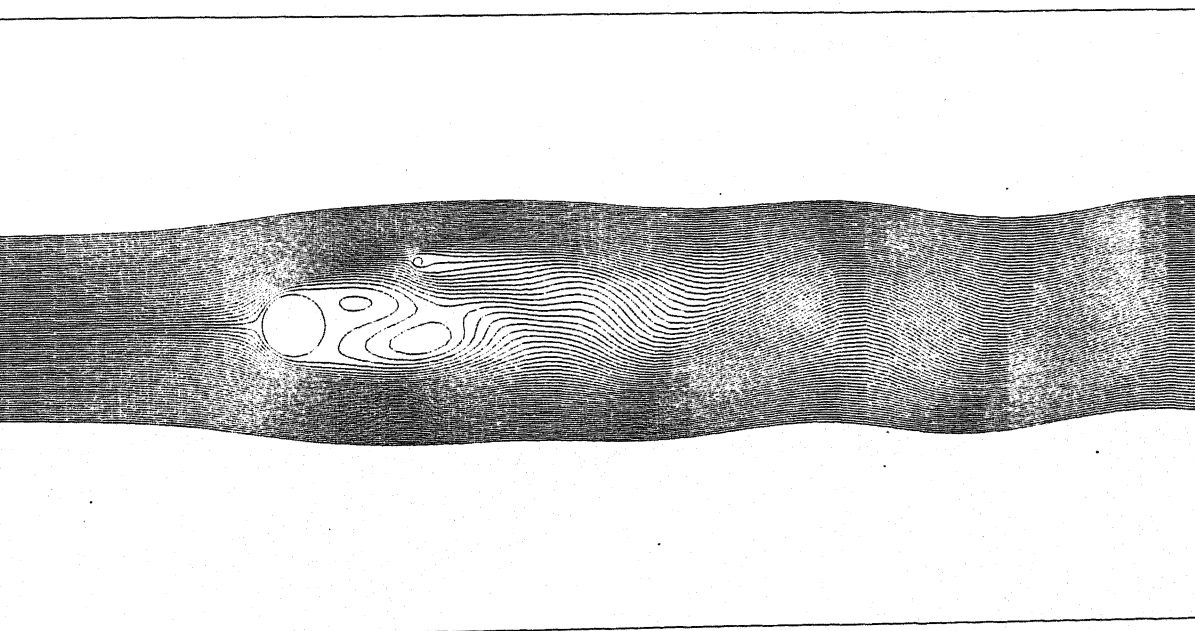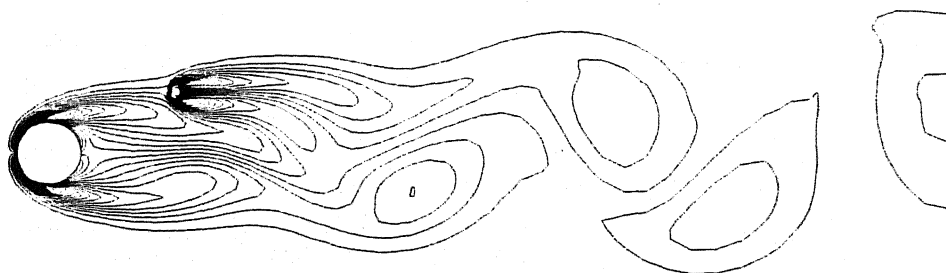
Figure 3.19: Pressure, Vorticity and Streamlines contours at Re = 100 for control cylinder problem using Fine Grid: Control cylinder at X/D = 2.0, Y/D = 1.0
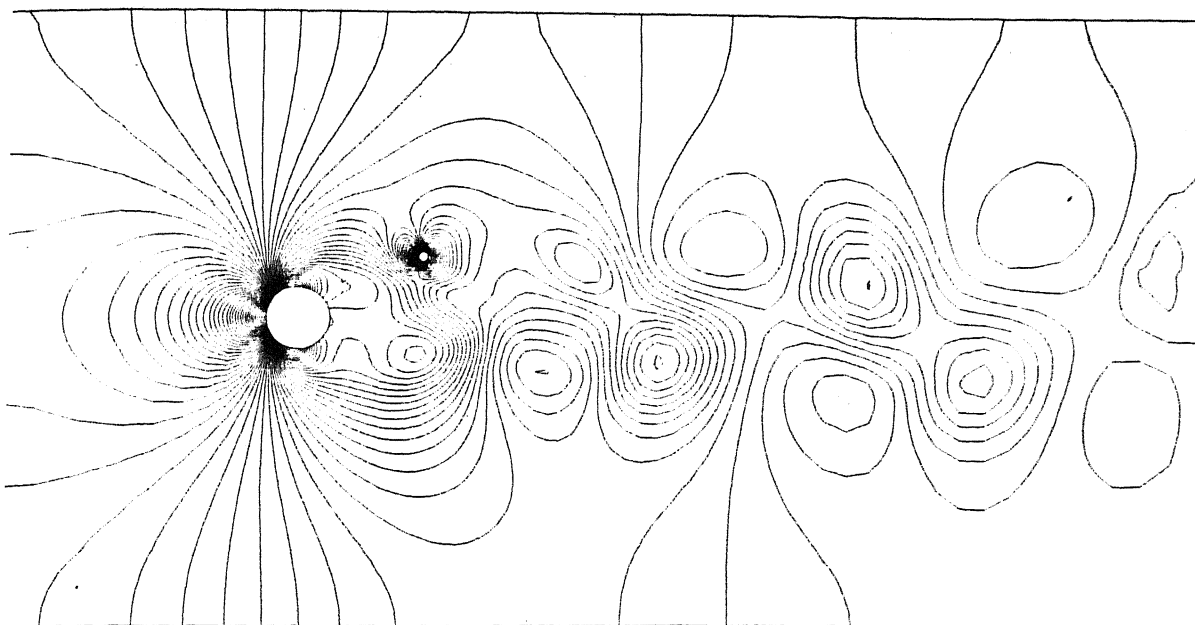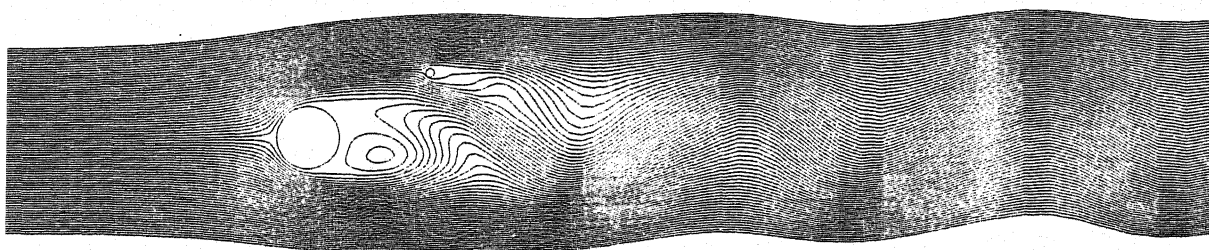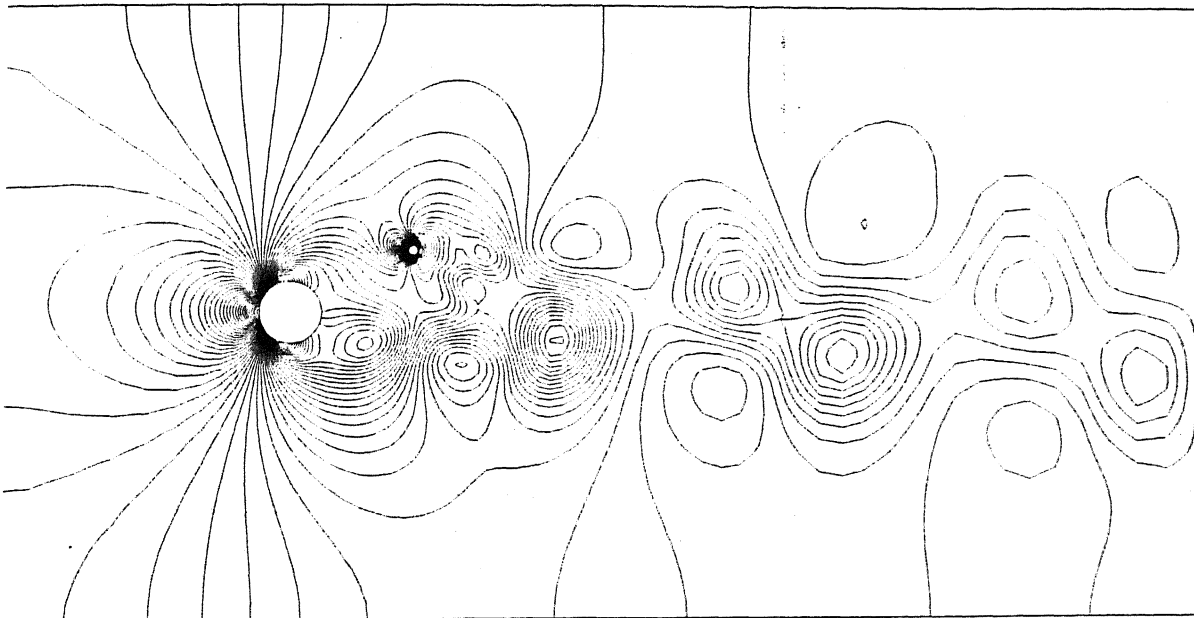
Figure 3.21: Pressure, Vorticity and Streamlines contours at Re = 100 for control cylinder problem using Fine Grid: Control cylinder at X/D = 2.0, Y/D = 0.8

Figure 3.22: Pressure contours at Re = 80 for control cylinder problem using Fine Grid: Control cylinder at X/D = 2.0, Y/D = 0.8

Figure 3.23: Close view of Pressure contours at Re = 80 for control cylinder problem using Fine Grid: Control cylinder at X/D = 2.0, Y/D = 0.8
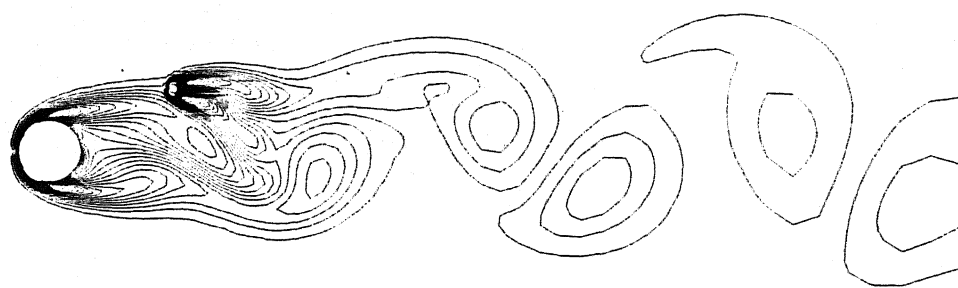
Figure 3.24: Vorticity contours at Re = 80 for control cylinder problem using Fine Grid: Control cylinder at X/D = 2.0, Y/D = 0.8

Figure 3.25: Close view of Vorticity contours at Re = 80 for control cylinder problem using Fine Grid: Control cylinder at X/D = 2.0, Y/D = 0.8
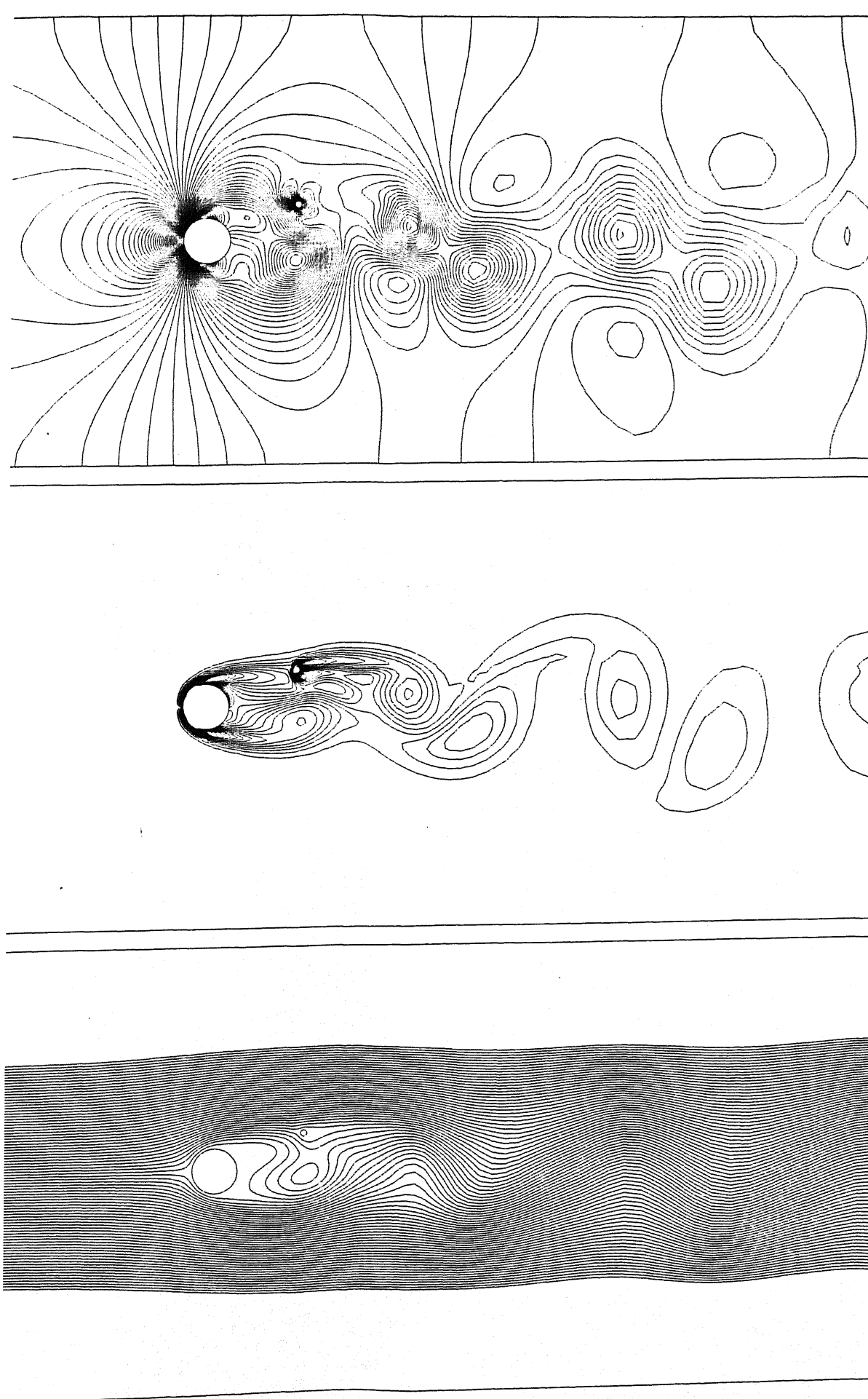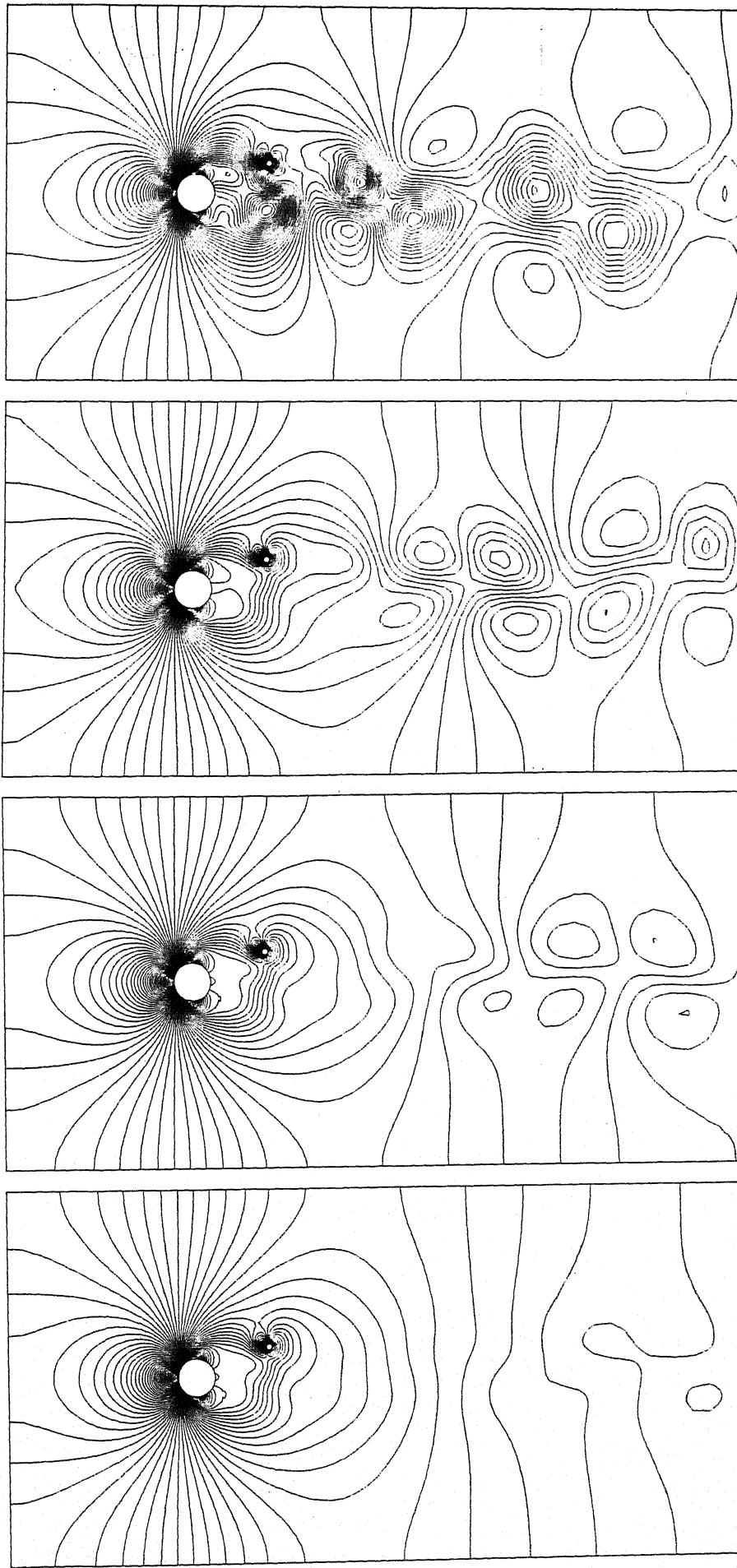
Figure 3.26: Streamlines at Re = 80 for control cylinder problem using Fine Grid: Control cylinder at X/D = 2.0, Y/D = 0.8
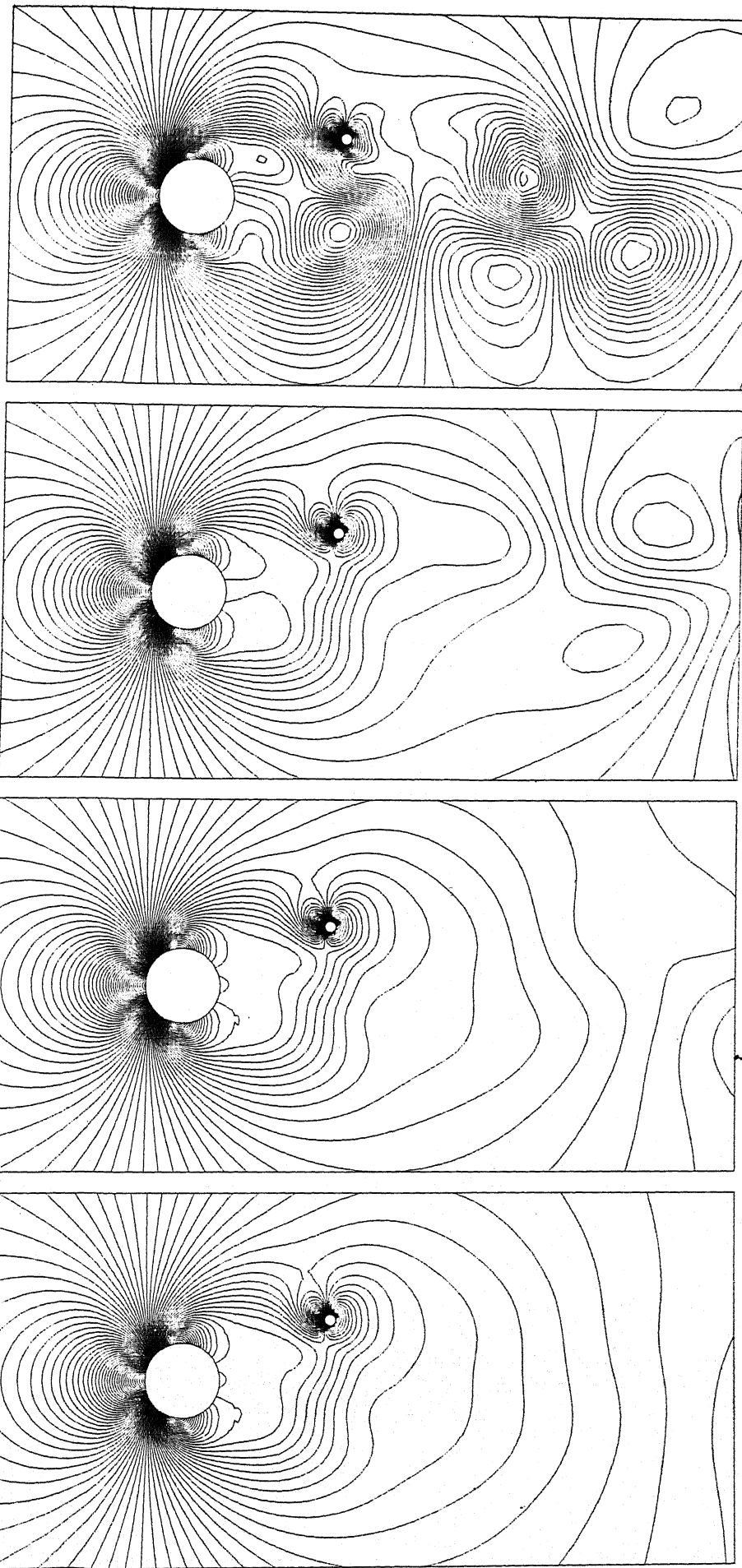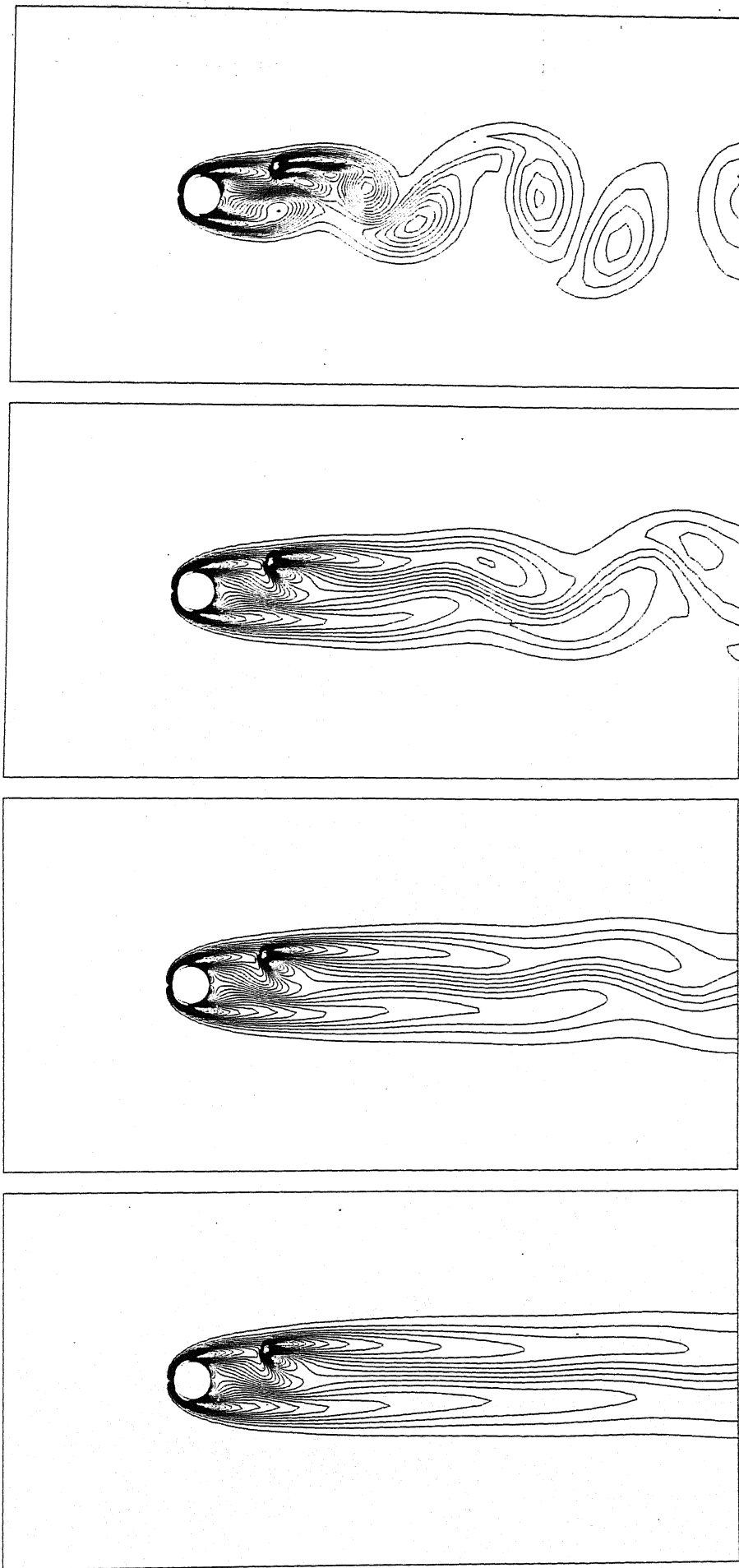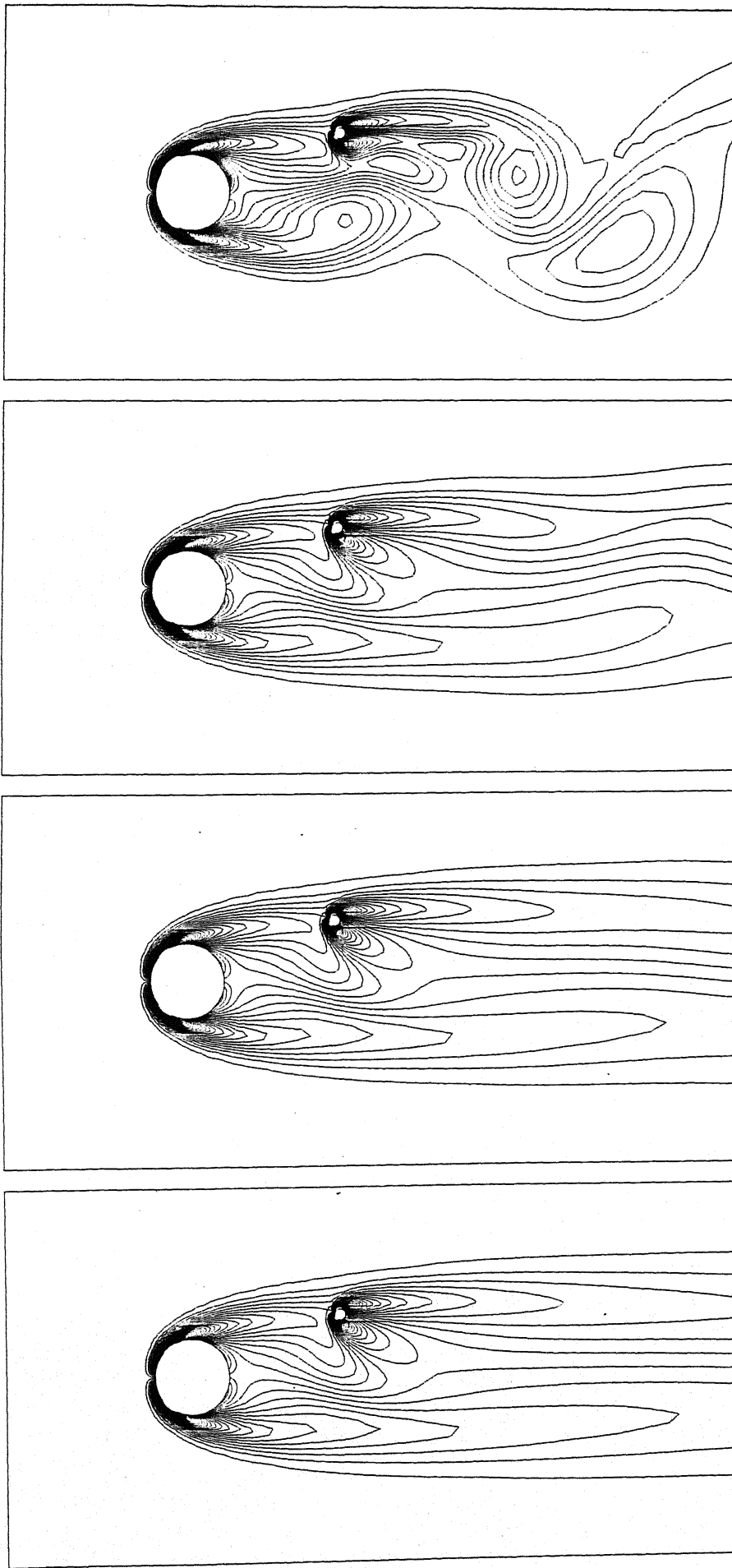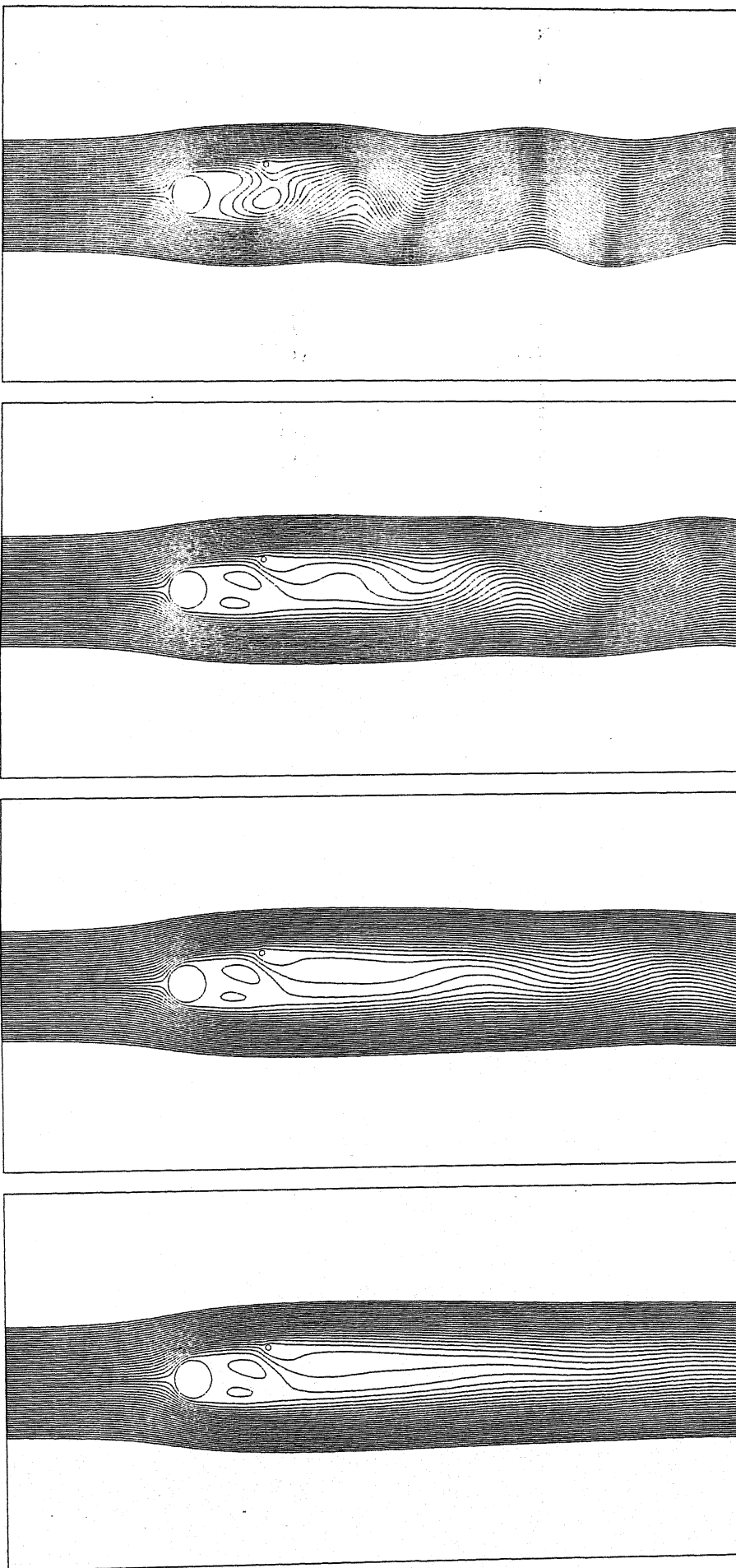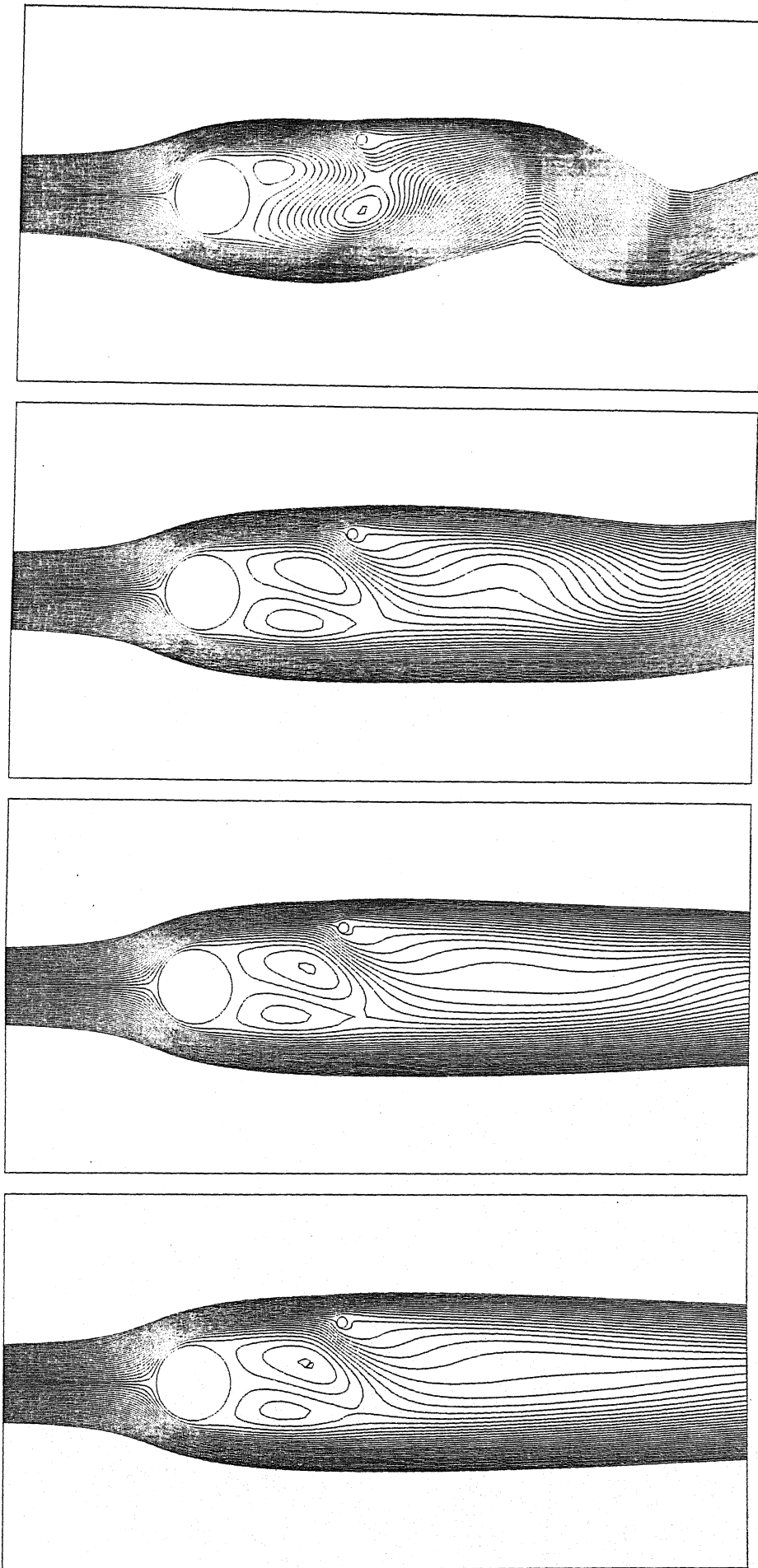
Figure 3.27: Close view of Streamlines at Re = 80 for control cylinder problem using Fine Grid: Control cylinder at X/D = 2.0, Y/D = 0.8

Chapter 4

Two cylinders in crossflow

4.1 Introduction

The flow around a pair of rigid circular cylinders is very complex, and has been studied extensively, yet understanding of these flows is far from complete. Some objectives of these studies have been to measure the fluid force and/or pressure distribution acting on each cylinder, flow velocity profile, and vortex shedding, and to understand the resultant flow patterns. Our study aims to get a better understanding of these flow problems. In this chapter results are presented for computations of flows involving stationary and oscillating cylinders. The computations for fixed cylinders are based on the stablized, semi-discrete finite element formulation while those for oscillating cylinders are based on stabilized space-time formulations.

In a fluid flow across a cylinder array, a fraction of the fluid energy is transmitted to the cylinders resulting in cylinder vibration. Cylinder vibrations resulting from cross flow generally are much more severe than vibrations resulting from axial flow. Shoei-Sheng Chen [2] gives following reasons for cross flow vibrations:

4.2   Mechanisms of cross flow vibration

Turbulent Excitations In a cylinder, there exist random noises, including turbulent pressure fluctuations and far field flow noises with some or little coherence; these randomly varying pressures on the surfaces of the cylinders generally produce relatively low amplitude cylinder vibration.

Vortex Induced Vibration These vibrations are induced by periodic vortex shedding from cylinders. While vortex shedding initiates cylinder vibration, the vortex shedding process can be modified by cylinder motion and synchronized with cylinder oscillations.

Fluid-elastic Instability At a certain flow velocity, fluid energy may feed into cylinders, resulting in large cylinder vibrations. The dominant fluid forces are the motion dependent fluid forces. Severe damage can result in short period of time.

Acoustic Excitation Acoustic excitation causes cylinder vibration , generally normal to flow direction and cylinder axis. When the natural frequency of vortex shedding at a particular flow rate coincides with the acoustic frequencies, two systems (fluid flow and acoustic field) are coupled and reinforce each other. The worst case is that in which the acoustic frequency, the cylinder frequency, and the vortex shedding frequency are the same.

Though all these mechanisms are important in causing vibration of cylinders, we have confined our study to understanding the role of vortex shedding in inducing the vibrations.

When one or both cylinders vibrate, the flow field becomes significantly more complicated because of the interaction of the fluid flow and the cylinder motion. Efforts have been made to understand the phenomena involved. Motivated by

concern over the large oscillations frequently occurring in transmission lines exposed to high wind, most of the studies of the cylinders have focused on characterizing the motion of two cylinders in tandem and staggered arrangement. The disturbed flow caused by the windward cylinder striking the leeward cylinder can induce dynamic instability, called wake induced flutter. Cylinders are also subjected to other fluctuating forces associated with vortex shedding and turbulence generated by the cylinder motion.

4.3   Flow Interference Regimes

The interference between the two cylinders will occur either when they are sufficiently close to each other or when the rear cylinder is adjacent to or within the wake of the upstream cylinder. Based on the arrangement of the two cylinders, M. M. Zdravkovich [5] has grouped the different situations into four regimes, as shown in figure 4.3.

Proximity Interference The flow field or motion of either cylinder affects the other; this occurs in both side by side and slightly staggered arrangements.

Wake Interference The flow field or motion of the upstream cylinder affects the cylinder in the wake; this happens in both tandem and staggered arrangements for $X/D > 4$.

Proximity and Wake Interference At small spacings, the wake behind the upstream cylinder is disrupted by the downstream cylinder; this occurs in both tandem and staggered arrangement for $X/D < 4$.

No Interference The flow field and motion of either cylinder is not affected by the other.
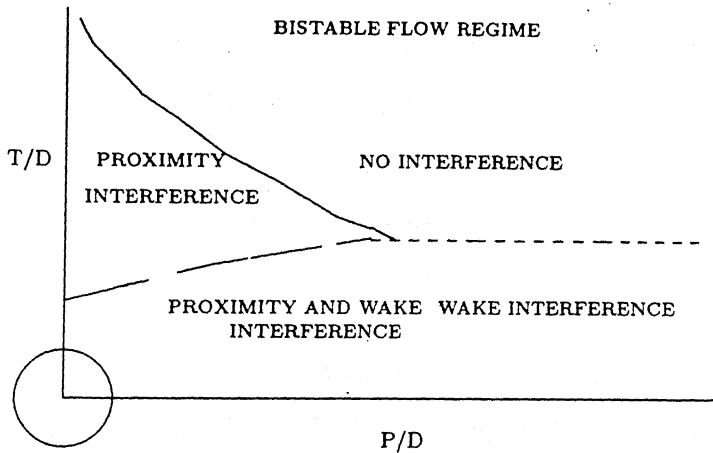
Figure 4.1: Interference regimes for two cylinders

The boundaries of different regimes are affected by different system parameters. Precise boundaries have not been defined in the figure 4.3 which is included only to illustrate the general location of the four major flow regimes.

4.4 Classification of the problem

Flow patterns across cylinders depend on cylinder arrangement as well as other parameters. Cylinder spacing is one of the important parameter. Depending on the cylinder's spacing, and flexibility of the support on which we mount the two cylinders our computational study delves into following three problems:

- In the first problem, the second cylinder is located at $X/D = 5.0, Y/D = 0.0$ in the wake interference region (in tandem position) with respect to first cylinder. In this case we do not allow any of the cylinder to move. We compute this problem for Reynolds number of 100.

- The second cylinder is located at $X/D = 5.5, Y/D = 0.7$ in the wake interference region of first cylinder in the second problem. Both of the cylinder are fixed in this case too. Reynolds number for this case also is 100.

- In the third problem locations of the two cylinders are same as in the second case, but the two cylinders are mounted on flexible supports. Therefore the two cylinder can move in both inflow and cross flow directions. But the cylinders are not allowed to rotate because of the various forces acting on them. For this case computations have been done for Reynolds number of 80 and 100.

In the present chapter finite element formulations are applied only in space for first and second problem, and both space and time for the third problem which involves moving boundaries of the two cylinders. The moving boundaries involve large displacements (linear) of rigid bodies. By employing smart mesh moving schemes, we are able to handle these displacements without any remeshing. Therefore, our solutions are free of projection errors associated with remeshing.

4.4.1 Computational domain

The dimensions of computational domain are $(-5.0 < X/D < 21.5)$ and $(-8.0 < Y/D < 8.0)$ with origin at the center of upstream cylinder. The diameters (D) of the two cylinders are equal to 2.0. Time step 'dt' for all the three problems is 0.1. Symmetric conditions are imposed at the upper and lower computational boundaries and the traction free condition is imposed at the outflow boundary. Grids for all the three problems contained 7260 nodal points and 7054 number of elements. Grid for the present problem is shown in figure 4.2.

4.5 Fixed Cylinders

The staggered arrangement is most likely to occur in practical situations. As mentioned earlier we computed the flow in this problem for two cases. In the first case both the cylinders are fixed. These computations are carried out for non-dimensional time of 350, and for Reynolds number of 100. In the second case the

two rigid cylinders are assumed to be attached to a linear spring and a dash pot for each of its degree of freedom of motion and are free to respond to fluid forces in both in-flow and cross flow directions. It is also assumed in this case that each of the degrees of freedom is decoupled from the other.

4.5.1   Two cylinders in staggered arrangement

Figure 4.4 shows time histories of coefficients of lift and drag for both the cylinders. Pressure, vorticity and streamlines have been plotted in figure 4.10. We find that after around $t = 80$, flow reaches periodic state as do the lift and drag fluctuations. Plot for C_L vs time (t) for first cylinder resembles that for the single cylinder case as reported by Mittal [6]. But average C_D for first cylinder which we found to be 1.42 is higher by around 5 % as compared to that for single cylinder flow computations. Average value of C_L is 0.05. Also C_D for first cylinder in two cylinder flow computations fluctuate with two frequencies as evident in its time history shown in plot 4.4. Coefficients of lift and drag for second cylinder show completely different behaviour, as compared to single cylinder case. Average of C_L for second cylinder is slightly higher in magnitude (0.2) as compared to that for single cylinder case. This can be explained by the fact that second cylinder does not face uniform upstream flow as is the case with first cylinder, and it tends to push some of the flow into the wake of the first cylinder. This is observed in control cylinder case also in which case it is the control cylinder which tends to push the flow into the wake of main upstream larger cylinder. We observe that because of this action control cylinder has some positive value of average lift coefficient. Average value of C_D is 0.9 for the second cylinder while average C_L is 0.185. C_D vs time (t) plot for second cylinder shows two frequency fluctuations. We also observe that Strouhal number for for this case approximately same value (0.165) as that for a single cylinder flow problem.

4.5.2 Two cylinders in tandem arrangement

Coefficients of lift and drag for the tandem arrangement of the two cylinders are given in figure 4.4. Computations are carried out till $t = 300$. Flow reaches periodic state after around $t = 200$. For first cylinder, average value of these coefficients is close to 0.0 and 1.42, which is approximately same as that in staggered arrangement. These coefficients have approximately same values (0.0 & 0.98) for second cylinder also. In the tandem arrangement first and second cylinder drag coefficient show only one frequency fluctuations. Pressure, vorticity and streamlines have been plotted in figure 4.9 for the tandem arrangement of the two cylinders. Comparing these plots for tandem and staggered arrangement reveals difference in the interference due to second cylinder in the vortex shedding and the diffusion of vorticity in the wake. We observe that while in the staggered arrangement flow gets pushed down into the wake of first cylinder due to presence of second cylinder, in the tandem arrangement the vortex shed from the first cylinder hits the second cylinder completely.

4.6 Flow induced vibration of circular cylinders

In this subsection results and general observations regarding oscillating flows are given. The position of the two cylinders is same as that for the fixed cylinders problem discussed in subsection 4.5. In the present case the two cylinders are assumed to be attached to spring-mass-damper system for each of there degree of freedom. Thus cylinders can oscillate about their mean position in both in-flow and cross-flow directions. As mentioned earlier we carried out the computations for this case for Reynolds number 100 and 80.

4.6.1 vibrations at Reynolds number 100

For this case the time histories of lift and drag coefficients are given in figure 4.5. If we compare these with that for fixed cylinders case of subsection 4.5, we observe that though mean values of the two drag coefficients for the two cylinders are lower but qualitatively their nature is quite similar. Drag histories of the two cylinders show presence of two frequencies . Lift coefficient histories for both the cylinder show single frequency oscillations, similar to that we observe for fixed cylinder case. We also observe oscillations in the maximum amplitudes of lift coefficients for the two cylinders, though we do not observe any such oscillations for fixed cylinder case. This indicates that flow is not fully developed yet and computations need to be carried out for more time steps for the flow to develop completely. Mittal has mentioned in the study [6] of single oscillating cylinder that this may be because of the difference in the natural frequency of vibration of spring-mass-damper system and Strouhal number (St) for the flow. Mean values for the lift coefficients are 0.186 for this case and the fixed cylinder case. Figure 4.7 show oscillations in X & Y coordinates of the two cylinders. We observe that maximum amplitude of these oscillations fluctuate with non-dimensional time (t). Though maximum amplitudes in X direction for the two cylinders and that in Y direction for the first cylinder are less than 8 % of radius of the cylinders but second cylinder oscillate in Y direction with as much as 80 % of the radius of the cylinders. In X direction too second cylinder oscillate with larger amplitude compared to that for first cylinder. In figure 4.12 pressure, vorticity contours and streamlines have been given. Along with boundaries of the cylinders at the end of the computations, boundaries of the cylinders in the fixed cylinder, staggered arrangement case have also been drawn to estimate how much cylinders have moved from there original positions.

We find that Strouhal number for this case is 0.171. The reduced natural frequency of the spring mass system for each of the cylinder is 0.165. Using Roshko's

[8] formula we find that this vortex shedding frequency occurs at Reynolds number 80. So we decided to carry out further computations with Reynolds number of 80. Roshko's formula is valid only for single cylinder problem, so our calculation will lead us to only another guess for the Reynolds number at which the Strouhal number of the flow is equal to the natural frequency of vibration for the spring-mass-damper system.

4.6.2 vibrations at Reynolds number 80

Figure 4.6 shows coefficients for lift and drag for this case. We observe that mean coefficient of drag for the first cylinder is changing with non-dimensional time (t) and has a value of 1.585 at the end of the computations. Coefficient of lift for the first cylinder has mean value of 0.05. Mean values of lift and drag coefficients for the second cylinder are 0.1 & 0.8. Coefficient of drag for the second cylinder and coefficient of lift for both the cylinder have constant mean values. We observe that by reducing the Reynolds number from 100 to 80 mean value of coefficient of drag for the first cylinder has increased by approximately 6 %, while coefficient of drag for the second cylinder retains the same value (0.8). Mean value of coefficient of lift also do not change from it's initial value of approximately 0.0 for both the cylinders. Maximum amplitudes of the coefficients of lift and drag also do not change significantly, except in the case of coefficient of lift for the second cylinder which has reduced considerably. Reduction of Reynolds number also results in larger amplitude of vibrations by the two cylinder. Though mean positions of the two cylinders remain the same in Y direction we observe that in X the cylinders have drifted in the direction of the flow by a small amount. First cylinder vibrates with maximum amplitude of 1.8 % of the diameter in the X direction while in Y direction maximum amplitude of vibration of vibration is 26 %. Second cylinder vibrates with larger maximum amplitude, 10.0 % of diameter in X direction and

60.0 % of diameter in Y direction. Pressure, vorticity contours and streamlines have been plotted in figure 4.13 for the present case. Along with the location of the cylinders at the end of the computations, locations of the cylinders in the fixed cylinder, staggered arrangement case are also drawn in these plots to compare the two locations of the cylinders. In the plots shown the first cylinder is at it's extreme x and y location.

4.7   Discussions & Conclusions

In our study on fixed cylinders in staggered and tandem arrangement, we observe that the presence of the second cylinder in the wake of another cylinder can alter the nature of the flow to a great extent and modify the wake street dramatically. Since second cylinder is placed in the wake interference region, only flow field or motion of the upstream cylinder affects the cylinder in the wake in both staggered and tandem arrangements.

In our third study we observe that the vortex induced oscillations are strongly dependent upon the arrangement of cylinders. The oscillation of one cylinder can strongly affect vortex shedding and the synchronization of the other cylinder. The rear cylinder oscillate with large amplitude while the front cylinder displays oscillations of smaller amplitude. In this study computations have not been carried out for large time steps and thus flow has not reached periodic state and is still developing. Amplitude of vibrations is larger in cross flow direction as compared to that in in-flow direction. An extremely complex relationship is found between the type of oscillations and the arrangement of the two cylinders. As observed by Zdravkovich [5] we found the amplitude of oscillations of the second cylinder much larger in cross flow direction than in in-flow direction.

Our study on the vortex induced oscillations gives only a glimpse into the
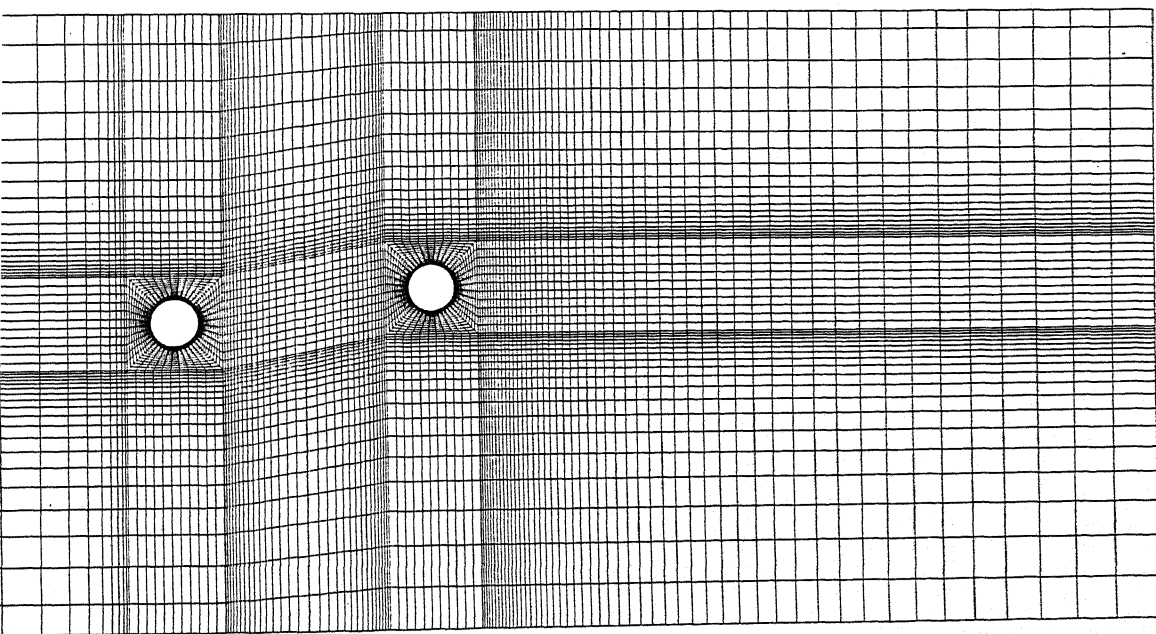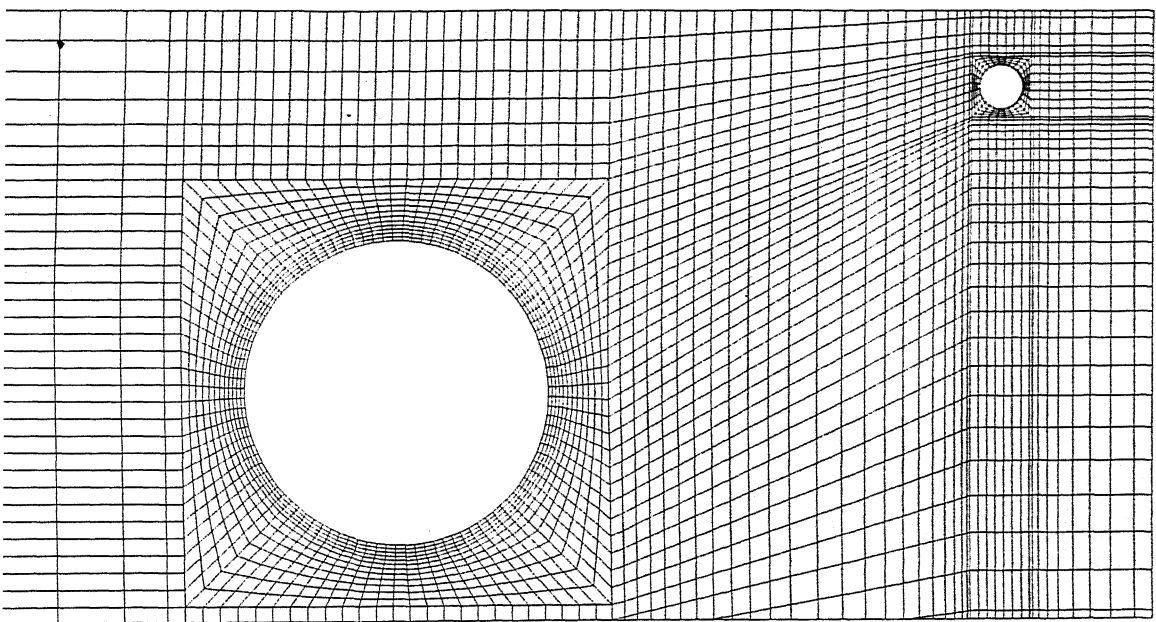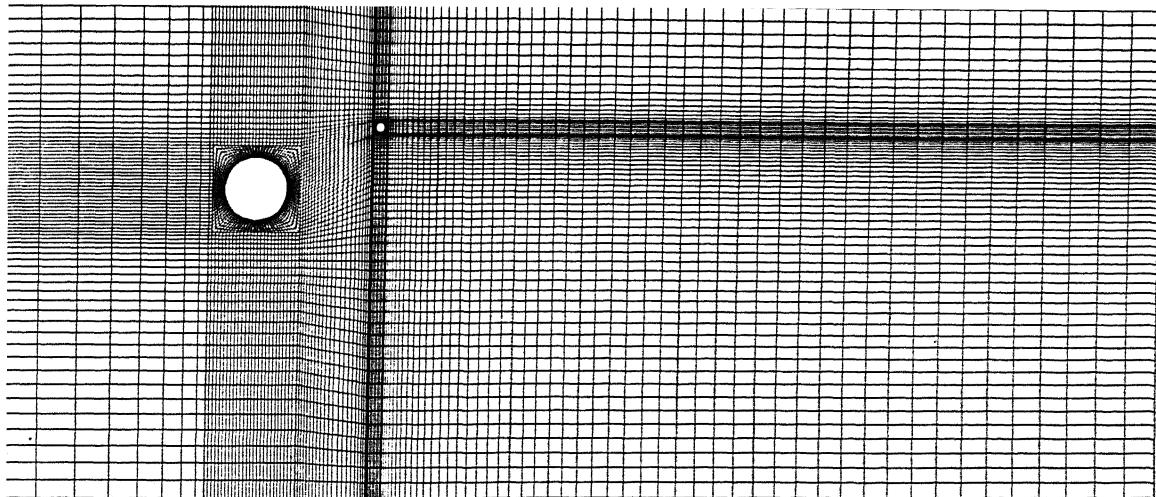
Figure 4.2: 1. Control Cylinder grid, 2. Grid around Main and Control Cylinder 3. Moving Cylinders problem
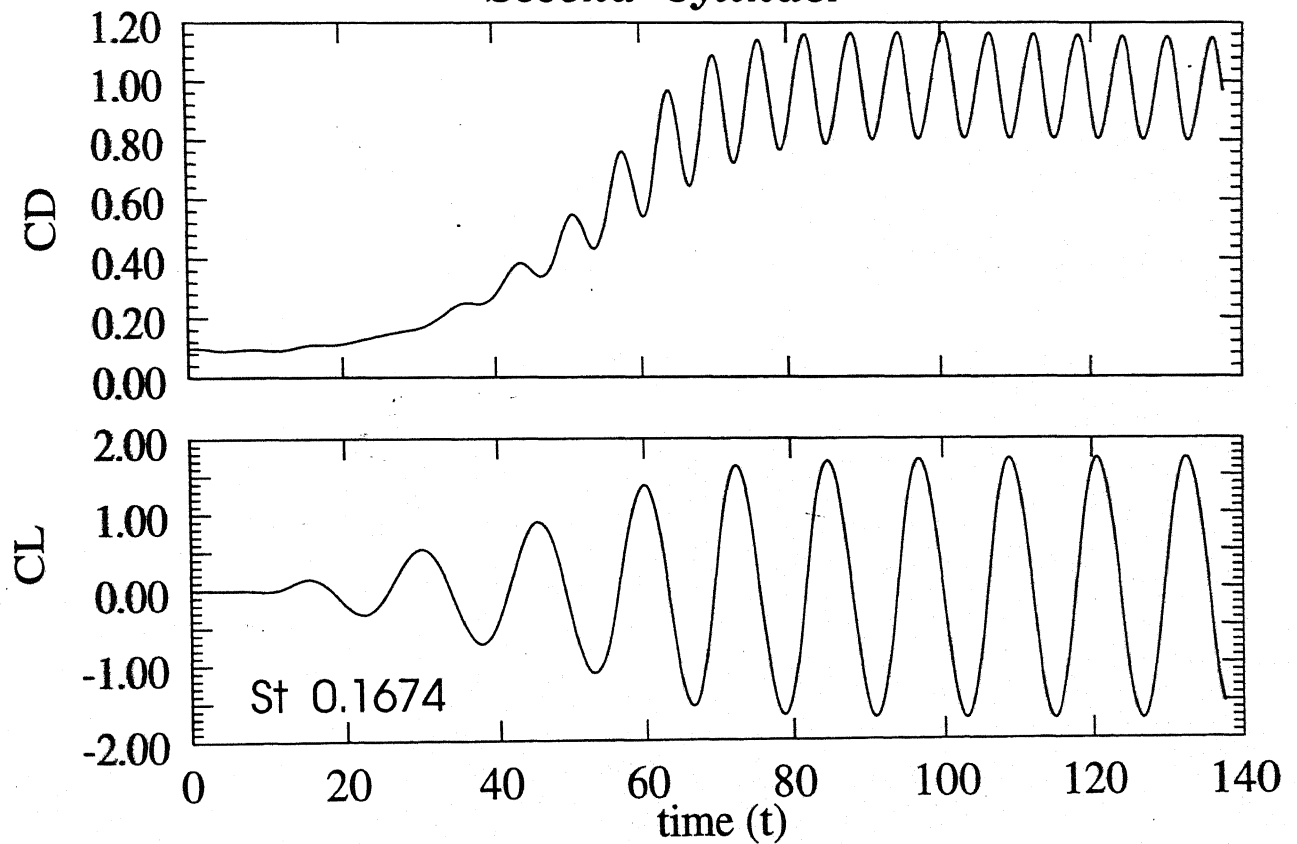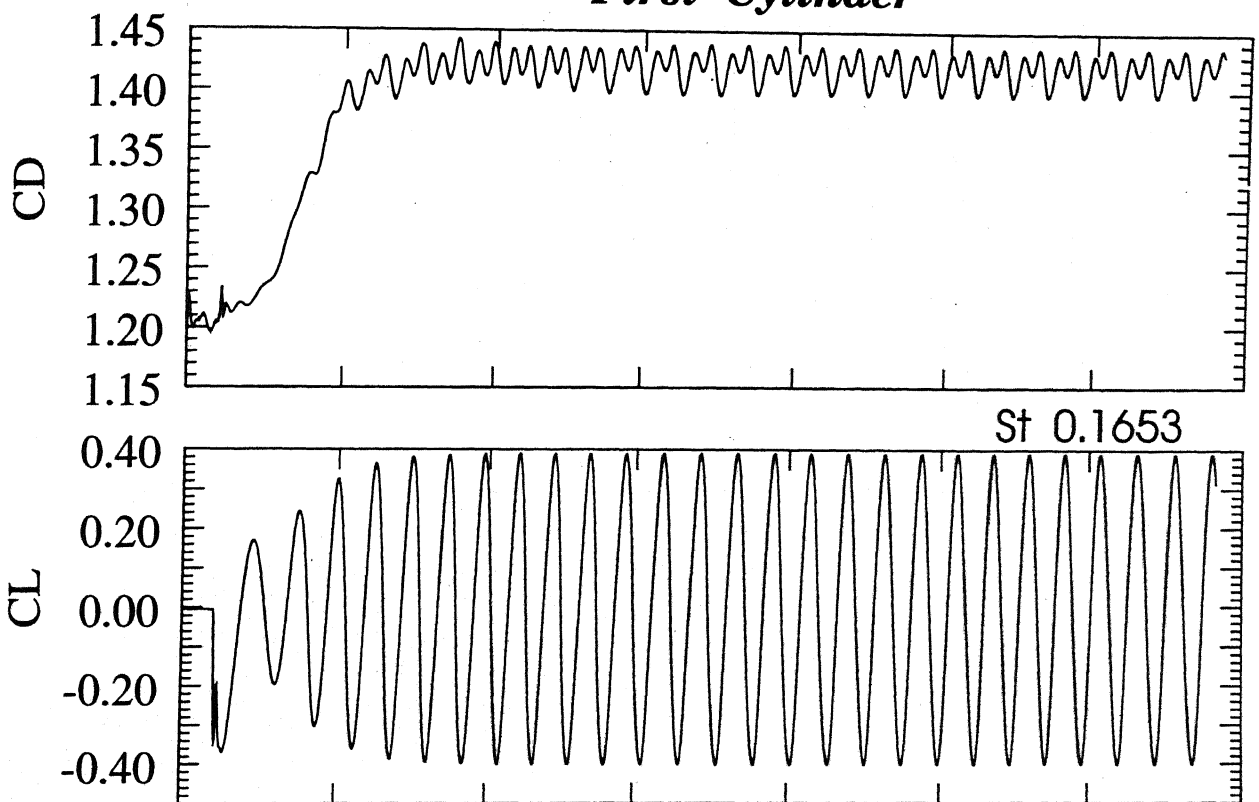
Figure 4.3: Coefficients of lift and drag for fixed cylinders in tandem arrangement at Re = 100. Second Cylinder at X/D = 5.5, Y/D = 0.0
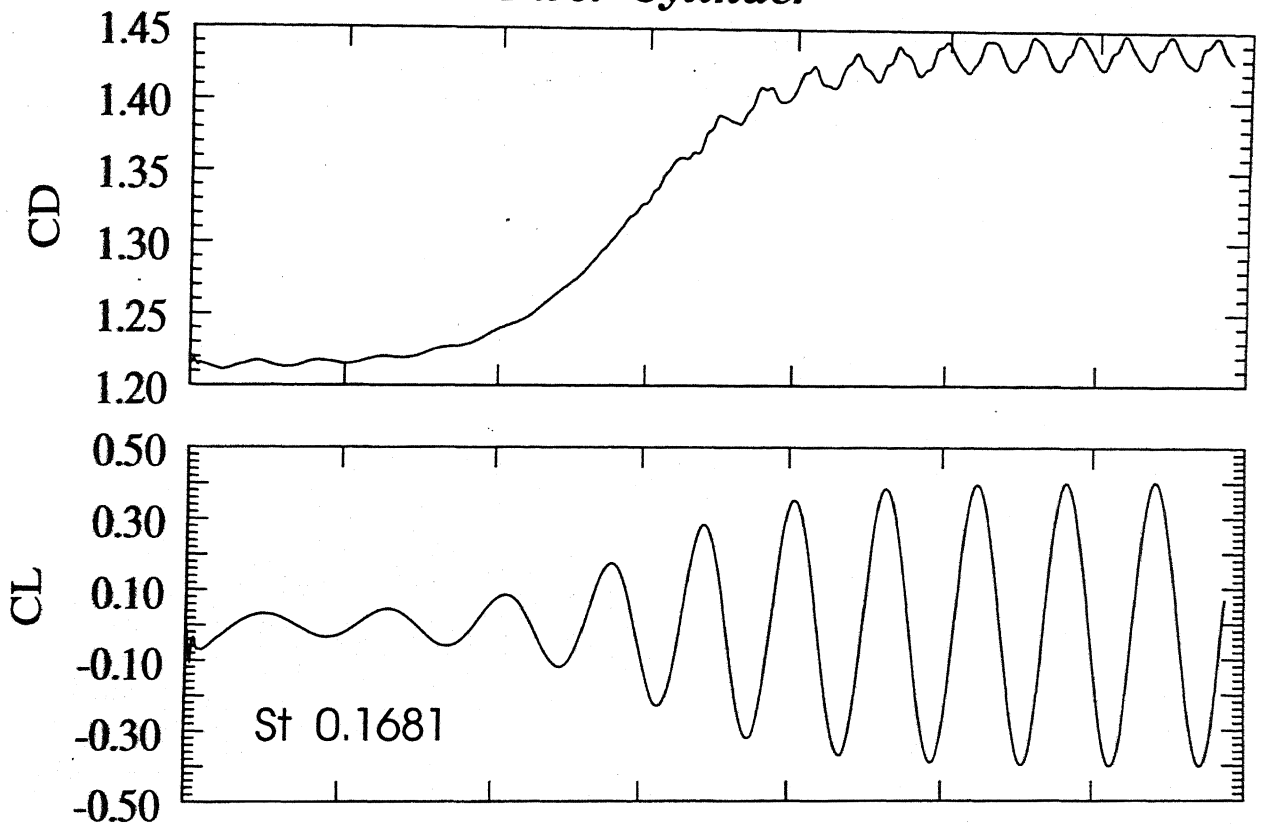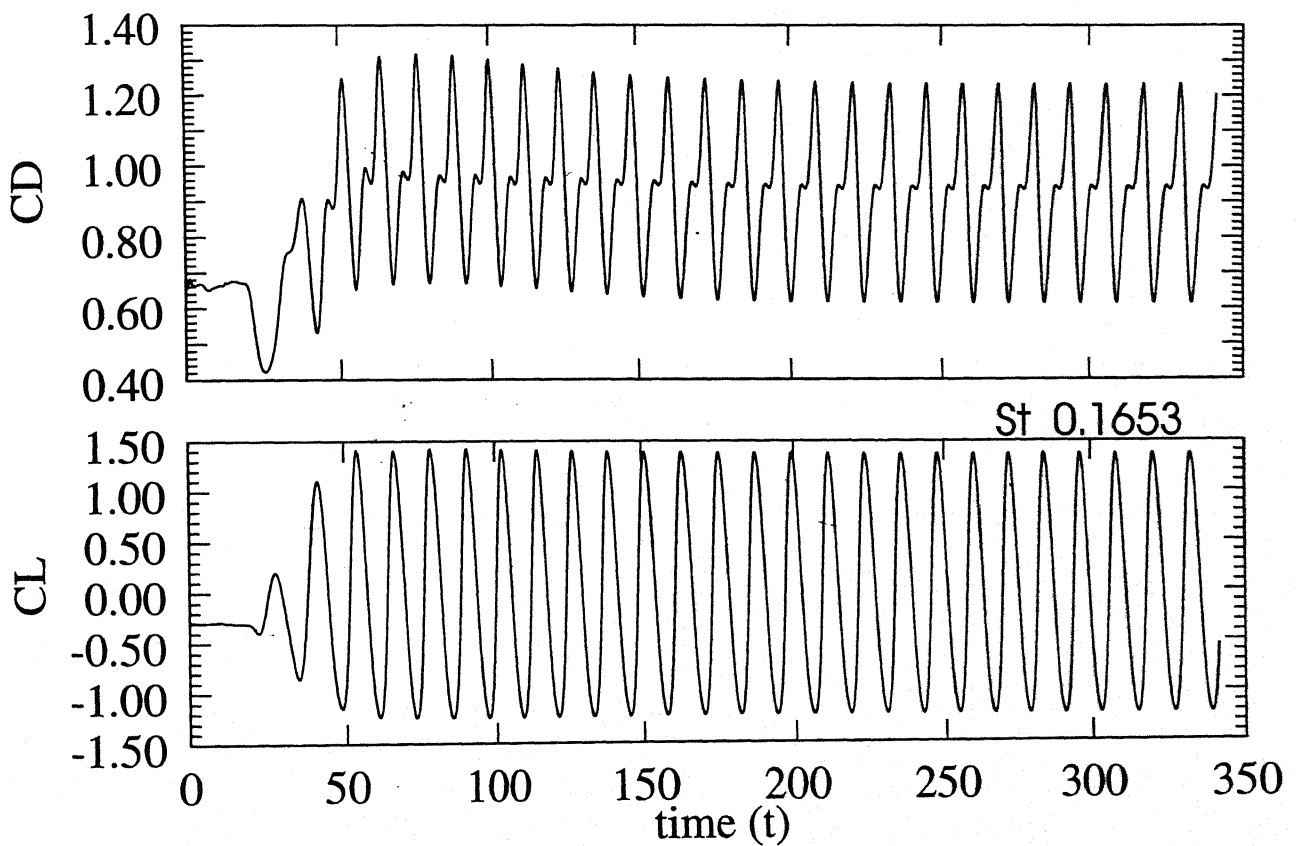
First Cylinder

Second Cylinder

Figure 4.4: Coefficients of lift and drag for fixed cylinders in staggered arrangement at Re = 100.
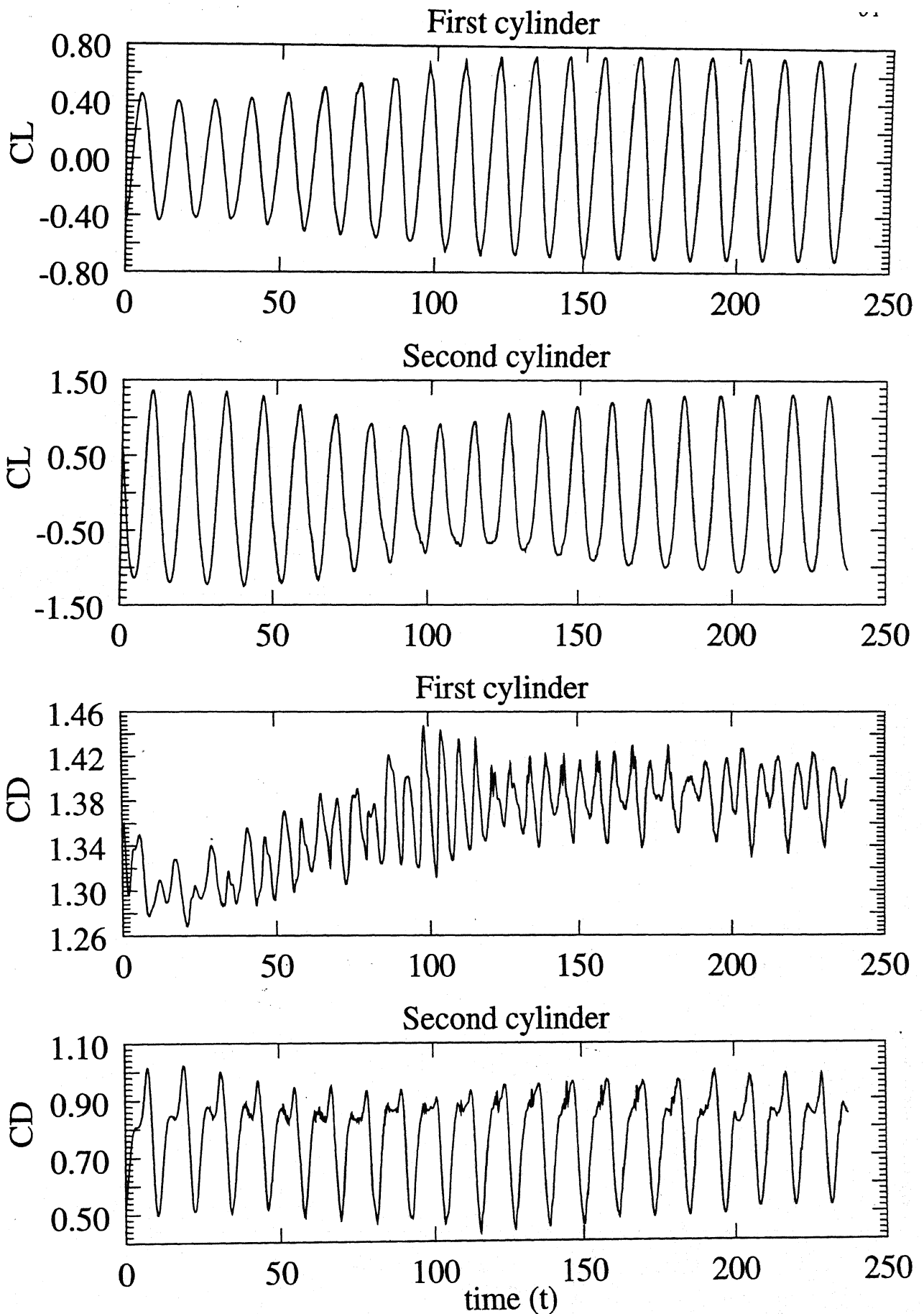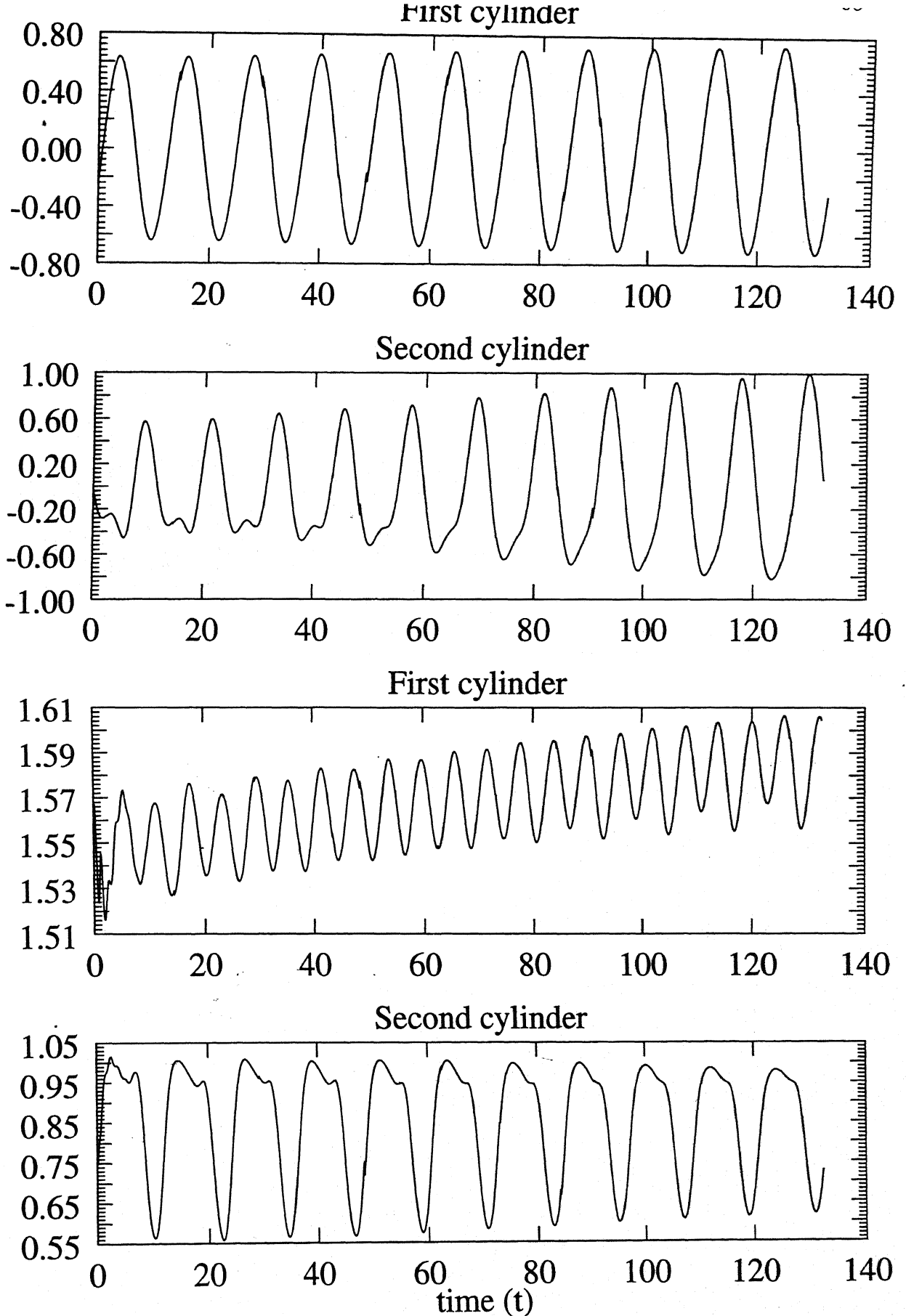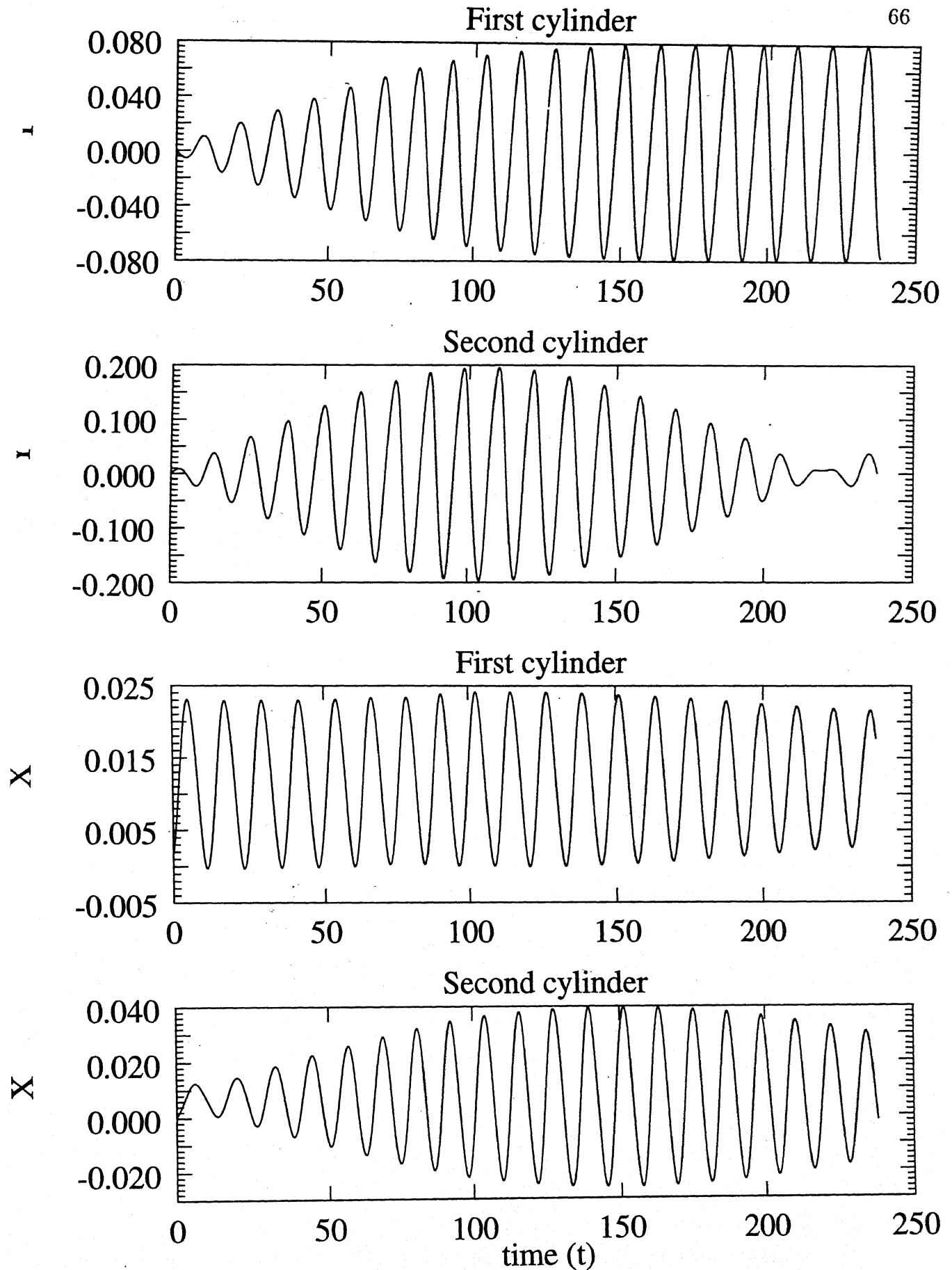Second Cylinder at X/D = 5.5, Y/D = 0.7

Figure 4.5: Coefficients of lift and drag for moving cylinders in staggered arrangement at Re = 100. Second Cylinder at X/D = 5.5, Y/D = 0.7

Figure 4.6: Coefficients of lift and drag for moving cylinders in staggered arrangement at Re = 80. Second Cylinder at X/D = 5.5, Y/D = 0.7

Figure 4.7: Displacements of the two moving cylinders in staggered arrangement at Re = 100.
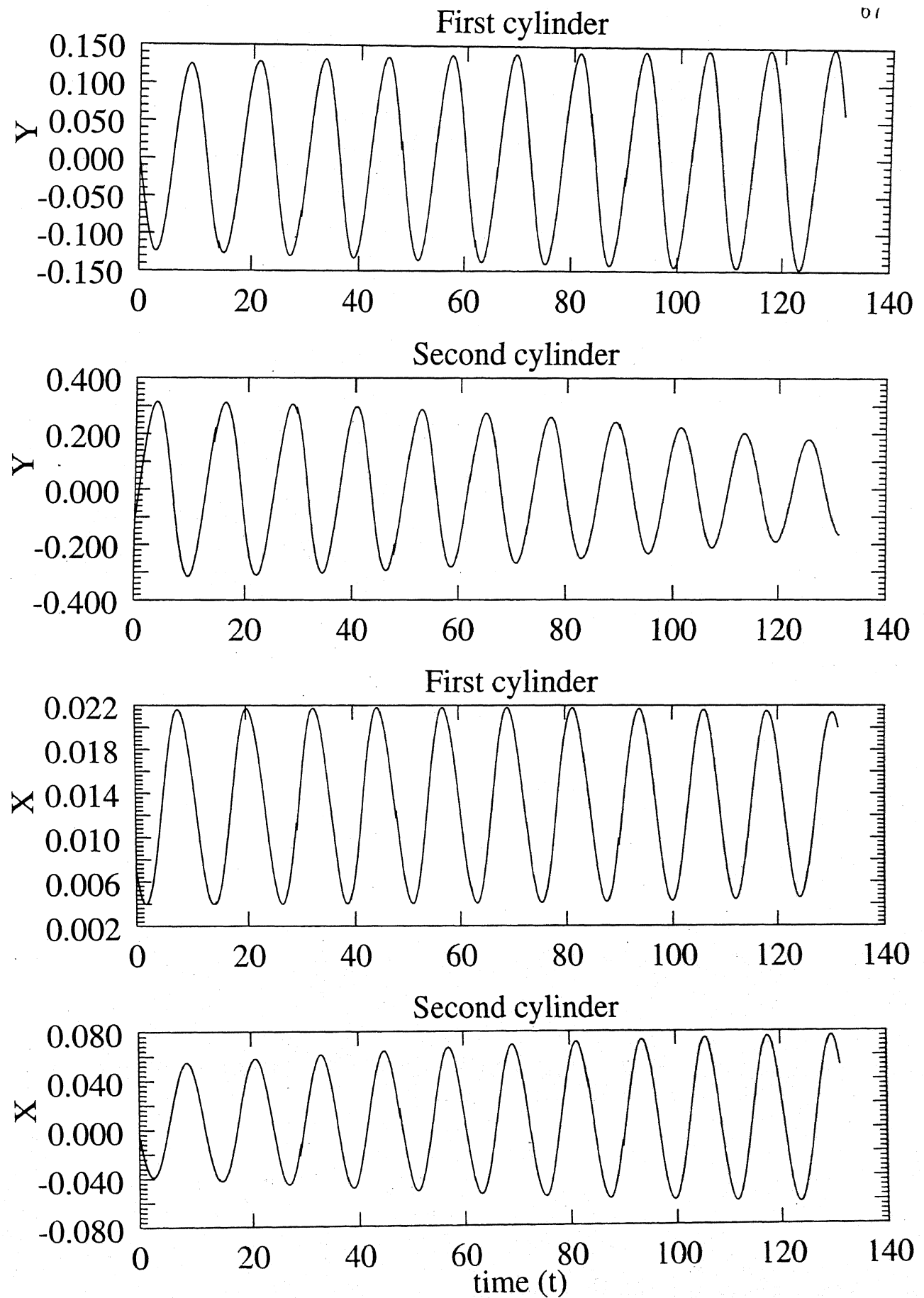
Figure 4.8: Displacements of the two moving cylinders in staggered arrangement at Re = 80. Second Cylinder at X/D = 5.5, Y/D = 0.7
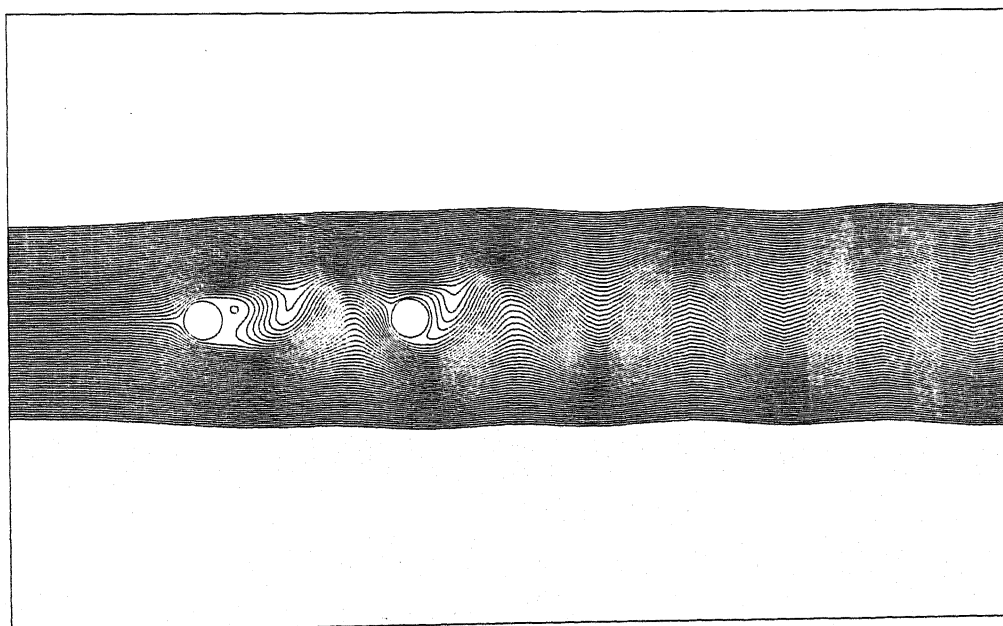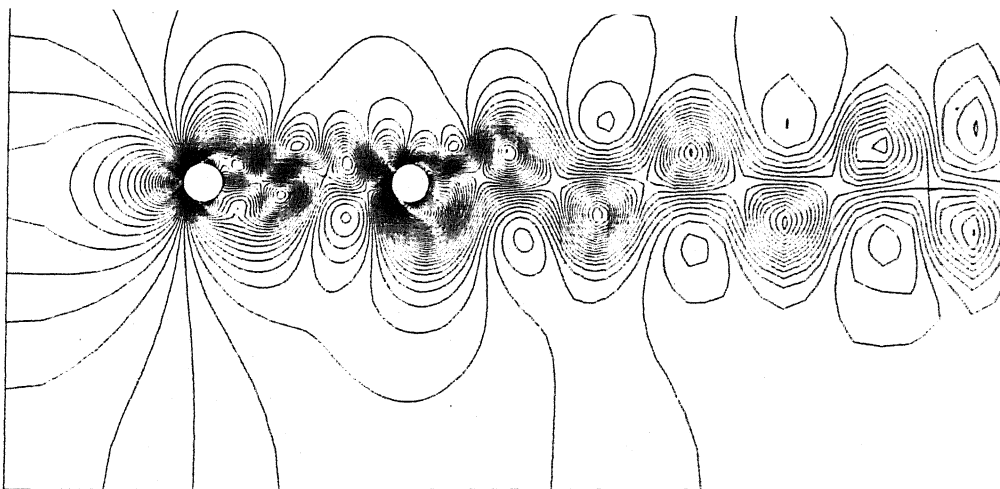
Figure 4.9: Pressure, Vorticity and Streamlines plots for fixed cylinders in tandem arrangement at Re = 100. Second Cylinder at X/D = 5.5, Y/D = 0.0
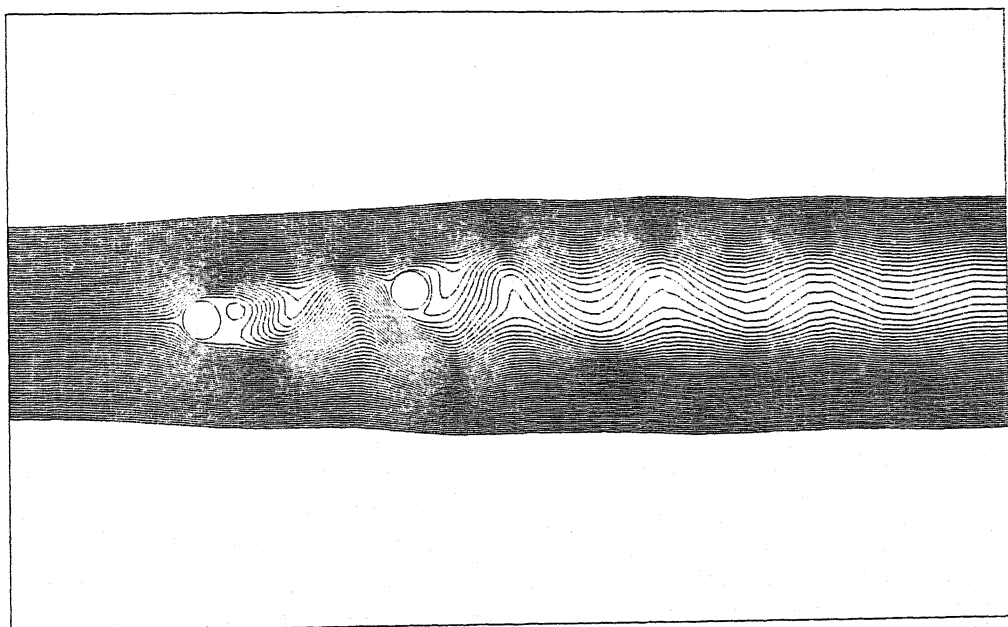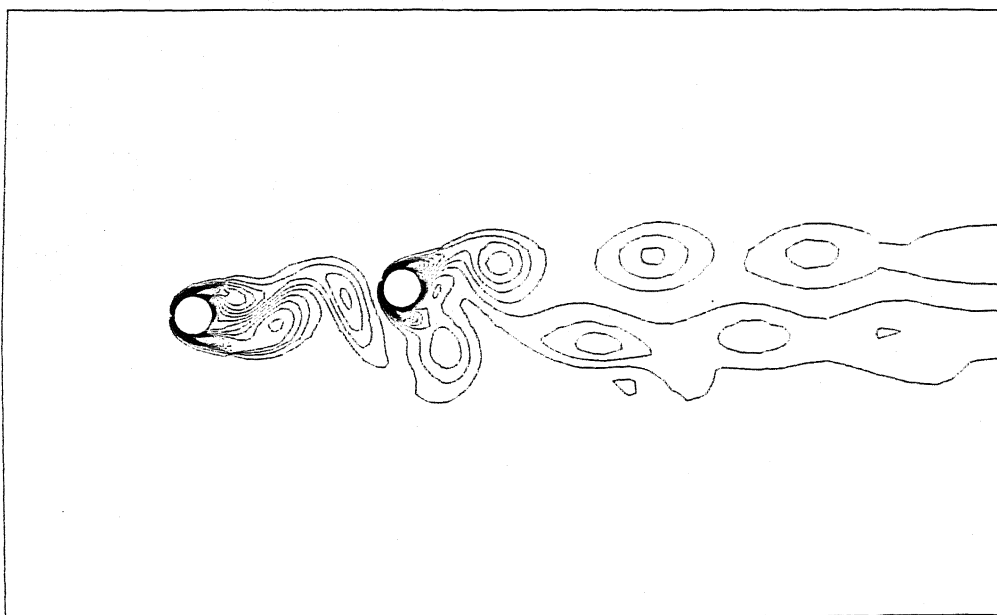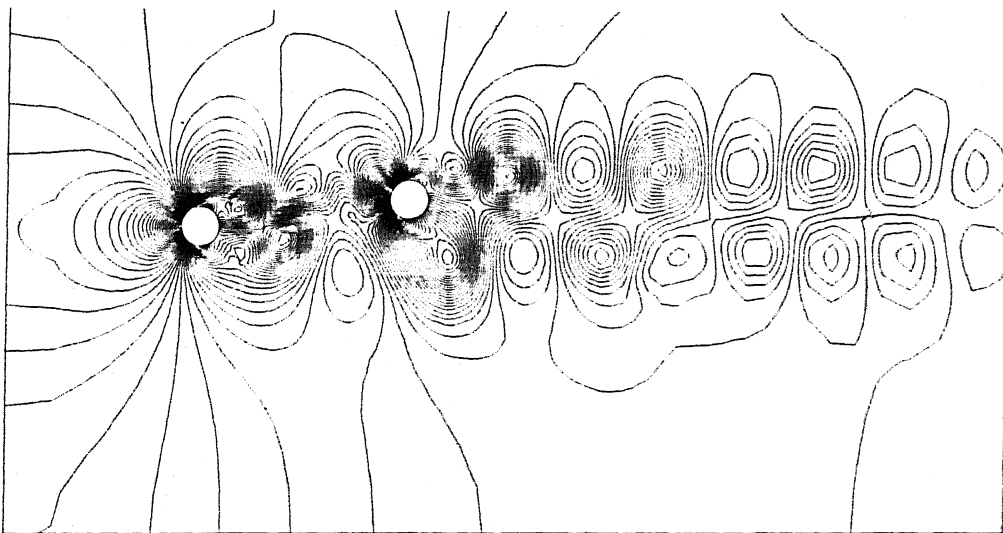
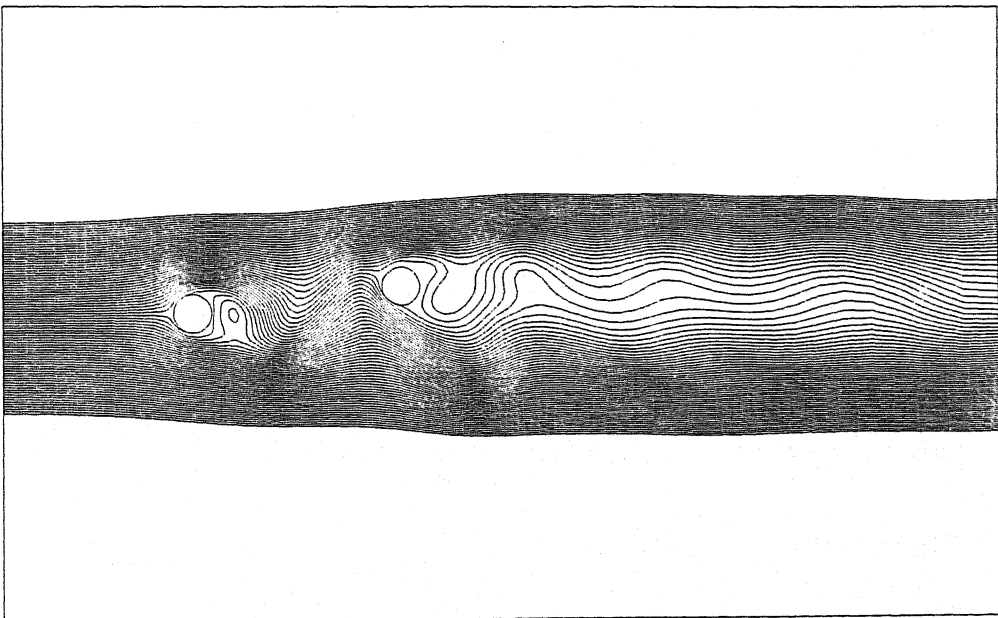Figure 4.10: Pressure, Vorticity and Streamlines plots for fixed cylinders in staggered arrangement at Re = 100. Second Cylinder at X/D = 5.5, Y/D = 0.7
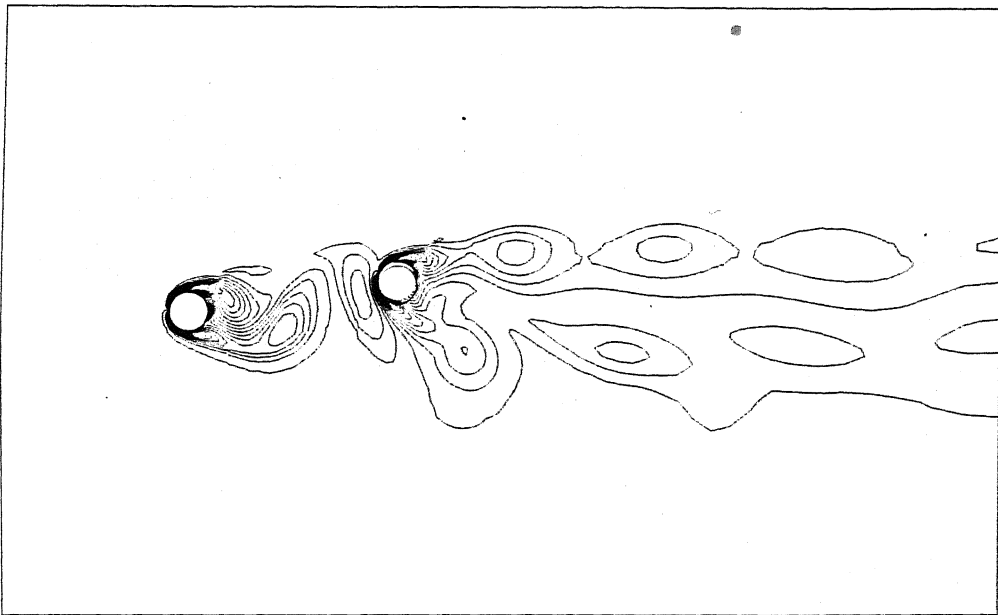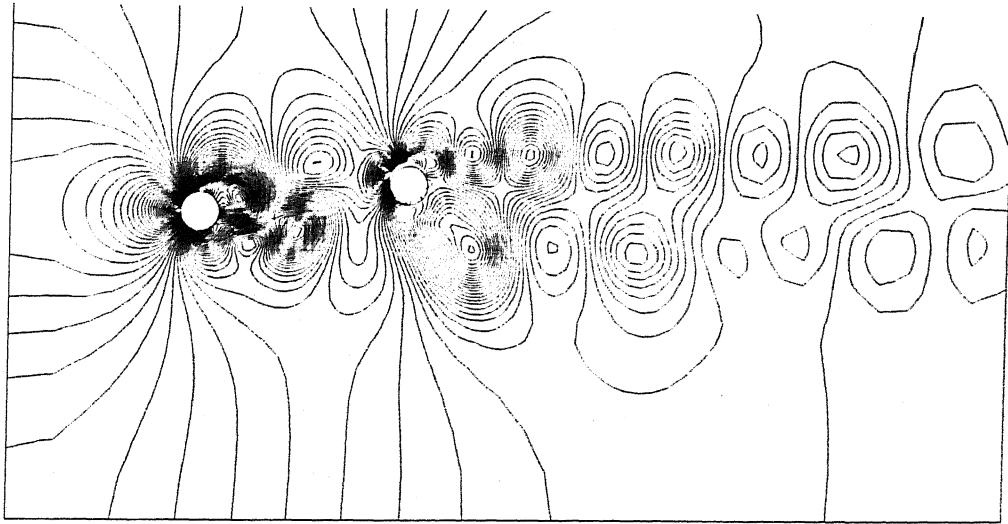
Figure 4.11: Pressure, Vorticity and Streamlines plots for fixed cylinders in staggered arrangement at Re = 80. Second Cylinder at X/D = 5.5, Y/D = 0.7
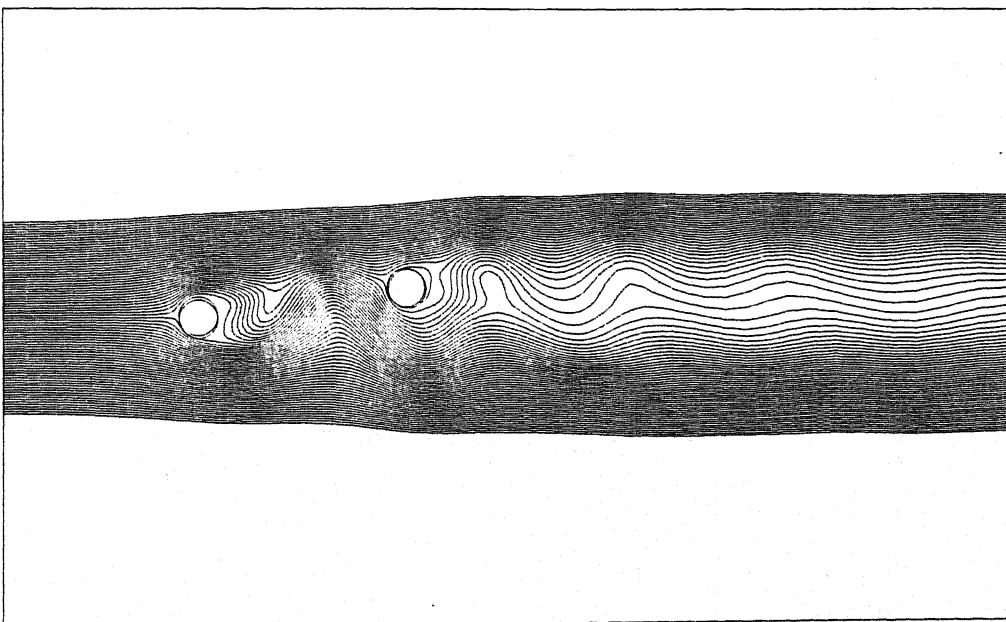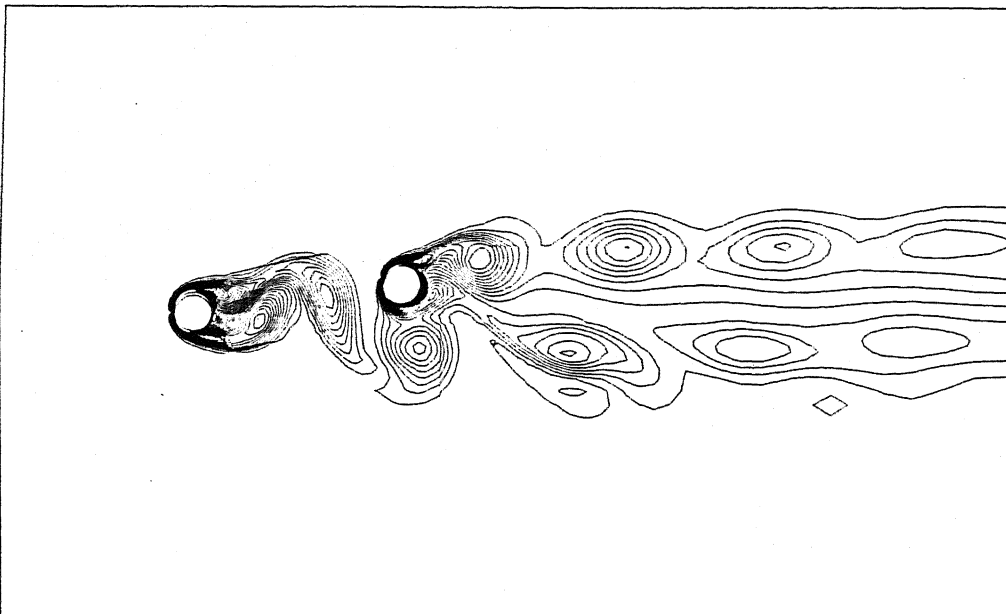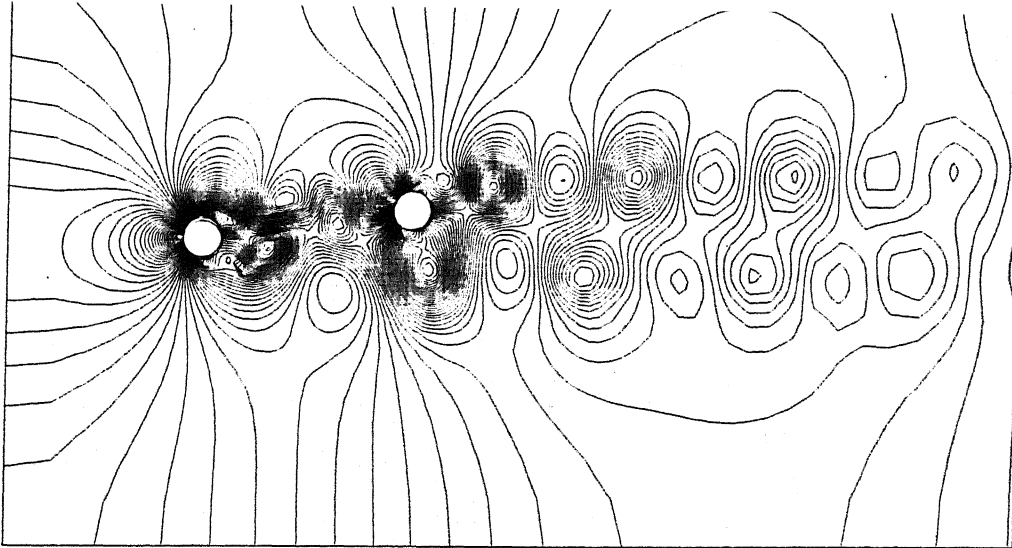
Figure 4.12: Pressure, Vorticity and Streamlines plots for moving cylinders in staggered arrangement at Re = 100. Second Cylinder at X/D = 5.5, Y/D = 0.7
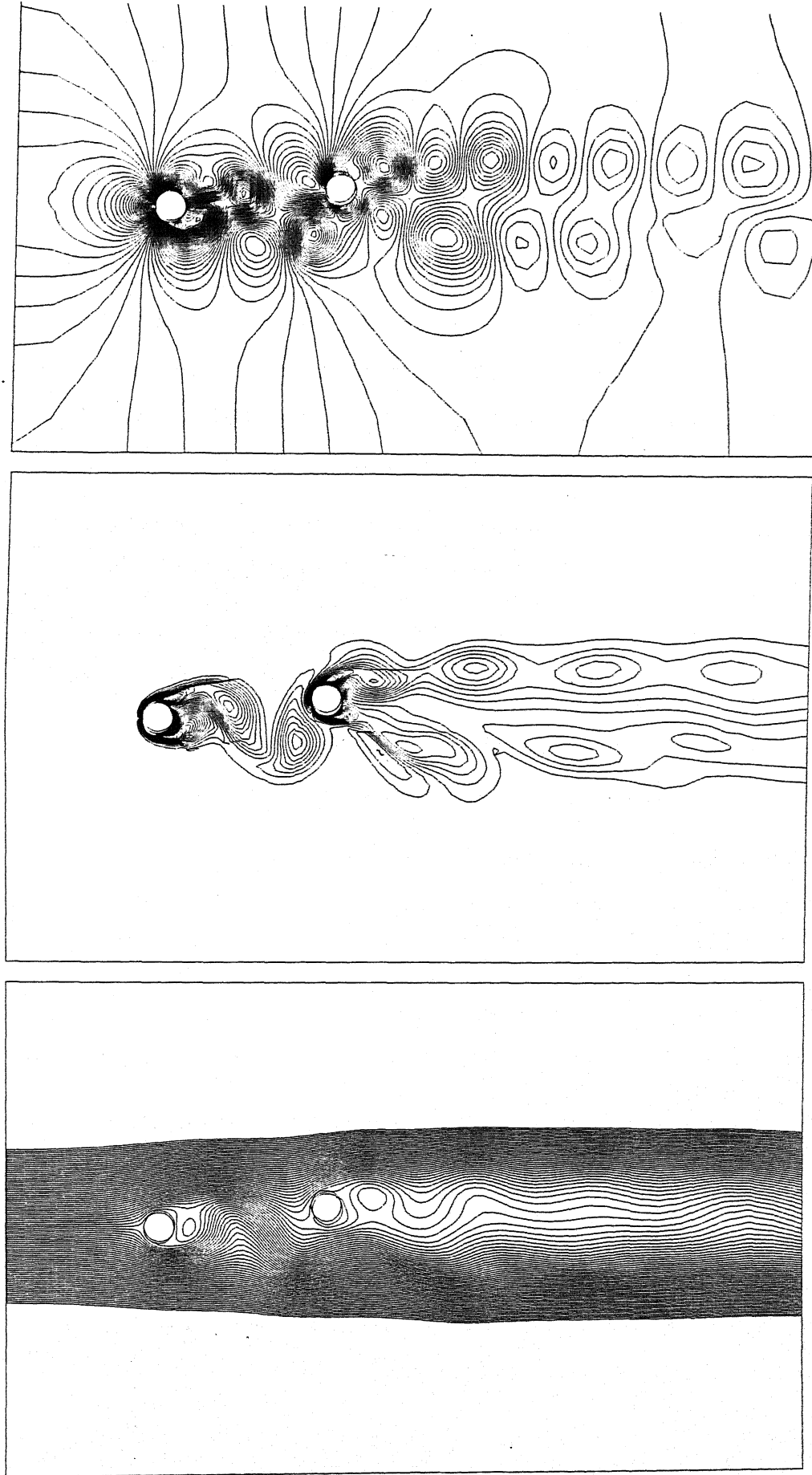
Figure 4.13: Pressure, Vorticity and Streamlines plots for moving cylinders in staggered

References

[1] E. Berger. Suppression of vortex shedding and turbulence behind oscillating cylinders. *Phys. Fluids Suppl*, pages 191–193, 1967.

[2] Shoei-Sheng Chen. *Flow-Induced Vibration Of Circular Cylindrical Structures*. Hemisphere Publishing Corporation, 1987.

[3] Abernathy F.H. and Kronauer R.E. The formation of vortex streets. *Journal Of Fluid Mechanics*, 13:1–20, 1961.

[4] Gerrard J. H. The mechanics of the formation region of vortices behind bluff bodies. *Journal Of Fluid Mechanics*, 25:401–413, 1966.

[5] Zdravkovich M. M. Classification of flow-induced oscillations of two parallel circular cylinders in various arrangement. *In. Sym. On Flow-Induced Vibration*, 2:1–18, 1984. ASME.

[6] Sanjay Mittal. *Stabilized Space Time Finite Element Formulations*. PhD thesis, Minnesota Institute Of Technology, 1992.

[7] P. J. Strykowski and K.R. Sreenivasan. On the formation and suppression of vortex 'shedding' at low reynolds numbers. *Journal Of Fluid Mechanics*, 218, September 1990.

[8] C. H. K. Williamson and A. Roshko. Vortex formation in the wake of an oscillating cylinder. *Journal of Fluid and Structure*, pages 355–381, 1988.

A121236

AE-1996-M-RAG-FIN